The Sun

7

Our Sun is the only star whose surface we can study in detail due to its proximity. Through space missions are also *in situ* measurements possible. The importance of our sun was already recognized by the ancient civilized peoples. The names of the sun deity (sun cult) are Aton, Ra, Re, Horus (Egyptians), Huitzilopochtli (Aztecs), Sunne, Sol (Germanic peoples), Apollo, Helios (Greeks), Surya (Hindu), Lugh (god of light, Celts), Inti (Inca), Mithra (Persians), Apollo, Sol (Romans), Svarožić (Slavs).

Solar physics has established as an own branch of astrophysics, and here has arisen a line of research topics of great practical relevance: The study of solar-terrestrial relations.[1]

7.1 Basic Data and Coordinates

What are the most important state variables that characterize our Sun, and how can these variables be determined? How can phenomena of the solar atmosphere be defined in a coordinate system?

[1] Formerly solar-terrestrial relations, now Space Weather.

A. Hanslmeier, *Introduction to Astronomy and Astrophysics*,
https://doi.org/10.1007/978-3-662-64637-3_7

7.1.1 Basic Data

The most important state variables of the Sun are:

Mass	333,000 Earth masses = 1.98×10^{30} kg
Radius	109 Earth radii = 6959×10^{8} m
Luminosity	3.826×10^{26} W $= 3.826 \times 10^{33}$ erg/s
Apparent brightness	$m_V = -26.^{\mathrm{m}}87$
Effective temperature	5777 K
Rotation period	≈25.38 days

In astrophysics, one often gives the data of objects in units of the corresponding value for the Sun, e.g., the mass of a star is 1.4 $M_\odot$.

From its values the Sun is an average star, many stars are even smaller than the Sun and less massive.

7.1.2 Coordinates

A reliable and save method to observe the Sun is the *projection* of its image onto a screen behind the eyepiece of a telescope. To determine the position of phenomena on the surface of the Sun, one uses the coordinates sketched in Fig. 7.1. The *Position angle P* is taken from an astronomical yearbook, in Fig. 7.1 one sees the definition of the sign (+ or −). The *heliographic latitude* B_0 of *center of the sun* is also taken from a Yearbook:

- $B_0 > 0$ one looks rather at the northern hemisphere of the sun,
- $B_0 < 0$ one looks rather at the southern hemisphere.

The sun rotates differentially, i.e. faster at the equator than at the poles. Therefore one has introduced the *Carrington rotation* that refers to the solar rotation at 16 degrees of heliographic latitude. . Moreover, solar rotations have been numbered by since November 9, 1853, and the mean rotation period is 27.2753 days (synodic value, sidereal value is 25.38 days). Carrington rotation number 2238 began on November 28, 2020.

Determination of *heliographic coordinates:* One first calculates the latitude B_0 of the sun's center and selects the appropriate grid of degrees onto which the sun's image is projected. Then one sets the east-west direction—one turns the measuring template until the sun's edge or a spot runs exactly on the E-W line. Then the position angle is set. Finally, the coordinates can be read directly.

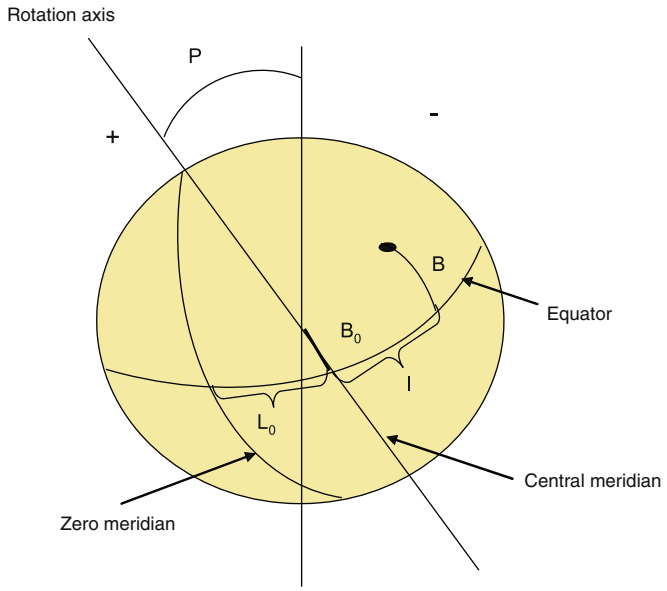

Fig. 7.1 Solar coordinates

7.1.3 Distance

The attempt to determine the distance Earth-Sun is old. *Aristarchus of Samos* (320–250 B.C.) first established the heliocentric world system and tried to determine the distance of the sun (Chap. 3).

Another method is the application of the *third Kepler law* (Sect. 3.3.5). Take a planet which comes closer to the earth than the sun (Venus or Mars), determine its distance in kilometers by means of parallax measurement, and then all distances in the solar system result, since according to Kepler's third law for any two planets 1 and 2 with the orbital semi-axes $a_1,\ a_2$ as well as the orbital periods $P_1,\ P_2$ are valid:

$$\frac{a_1^3}{P_1^2} = \frac{a_2^3}{P_2^2} \tag{7.1}$$

The distance determination with *Parallax measurement* is simple: sight an object from two locations as far apart as possible whose distance is known. Then this object appears at different angles relative to objects further away, and from the *Parallax* π one has according to

$$\sin \pi = \frac{a}{r} \tag{7.2}$$

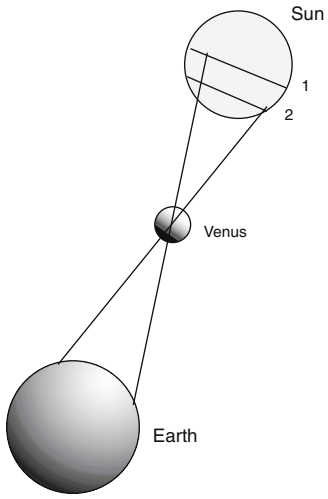

Fig. 7.2 Determination of the Venus parallax during a *Venus transit (transit)* in front of the the solar disk. From two distant observing sites on Earth, the planet can be seen passing in front of the solar disk on path 1 and path 2, respectively. The last observable Venus transit was 2004, the next will be 2117

the distance r, where a is the base length. Even simpler is the determination of the distance from the measurement of *signal propagation times.* One sends a radar beam to Venus and measures when it arrives again after reflection at the surface of Venus. The method is however somewhat uncertain, since one does not know the layer, in which the signal is reflected, sufficiently exactly.

A direct determination of the solar parallax is difficult, because during the day, when the sun is above the horizon, no reference stars are visible. Figure 7.2 shows the determination of the Venus parallax.

7.1.4 Solar Mass

As shown in Sect. 3.3.5, the solar mass can be calculated from the exact form of the 3. Kepler's Law:

$$\frac{a^3}{P^2} = \frac{G}{4\pi^2}\,(M_1 + M_2) \tag{7.3}$$

For example, let's insert: M_1 Mass of the Sun, M_2 Earth mass, P orbital period Earth around the Sun (1 year), a known Earth-Sun distance. Then we immediately get the mass of the sun. Earth's mass, M_2 can be neglected here.

7.1.5 Radius

If the solar distance is known, then the solar radius in kilometers follows from the apparent solar diameter. In the course of a year the apparent Sun radius varies between $32'26''$ (Earth

at perihelion, near the Sun, currently on January 4) and $31'31''$ (Earth at aphelion, far from the Sun, currently on July 4).

7.1.6 Luminosity

Principle of determination: one measures the energy received on earth from the sun and then takes into account the distance of the sun. Per square meter we receive on earth a radiant power of $S = 1.37\,\mathrm{kW}$ from the sun, the *Solar constant S*. This value is important for solar pannel operators. But one should not expect $1\ \mathrm{m}^2$ collector area actually provides this energy, since:

- is the value for outside the earth's atmosphere,
- this is only true for perpendicular incidence of the sun's rays,
- one must take into account the efficiency of the system.

The luminosity of the sun follows from:

$$L = 4\pi r^2\, S \tag{7.4}$$

r—Earth-Sun distance.

The solar constant S indicates the amount of energy that can be absorbed at the Earth's location (i.e., in $r = 1.496 \times 10^{11}\,\mathrm{m}$ distance) on an area of $1\,\mathrm{m}^2$ per second, i.e. $S = 1367\,\mathrm{Js}^{-1}\mathrm{m}^{-2}$. This energy is distributed over the surface $O = 4\pi R^2 = 4\pi(1.496 \times 10^{11}\,\mathrm{m})^2$, and the total radiant power (luminosity) of the Sun is :

$$L = O \times 1367\,\frac{\mathrm{J}}{\mathrm{m}^2\mathrm{s}} = 3..845 \times 10^{26}\,\mathrm{W}$$

The solar constant indicates the solar radiant power arriving at the earth.

7.1.7 Effective Temperature

We treat stars as black bodies, since Planck's law of radiation applies to them. In thermodynamic equilibrium (in a cavity of temperature T), the emission and absorption of any volume element must be equal. If the emission is described by an emission coefficient ϵ_ν and the absorption is given by an absorption coefficient κ_ν then in the case of a

thermodynamic equilibrium (TE, thermodynamic equilibrium):

$$\epsilon_\nu/\kappa_\nu = B_\nu(T) \tag{7.5}$$

where $B_\nu(T)$ is the Planck function described above (Eq. 5.34); this is known as *Kirchhoff's theorem* .

According to the *Stefan-Boltzmann's law of radiation* the total radiative flux πF of a star (by this is meant the energy flow coming from the interior per square centimetre of the star's surface, for example):

$$\pi F = \sigma T_{\text{eff}}^4 \tag{7.6}$$

and one obtains for the Sun an effective temperature/indexSun!effective temperature eff $=$ 5770 K. The measurement of πF is based on the measurement of the solar constant S.

Thus, we have given the main state variables of the Sun.

In Fig. 7.3 the spectrum of the Sun is shown. Likewise, the radiation curve of a black body with $T = 5800$ K is underlaid.

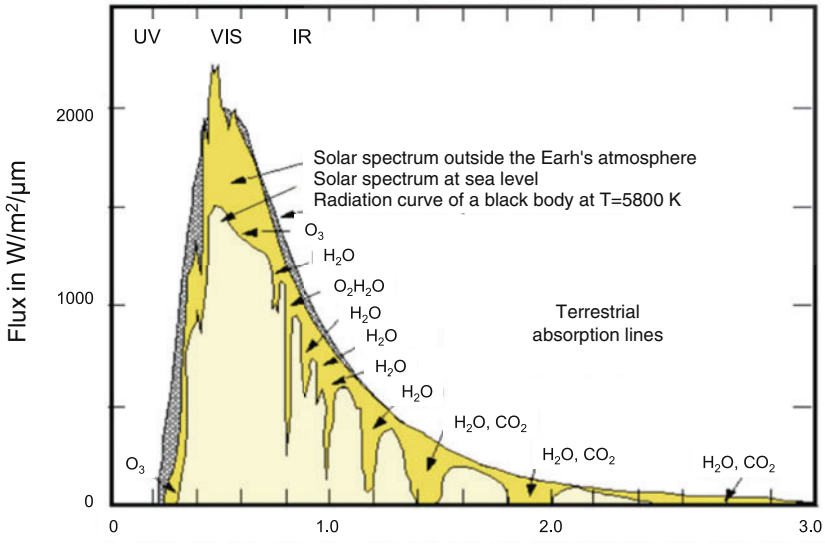

Fig. 7.3 Spectrum of the sun outside the earth's atmosphere and at sea level. You can see the absorption by the Earth's atmosphere. Abscissa: Wavelength in µm

7.1.8 Sun: Observation

Important Never observe the sun with unprotected eyes. The simplest observation is to project the image of the sun on an observation screen (stencil) behind the telescope. Neutral filters in front of the telescope lens can also be used to attenuate the sunlight.

Observation Experiment: Observe the sun with a small telescope in projection. It is very easy to see the center to limb variation, possibly sunspots and flares. By means of sketches one can follow the migration of the spots in a few days which is due to rotation of the Sun.

Special solar telescopes are used in research (see Chap. 5).

- Tower telescopes: At the top of a vertical tower there is a *Coelostat* system that reflects the light into a vertical tower, which is often evacuated to avoid heating up. The tower host the telescope mirrors.
- Coronagraph: The solar disk is darkened by a cone aperture and filters and thus an artificial solar eclipse is produced; one can observe the corona (this outermost part of the solar atmosphere has about the brightness of the full moon). Problem: Stray light in the earth's atmosphere.
- H-Alpha (Hα) telescope: Observation of the sun in the light of the hydrogen line Hα at 656.3 nm; with this one can see sunspots, prominences, filaments, flares. Thus also structures of the chromosphere become observable.
- Spectroheliograph (Hale, 1890): The image of the sun falls on a narrow slit of a monochromator. One observes the sun in a narrow wavelength range, and through a scan one sees the whole sun.
- Lyot Filter: Consists of several birefringent quartz plates. Each plate is half the thickness of the previous one. Due to the property of birefringence, light splits into an ordinary ray I_o and an extraordinary ray I_{eo} each with a different refractive index and phase velocity. Waves in the same polarization state can only occur if the optical path length of I_o, I_{eo} are an integer multiple of the wavelength. By adding a polarizer, to the plates, which is a filter, you get a transmission function with peaks. By using liquid crystals you get a *tunable filter.*
- Radio heliograph: e.g. Nancay, the sun is observed at five frequencies between 150 and 420 MHz. Thereby one detects different heights in the solar atmosphere ($\rightarrow$ the higher the frequency, the deeper one sees into the solar atmosphere, i.e. closer to the solar surface).

An example of a modern solar telescope commissioned in 2012 is GREGOR (Fig. 7.4). It has a diameter of 1.5 m. The telescope is located at an altitude of about 2400 m on the Canary Island of Tenerife.

The *DKIST* solar telescope (see Chap. 5) became operational in 2020 and, with a diameter of 4 m, is the largest solar telescope ever built. In Europe there are plans for an

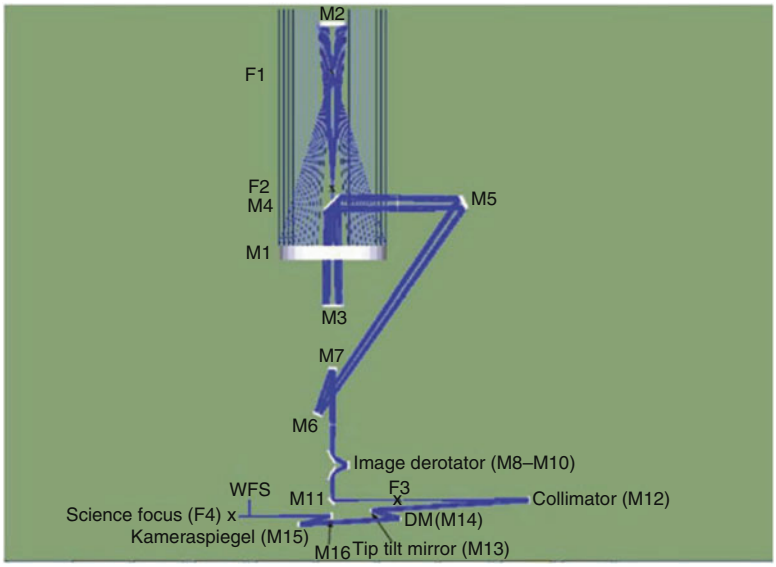

Fig. 7.4 The new GREGOR telescope. Tip Tilt is a tiltable mirror which can partially compensate for air turbulence and allows better solar images. (Source: KIS, Freiburg)

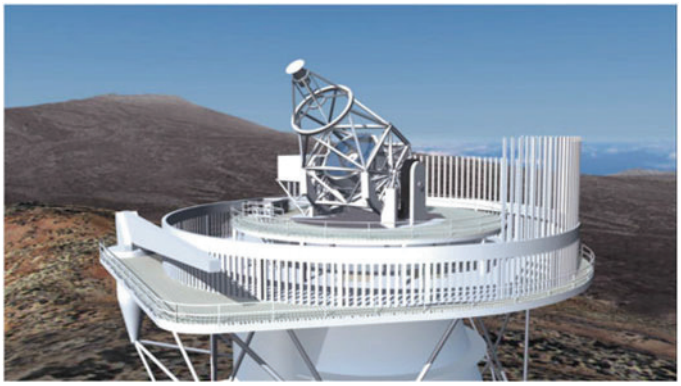

Fig. 7.5 The planned European Solar Telescope, EST [EST consortium]

EST, European Solar Telescope (Fig. 7.5), which could be operational in 2029 and whose diameter would be similar to that of DKIST. Since DKIST is located in Hawaii and EST on the Canary Islands, a round-the-clock solar observation would become possible.

The Sun, our nearest star, is the only star where details can be observed!

7.2 The Structure of the Sun, the Quiet Sun

What layers does the sun consist of and how do these layers come into being? We have to distinguish between the layers of the solar interior and the solar atmosphere.

7.2.1 General Structure of the Sun

The structure of the sun can be roughly subdivided in:

- Sun interior
  - core,
  - radiation zone,
  - convection zone,
- solar atmosphere
  - photosphere,
  - chromosphere,
  - corona.

In general, we can say that our Sun is the only star where surface details can be observed directly. Thereby seen from Earth an angle of $1''$ corresponds to about 720 km on the solar surface. Only recently quasi *in situ* measurements by space probes are possible.

The Sun is a gas sphere in which the density decreases almost monotonically towards the outside. Physical quantities relating to the Sun are denoted by the subscript solar sign $_\odot$.

From Table 7.1 one sees that within 0.5 $R_\odot$ 96% of the mass is already concentrated. In the following we discuss the individual layers of the sun and the phenomena of the quiet (i.e. not active) sun occurring in them.

Table 7.1 Variation of the density in the solar interior

$r/R_\odot$	$r/10^{10}$ cm	$T[10^6\,\mathrm{K}]$	$\rho[\mathrm{g/cm^3}]$	M_r	$P[\mathrm{N/cm^2}]$
0.00	0.00	20	158	0,0	4×10^{12}
0.1	0.7	16	118	0.0089	2.5×10^{12}
0.2	1.39	11	45	0.44	6×10^{11}
0.5	3.48	3.9	0.74	0.96	4×10^{9}
0.9	6.27	0.44	0.001	1.0	7×10^{5}

7.2.2 Sun's Interior

Near the center the *Fusion* from Hydrogen, H, to Helium, He, takes place. This *Hydrogen burning* (actually a nuclear fusion) is described in more detail in Chap. 8 on stellar structure. Our Sun has already burned about 50% of the available hydrogen. Fusion produces *neutrinos,* which pass through the sun unhindered due to their small effective cross-section. On Earth, special detectors can be used to detect these neutrinos originating from the interior of the Sun and thus verify the theories of solar structure. Since the measured neutrino fluxes do not correspond to the theory, there exists a *neutrino problem* in solar physics. We have to consider :

- Neutrinos: arrive at Earth with only eight minutes delay, so they reflect the current rate of nuclear fusion in sun;
- Photons: are emitted at the surface of the sun. However, it takes many 10^5 years until a photon reaches the surface from the place of its origin (thereby changing from extremely short-wave to long-wave) and is emitted. This is due to the many scattering processes of the photons. The light of the present sun thus comes quasi from nuclear reactions which took place many 10^5 years ago.

Another way to explore the interior of the sun is through the use of Helioseismology. The sun oscillates, and from the analysis of these oscillations the physical parameters of the sun's interior can be determined. Analogue: From the sound of a bell, the bell material can be inferred.

> The evaluation of the neutrino flux from the Sun and helioseismology make it possible to explore the interior of the Sun directly.

From this, it appears that our ideas about the structure of the Sun agree quite well with observations.

Nuclear fusion in the solar interior can be roughly stated as:

$$4p \rightarrow {}^4\mathrm{He} + 2e^+ + 2\nu_e \tag{7.7}$$

So neutrinos are produced, ν_e or, to be more precise, electron neutrinos. The first neutrino experiment goes back to *R. Davis* Some chlorine atoms of the cleaning liquid C_2Cl_4 in a large underground tank are converted to ^{37}Ar. This experiment was performed for the first time in 1964, and only 1/3 of the expected neutrino flux was measured. In the Superkamiokande experiment (1988), a tank filled with 50,000 t of highly pure water is used about 1000 m below the earth's surface. Free electrons are produced when neutrinos

react with water molecules in the tank. The neutrinos are detected by the occurring Cerenkov radiation of free electrons.

The measured low neutrino flux is explained by the fact that neutrinos change their properties on their way to Earth. They change into muon and tau neutrinos, but only the electron neutrinos can be measured. These neutrino oscillations would then also require a finite rest mass. Sudbury neutrino experiment (SNO) can detect all three types of neutrino (1999–2006), and neutrino oscillations are considered to be secured to explain the neutrino problem of the Sun.

Energy is released during nuclear fusion in the form of gamma ray quanta. These are absorbed and re-emitted in the radiation zone. Thus, in the radiative zone, energy transport occurs by radiation. In the convection zone, energy transport then starts by convection: Hot plasma flows upward, cools down, sinks downward, heats up again, etc.

The expansion of the three regions of the solar interior corresponds roughly to $(1/3)R_{\odot}$ in each case , i.e., the convection zone extends, for example, to about 200,000 km below the solar surface.

7.2.3 Photosphere

This layer emits almost the entire Solar radiation, whereby the maximum of the radiant power lies at 500 nm. The thickness of the photosphere is about 400 km and is very thin compared to the solar radius of about 700,000 km. Within the photosphere the temperature decreases from 6000 K to 4000 K, the density from 10^{-7} to 10^{-8} g cm^{-3}. The optical depth is : $\tau = 0.5$ at $T = 5800$ K and $\tau = 0.05$ at $T = 4800$ K.

If you look at a solar image in visible light, you can see *center to limb variation*. The solar disk appears brighter in the center than at the edge. If one looks towards the solar limb, the visual ray must take a longer path through the solar atmosphere, and one therefore sees into less deep and thus cooler layers than in the centre of the solar disc(cf. Fig. 7.6). Important: The center to limb variation is wavelength dependent and becomes more pronounced in the blue than in the red. In the radio wave range at $\lambda > 1$ cm one has *Limb brightening*, since here the radiation comes from higher layers where the temperature increases outward.

The center to limb variation indicates that the temperature increases inward from the solar surface.

The solar spectrum is shown in Fig. 7.7 shown.

The surface of the Sun in the photospheric region is not homogeneous, but shows a cellular pattern, which, because of its granular appearance, is also known as *granulation* (Fig. 7.8) . These cells have an average extension of about 1000 km and a lifetime of ten

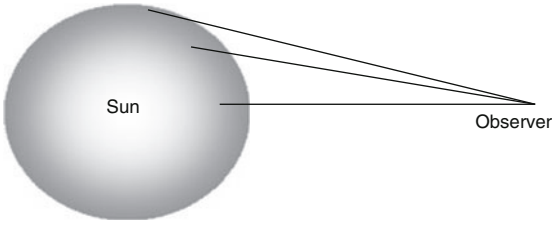

Fig. 7.6 Limb darkening: The visual ray going to the sun's limb penetrates less deep

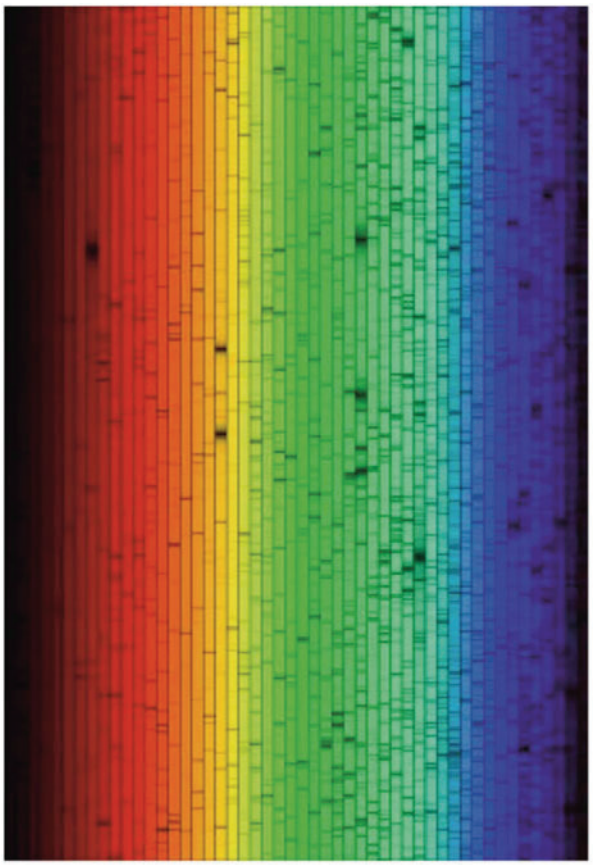

Fig. 7.7 Solar spectrum (credit: AURA)

minutes. From a depth of 200,000 km below the surface of the sun the energy transport to the surface is by *convection*:

Hot plasma flows up, cools, and sinks back down, etc. The bright granules are 200 K to 300 K hotter than the dark intergranular spaces where the plasma sinks down. If you bring a spectrograph slit into an image of the Sun near the center of the Sun, the lines coming from the photosphere appear wiggly (*wiggly lines,* Fig. 7.9). Lines coming from the granulum are blue shifted, because the matter rises upwards, i.e. towards the observer, and lines coming from the dark intergranulum are red-shifted, because here the matter

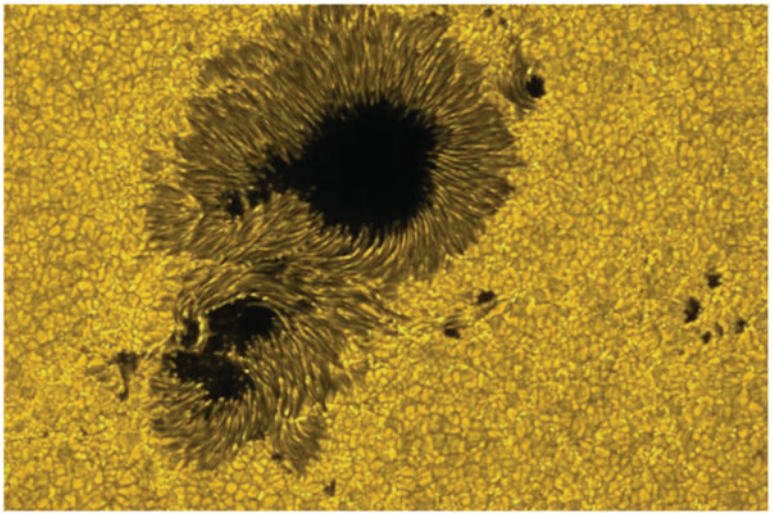

Fig. 7.8 Solar granulation with sunspot; image taken by Hinode satellite

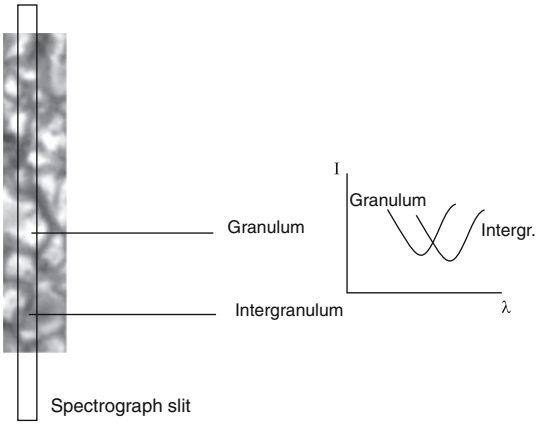

Fig. 7.9 The spectrograph slit lies over granular/intergranular regions. This results in a blue shift for the rising granulum and a red shift for the sinking intergranulum when observed at the center of the solar disk

sinks back into the interior of the sun. If one cannot separate granulum and intergranulum, one gets a superposition of these line profiles, and since the bright and thus ascending elements dominate in size, one gets a mostly C-shaped *Bisector* (which is the line that bisects a line profile at equal intensities). The line profile is therefore asymmetrical. So asymmetric line profiles at stars are always a sign, that there is convection also at their surfaces.

7.2.4 Chromosphere

The chromopshere is extending outward of the photosphere up to about 10^4 km height (1.00–1.015 $R_\odot$). The density decreases to $10^{-11}\,\mathrm{g\,cm^{-3}}$, the temperature increases again to 10^5 K. Because of the low density, the radiation of the chromosphere contributes almost nothing to the total radiation, despite the high temperatures. During a total solar eclipse one observes the *Spicules,* a bristly structure that aligns with magnetic fields. In the spectrum of the chromosphere, which is seen to flash only briefly during a total solar eclipse and is therefore known as the *Flash spectrum* one sees emission lines. These arise as follows:

- Lines that appear in absorption in the photosphere spectrum are visible as emission lines in the chromosphere.
- Due to the high temperatures in the chromosphere, lines of highly excited or ionized atoms are observed.

Both indicate high temperatures.

The chromosphere can also be observed outside a total eclipse. Spectroheliograms are used to take monochromatic images. One measures through a *narrowband filter* the radiation in the centers of strong absorption lines: at $\lambda = 656.3\,\mathrm{nm}$ H_α, at $\lambda = 393.3\,\mathrm{nm}$ and $\lambda = 396.8\,\mathrm{nm}$ the so-called H and K lines of Ca II (singly ionized calcium). In the latter one sees the *chromospheric network* (supergranulation cells) about 30,000 km in diameter, at the edges of which are strong magnetic fields. In other lines (e.g. Hα) one sees prominences protruding beyond the solar limb, which can be seen as dark filaments in front of the solar disk (Fig. 7.10).

7.2.5 Corona

In the outermost layer of the solar atmosphere, the corona, the density decreases to $10^{-18}\,\mathrm{g\,cm^{-3}}$ and the corona merges outwards into the *interplanetary medium*. Its shape depends on the activity of the Sun: At *maximum* it is symmetrical around the solar disc, in the *Minimum* it is more concentrated to the equator.

The *spectrum* of the corona consists of the following parts:

- Continuous spectrum, *K corona:* photospheric light scattered by free electrons at the corona. But then one should observe absorption lines. But because of the high temperatures these are blurred (temperatures of several 10^6, K resp. speed of $v = 8000\,\mathrm{km/s}$) and won't come up.
- *L corona:* emission lines; highly ionized elements, e.g. FeXIV (13-fold ionized iron), this is the *green corona line* at 530.3 nm. From the ratio FeXIV/FeX one can determine the temperature according to the Saha formula.
- *F-Corona:* Normal solar spectrum; originates from scattering by interplanetary dust.

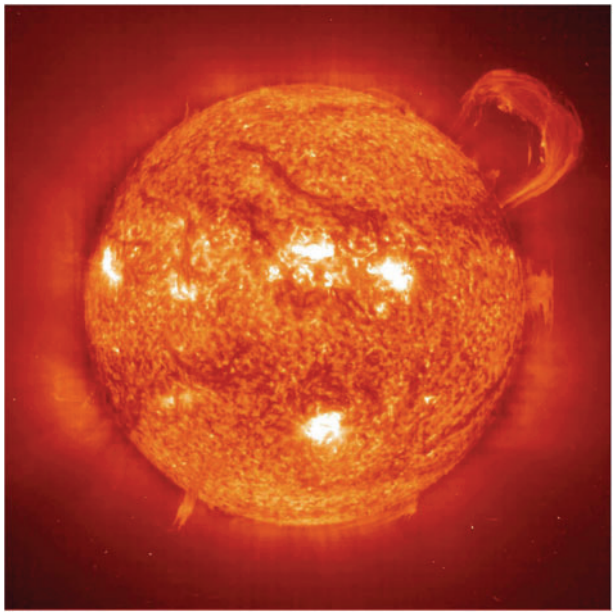

Fig. 7.10 Sun with prominences projecting brightly above the solar limb and appearing dark in front of the solar disk (source: SOHO/NASA)

An observation of the corona outside of total solar eclipses is possible in the UV and in the X-ray range as well as in the radio range (m-waves). In the X-ray light the *coronal holes* can be seen. Here the magnetic field lines, which determine all structures in the corona, are open over wide areas. Through these areas the *Solar wind* escapes.

If one observes the sun in the radio range, the *Plasma frequency* ν_0 should be noted; radio radiation below this frequency ν_0 (or above this wavelength) cannot escape because the refractive index becomes negative, < 0 .

$$\nu_0 = \sqrt{\frac{e^2 N_e}{\pi m}} = 9 \times 10^3 \sqrt{N_e} \qquad [\text{MHz}] \tag{7.8}$$

In this formula, the electron density N_e is given as particles per cm^3. The electron density in the corona decreases with increasing distance from the solar surface: At a distance of $1.03\,\text{R}_\odot$ it is at most $350 \times 10^6\,\text{cm}^{-3}$ at a distance of $2.0\,\text{R}_\odot$ it is $3.1 \times 10^6\,\text{cm}^{-3}$ and at $5\,\text{R}_\odot$ only more $0.05 \times 10^6\,\text{cm}^{-3}$.

When observing in different frequencies, one can probe different layers of the solar atmosphere.

If one observes the Sun in the radio range at higher frequencies, then one sees into deeper layers because the electron density is higher there. So you can do a kind of *tomography* of the solar corona when observing at different frequencies.

The temperature increases strongly in higher layers of the solar atmosphere. The reason for this is not yet fully understood.

7.3 The Active Sun

Our sun is not a static star—it is an active star (ex. Fig. 7.11), changing occur constantly. We will first discuss the individual phenomena and then their effects on Earth.

7.3.1 Sunspots

The easiest way to determine the solar activity on the surface of the sun is by looking at *Sunspots*. These were observed with the naked eye in ancient times when the sun was low in the sky. For a sunspot to be visible to the naked eye, it must have a total extent of about 40,000 km. Since it has been recognized that phenomena of solar activity affect radio communications, satellite positions, corrosion of pipelines, electric power lines, etc., close attention has been devoted to the study of the *Space Weather.*

The first telescopic observations of the spots were made by *G. Galilei* (1610) *Chr. Scheiner*, and other astronomers. At first sunspots were thought to be inner planets wandering around the Sun. Then it was realized that their migration around the Sun could be explained by the rotation of the Sun.

Spots consist of a dark core part, the *umbra,* which is surrounded by a filamentary brighter *penumbra* (Fig. 7.12). The temperature in the umbra is 4300 K and in the

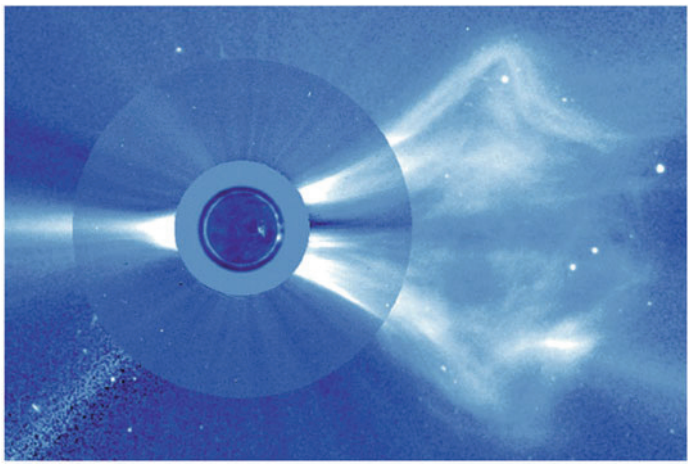

Fig. 7.11 Coronal Mass ejection (CME), recorded with LASCO-SOHO

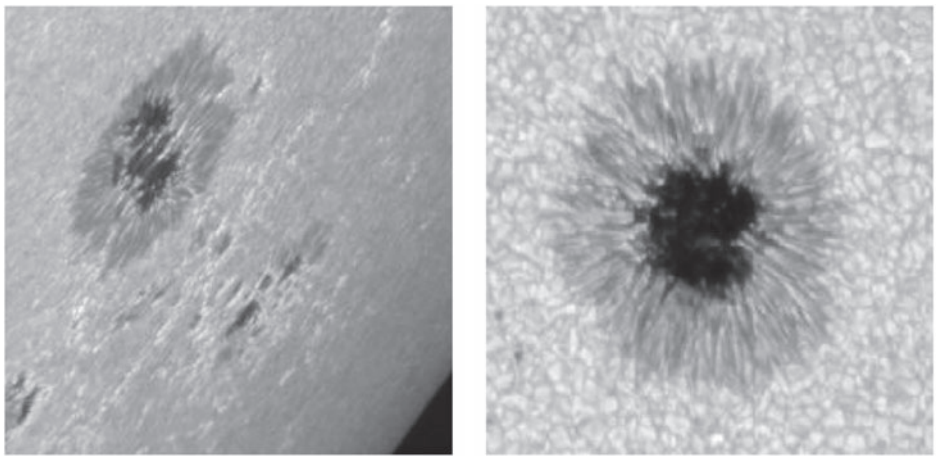

Fig. 7.12 Sunspot with flares at the edge of the sun and in the center of the sun disk; photograph La Palma, Vazquez, Bonet, Sobotka, Hanslmeier

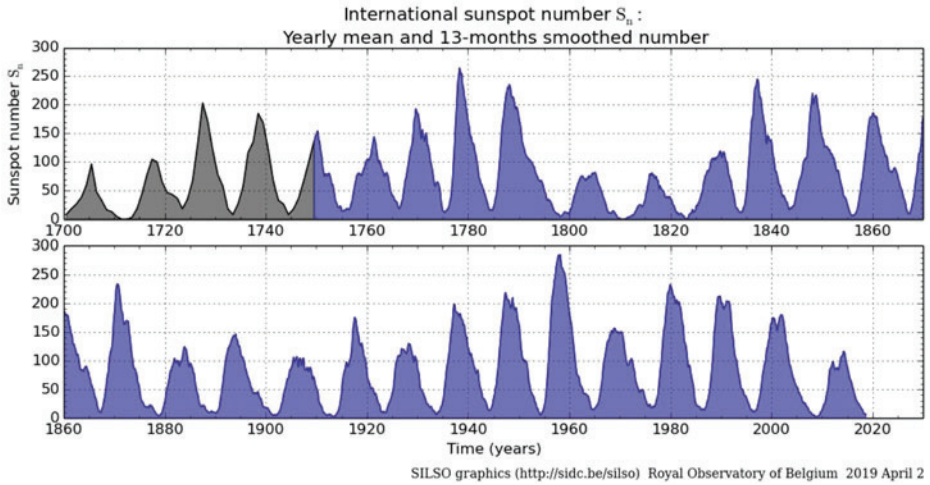

Fig. 7.13 Sunspot relative numbers (source: SIDC)

penumbra 5500 K. The intensity ratio between the spot and the photosphere is 0.13 at a wavelength of 300 nm, and at $\lambda = 1000$ nm 0.46.

The number of sunspots varies with an average period of eleven years, which is the *Sunspot cycle* (Fig. 7.13). The activity cycles have been numbered consecutively since 1760. In 2019, the cycle began with the number 25. Spots usually occur in groups of spots with several individual spots. If g is the number of groups and f is the number of single spots, then we determine the *Relative number R*:

$$R = k(10\,g + f) \tag{7.9}$$

Thereby k is a correction factor that takes into account the influence of the instrument. At the beginning of a new cycle, spots occur at higher heliographic latitudes at $\pm 35°$ on, in the middle of the cycle at $\pm 8°$. Thus one gets a *Butterfly diagram,* if one records the positions of the spots in the course of an eleven-year cycle.

There can be up to two years of overlap between spots of the old cycle and the new cycle. If one observes the spots at the solar limb, the penumbra on the side closer to the center of the sun appears shortened. This is the *Wilson effect.* Lines of equal optical depth are geometrically several 100 km deeper in large spots than in the photosphere; this leads to an asymmetry of the penumbra at the solar limb.

The lifetime of the spots is a few days, for 90% of the spots less than eleven days.

If one examines spectral lines that are created in the spots, one sees a splitting due to the *Zeeman effect.* Therefore spots are related to magnetic fields.

The magnetic flux densities measured in the spots[2] are up to 4000 Gauss[3] (Earth's magnetic field around 0.5 Gauss). The field lines pierce the photosphere vertically in the umbra region and diverge like a razor brush. If H_0 is the strength of the field at the center of the spot and r is the distance from the spot center, then one has:

$$H(r) = H_0(1 - r^2) \tag{7.10}$$

Why are spots cooler than the approximately 6000 K hot solar surface? Outside the field in the sun there is the pressure p_e. In the area of the spot to the pressure p_i there is also amagnetic pressure $B^2/2\mu$ where μ denotes the magnetic permeability. In order to have a stable structure, the following must hold true:

$$p_i + B^2/2\mu = p_e, \tag{7.11}$$

thus $p_i < p_e$ and because of $\rho_i = \rho_e$ it follows that $T_i < T_e$ is. The temperature inside a spot T_i is therefore lower than the surrounding photosphere temperature T_e.

91% of all spots occur in *bipolar groups*. These are magnetic tubes driven by magnetic buoyancy from the solar interior to the surface, and then produce a bipolar group at the two puncture points (Fig. 7.14).

The *Zurich classification* is sketched in Fig. 7.15 (after Bray). Criteria for this are whether a group is unipolar or bipolar, whether a penumbra is pronounced or not, and the heliographic length extent.

The spot preceding in solar rotation is called the p-spot and the one following is called the f-spot. If in a cycle of activity in the northern hemisphere the p-spot has a positive polarity and the f-spot a negative polarity, then in the southern hemisphere it is the other way round: the p-spot then has a negative polarity and the f-spot a positive polarity. On

[2] Often one simply speaks of field strengths, although $B = \mu H$, μ =Permeability.

[3] 1 Gauss = 1 G = 10^{-4} Tesla.

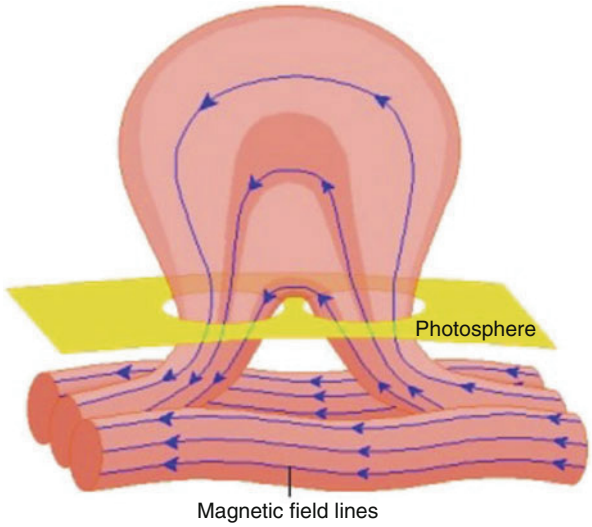

Fig. 7.14 A bipolar spot group is formed when magnetic flux penetrates to the surface of the photosphere

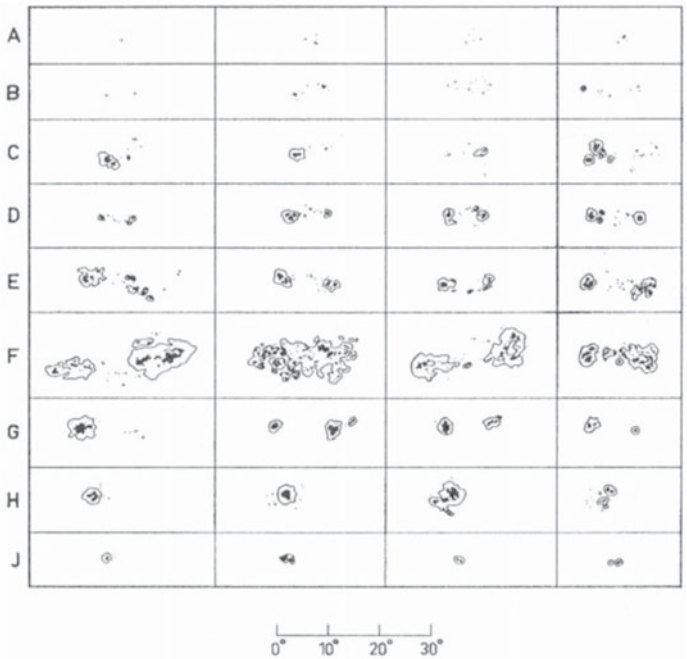

Fig. 7.15 Zurich sunspot classification; (**a**) unipolar (first row from top), (b) bipolar, without penumbra (second row from top), (**c**) bipolar, penumbra at one of the two main spots, (**d**) Penumbra at both main spots, small, etc.

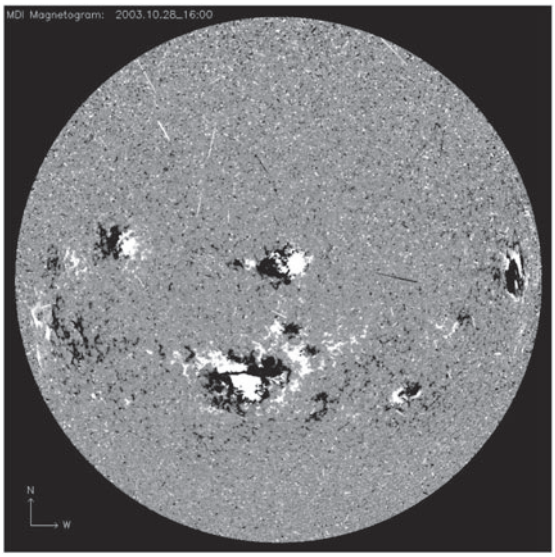

Fig. 7.16 Magnetogram of the sun. White and black denote different polarities (SOHO/MDI)

the next cycle, the whole thing is reversed: In the northern hemisphere of the Sun, the p-spot then has a negative polarity, and so on. This has been found by *Hale* and is known as *magnetic cycle* (Fig. 7.16).

The spectrum of spots is difficult to observe, it resembles that of a K star. New results of helioseismology show the dynamics below spots (Fig. 7.17).

Sunspots are areas of strong magnetic fields where convection is reduced.

7.3.2 Faculae

They are practically the counter part to the spots. They appear as extended areas of excessive brightness (10% more than in the photosphere). Faculae usually occur in the vicinity of sunspots; because of the contrast they are especially observable at the solar limb, i.e. they are an overheating of the higher solar layers. Usually, faculae are found at the same heliographic latitudes as the spots. The polar faculae occur at unusually high latitudes in the years before or during a sunspot minimum.

In the range around 430 nm *(G-band)* sees one finds many molecular lines (CH, vibrational states, rotational states) in the solar spectrum. At very good resolution with a G-band filter, one finds bright, about 0.1″ extended dots, *G-band bright points,* GBPs, which are small magnetic elements.

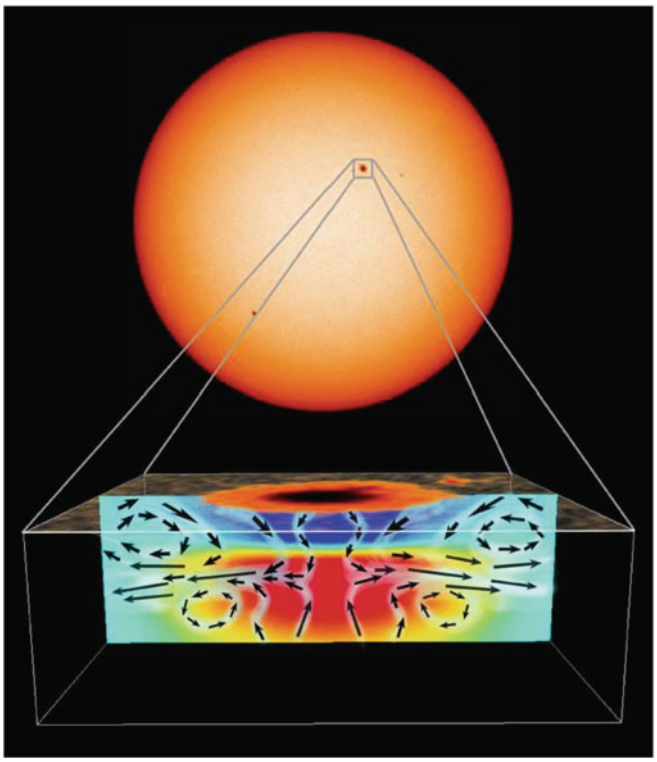

Fig. 7.17 Sunspot with structure below the photosphere (SOHO/MDI)

7.3.3 Prominences

These are clouds of matter in the corona. They can be observed as:

- At the solar limb: bright against the dark sky; either during a total solar eclipse or in the light of a chromospheric line such as Hα;
- on the solar disk: they appear there dark against the bright photosphere, i.e. in absorption, and are called *Filaments*.

Prominences are also subject to the eleven-year cycle. The main zone of their occurrence corresponds to the spot zone. Shortly before the minimum the polar zone appears, which moves poleward and reaches its maximum about two years before the spot maximum at the pole. One distinguishes:

- dormant prominences: long-lived; thickness about 7000 km. Height usually up to 40, 000 km, length 20, 000 km; they are long, thin, and lamellar. They often stand only on single feet in the chromosphere; their life is up to a year. They usually arise in groups

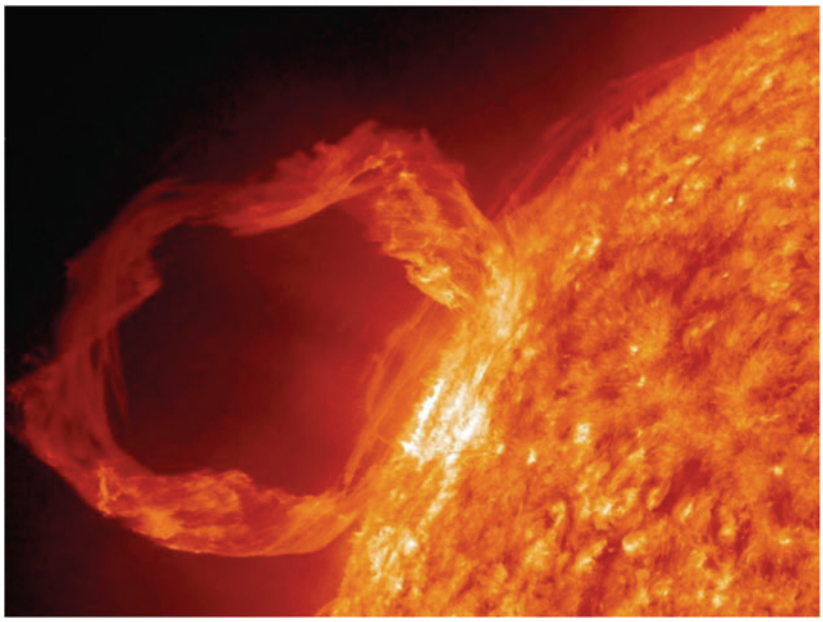

Fig. 7.18 Prominence taken with the SDO/AIA instrument.

of spots or in flares. The sun rotates differentially, i.e. faster at the equator than at the poles, therefore their position becomes more and more parallel to the equator.

- Active or eruptive prominences: usually associated with active spot groups. There are:

(a) Sprays: explosive rise with 1000 km/s (the maximum observed height was 1.5 million km!).
(b) Surges (splashes): ascent with 50–200 km/s; occur repeatedly in active spot groups.
(c) Coronal rain: After eruption, matter flows back like rain.
(d) Loops: Matter follows magnetic field lines.

The prominences (Figs. 7.10 and 7.18) always appear at the boundary between regions with different magnetic polarities *(neutral line)*. There the field lines run horizontally. The ionized matter is held in place by the magnetic field, and its density is 100 times greater than the ambient density; even in the case of the quiescent prominences, matter is constantly flowing away and being replaced.

7.3.4 Flares and Coronal Mass Ejections

Solar flares can be observed throughout the electromagnetic spectrum. *Carrington* and *Hodgson* observed for the first time in 1859 a *Flare* in visible light (which is very rare).

Hale invented the spectrohelioscope, which could be used to observe the Sun at a particular wavelength, and in 1920 found that flares were visible in the light of the hydrogen line Hα. Then, in 1940, flares were observed in the radio region and, with satellites, later in the UV and in X-rays.

The energy released in flares ranges from 10^{16} J *(nanoflares)* to 10^{25} J (large, so-called *Two Ribbon Flares*).

A comparison: The *Hiroshima bomb* had an explosive force of 15 kt, with

$$1\text{kt (kiloton TNT)} = 4.184 \times 10^{12}\,\text{J}. \tag{7.12}$$

The largest ever found explosed *Hydrogen bomb* had 50 megatons, and the explosive power of all conventional bombs in World War 2 reached about two megatons.

As an exercise you could estimate how large the energy release in a flare burst is compared to the Hiroshima bomb.

For *classification* of flares one uses two systems:

- Importance: 1, 2, 3, 4 and the additions *f* for *faint, n* for *normal* and *b* for *bright.* S indicates a subflare. So the brightest flares are 4b. The higher the value of this optical classification, the longer the apparition usually lasts.
- X-ray classification: Since 1970 there are X-ray observations of flares, and one classifies according to the flux in the range 1–8 Å in units of W/m^2. In powers of ten:

  Class A: $10^{-8}\,\text{W/m}^2$, class B: $10^{-7}\,\text{W/m}^2$, C, M, X.

  An M8 flare then has a maximum flux in the 1–8 Å range of. $8 \times 10^{-5}\,\text{W/m}^2$. Note that C1 flares can only be observed at the time of solar activity minimum, when the X-ray background is weak.

If a flare eruption (eruptive flares) occurs, then there is associated:

- shortwave radiation (< 200 nm): of the same order of magnitude as the total solar radiation in this region.
- X-ray radiation: Increased X-ray radiation causes disturbances in the Earth's ionosphere *(Mögel-Dellinger effect)*. Increased ionization of the D layer occurs; radio waves that, in order to be reflected from the F layer, must pass through the D layer twice, are strongly attenuated, thus interfering with radio traffic.
- Corpuscular radiation: The particles with velocities between 1000 km/s and 2000 km/s arrive at Earth one day after the flare outburst, causing magnetic storms, Auroras (green and red oxygen lines, these are forbidden transitions).
- Radio bursts in the m-range.

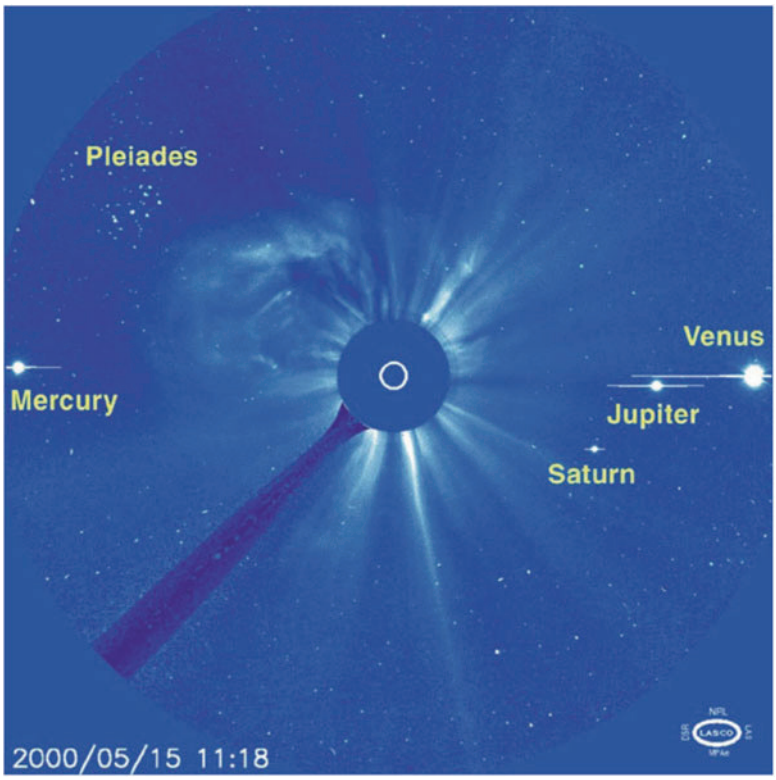

Fig. 7.19 A coronal mass ejection, CME, imaged by the SOHO solar satellite. The Sun itself is obscured and its actual size is indicated by the circular ring (You can also see 4 planets and a few stars in the image) (source: NASA/SOHO)

- Cosmic rays: particles are accelerated almost to the speed of light, in the upper atmosphere of the earth these produce secondary particles and high-altitude showers when they collide with atomic nuclei.

In 1970, *CMEs,* Coronal mass ejections (Figs. 7.11 and 7.19) were observed for the first time. The matter released during a CME leaves the Sun at a speed of up to 2000 km/s. The mass of the ejected matter is $10^{15} \ldots 10^{16}$ g. Eruptive flares are likely to be caused by CMEs. During the eruptive phase of a CME, the field lines are open, but then close again, magnetic reconnection occurs, and an eruptive flare bursts *(gradual flare)*. The intersection of these loops with the solar surface appears as two parallel bands in Hα, and it used to be referred to as *two ribbon flares* when the role of CMEs in flare outbursts was not well understood. The same physics seems to be behind eruptive prominences *(disparition brusque)*.

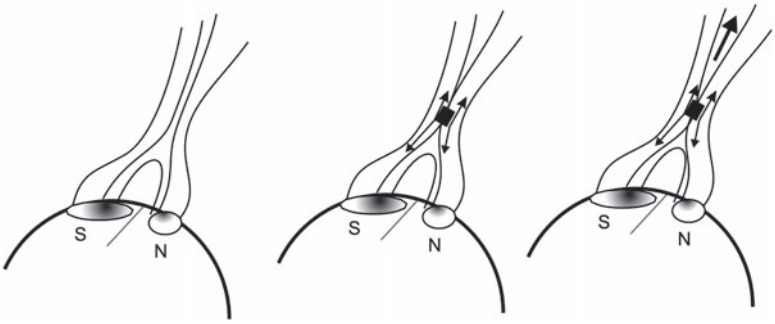

Fig. 7.20 Model for flare formation. At the beginning you have a bipolar group whose field lines are not connected in the corona loop. In the second phase, the flare begins when reconnection of the field lines occurs, and a current flows to the foot points in the photosphere. Finally, the flare moves up into the corona

A *Halo-CME* is a CME that appears to be pointing directly towards the Earth. In this case the CME appears as a halo around the sun. The CME is expanding and appears as an ever-growing halo around the Sun.

Most of the flares are impulsive flares. They can be modeled with a single static magnetic loop (Fig. 7.20). Again, there is a magnetic reconnection with subsequent acceleration of particles, but with no connection to CMEs.

Hale has introduced the following classification for Magnetic structures *(Mt. Wilson classification),* which is also important for the occurrence of flares:

- α: A single dominant spot, usually associated with areas of opposite polarity.
- β: Sunspot pair with opposite polarities.
- γ: Complex group with irregular distribution of polarities.
- δ: Umbrae with opposite polarities within a single penumbra.

In the δ-configuration there occur more flares than in the other groups. Such a configuration can occur in all other groups. Here one has two poles with strong vertical fields close to each other. One can give the following criteria for the occurrence of flares:

- large δ-Spots,
- Umbrae with large elongation,
- high shear in the transverse field or strong gradients in the longitudinal field,
- large spots always have strong flares.

Flares and CMEs arise from reconfigurations of the magnetic field, reconnection.

7.3.5 The Radio Radiation

One must distinguish between solar radio radiation of a slowly variable component and bursts.

The slowly variable component originates from discrete regions of the solar atmosphere, predominantly active regions. The radiation flux is closely correlated with the relative number; it is probably thermal radiation from the corona condensations. Its temperature is about 10^7 K and the wavelength of the radiation is between 1–100 cm, the maximum at 15 cm; the intensity at 10.7 cm is also used as a substitute for spot relative numbers uses.

Radiation bursts produce radiation in the range of 1 cm to 15 m. In the centimeter range, the intensity increases to 20–40 times the normal value, and in the m range, it increases to 10^5-fold of the normal value on.

Let us consider the so-called plasma frequency ω_p. We assume electrons moving with respect to ions at rest. In the case of a gas consisting only of electrons and ionized hydrogen atoms, we find for the charge density:

$$\rho = en_e \tag{7.13}$$

From $div\mathbf{E} = \rho/\epsilon_0$, $\epsilon_0 = 8.854 \times 10^{-12}$As/Vm, electric field constant (permittivity of the vacuum) becomes in the one-dimensional case:

$$div(\mathbf{E}) = dE/dx; \rightarrow E = en_e x/\epsilon_0 \tag{7.14}$$

and the equation of motion is:

$$\ddot{x} = F/m_e = eE/m_e = -\frac{e^2 n_e}{\epsilon_0 m_e} x \tag{7.15}$$

this is the equation of a harmonic oscillator, and one obtains the Plasma frequency To

$$\omega_p = \sqrt{\frac{n_e e^2}{\epsilon_0 \epsilon m_e}} \tag{7.16}$$

when the propagation in a medium of permittivity $\epsilon > 1$ is considered.

The higher the electron density, the higher the plasma frequency. The plasma frequency is also responsible for the reflection of radio waves in the Earth's atmosphere, or how deep into the corona one can look in the radio region.

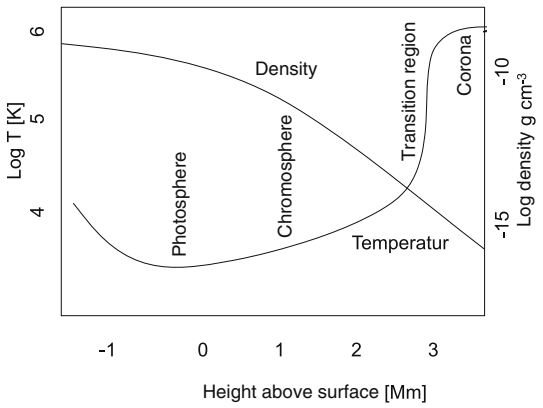

Fig. 7.21 Course of electron density and temperature in the different layers of the solar atmosphere; the transition zone from chromosphere to corona is also called the *transition region.*

Corona: Observations at high high frequencies you see regions of high electron density and therefore you look into deeper layers.

If you plot the *bursts* in the time-frequency diagram, one can see how the regions of stronger radio radiation move through the solar atmosphere. The electron density decreases outward and so does the plasma frequency (Fig. 7.21).

The *Bursts* are classified into:

1. Type I: m-range; short, steeply rising bursts; total duration less than 1 s; main component of noise storms.
2. Type II: m range; emission in a narrow frequency band, shifting from high to low frequencies with time; drift velocity in the frequency band is between 0.5 and 1 MHz/s. Duration about ten minutes; matter thus passes through the corona, i.e. from the frequency drift one can read the height and the velocity from 400–1000 km/s. Occurrence: relatively rare, in activity maximum one outburst every 50 h; correlation with geomagnetic storms (these start 2–3 days after the outburst).
3. Type III: m range; narrow-band, but faster frequency drift than type II (20 MHz/s). Duration 10 s, ascent rate 0.4 c. Height about 1 $R_\odot$; during the sunspot maximum three type III bursts per hour are observed. Occurrence mostly at the beginning of a flare (Fig. 7.22).
4. Type IV: throughout the radio range; fast electrons; height above photosphere 0.3–0.4 $R_\odot$; no more plasma oscillations, because matter density is too low.
5. Noise Storms: m range; large number of individual radiation bursts; duration hours to days; frequent at spot maximum. Type I bursts occur repeatedly; synchrotron radiation of fast electrons; 0.3–1 $R_\odot$ over the photosphere; preferably over spot regions.

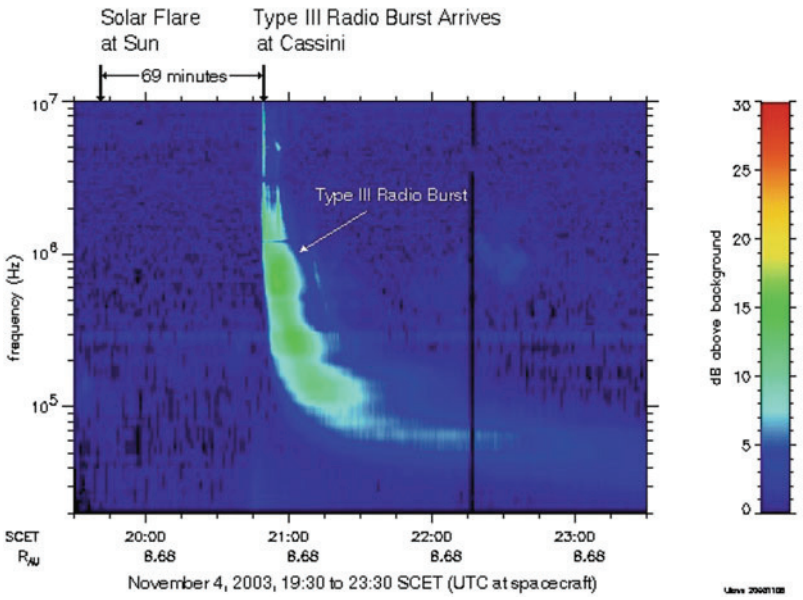

Fig. 7.22 Type III burst imaged by the Cassini spacecraft studying Saturn. More than an hour after the event on the Sun, Cassini shows the radio emission and, in the frequency-time diagram, the emergence of the radio emission at different altitudes in the solar atmosphere (lower frequencies at higher altitudes) (source: Cassini/NASA)

7.3.6 X-rays of the Corona

In visible light, the corona can be seen during a total solar eclipse (Fig. 7.23). The missions *SOHO, TRACE, YOHKOH* an d *RHESSI* enable also observations of the sun in the extreme UV- and X-ray range where the radiation of the Sun varies by the following factors during the eleven-year cycle:

- Variation in the UV range: ≈ 2,
- Variation in the X-ray range ≈ 100.

In Fig. 7.24 the sun is shown in the X-ray region shown. This is emitted due to the high temperatures in the corona. One can clearly see the difference between the emissions near the maximum and near the minimum of solar activity.

The energy of X-rays is a measure of the energy of the electrons that produce them. It is useful to remember:[4]

$$1\text{keV} = 1.6 \times 10^{-16}\,\text{J} \tag{7.17}$$

[4] In visible light at a few eV.

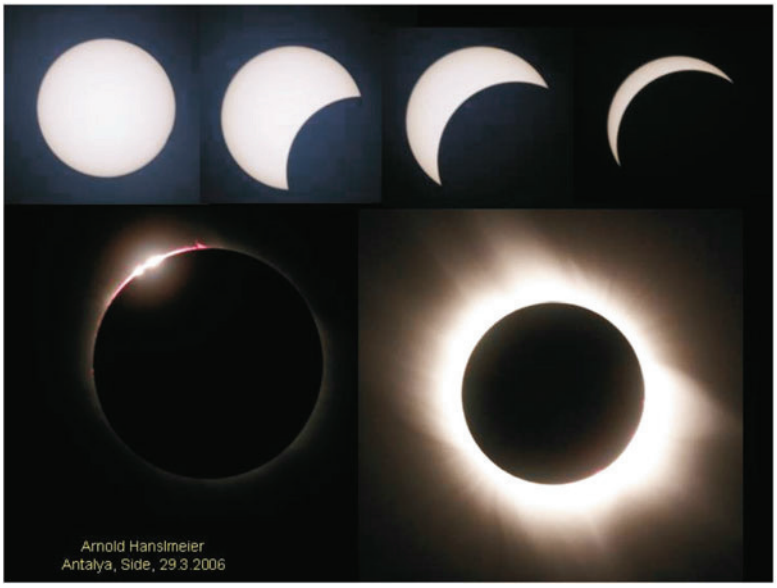

Fig. 7.23 Total solar eclipse of 29.03.2006. Shortly before totality (diamond ring phase) some red glowing prominences are visible, lower right: totality. Corona well visible (image A. Hanslmeier)

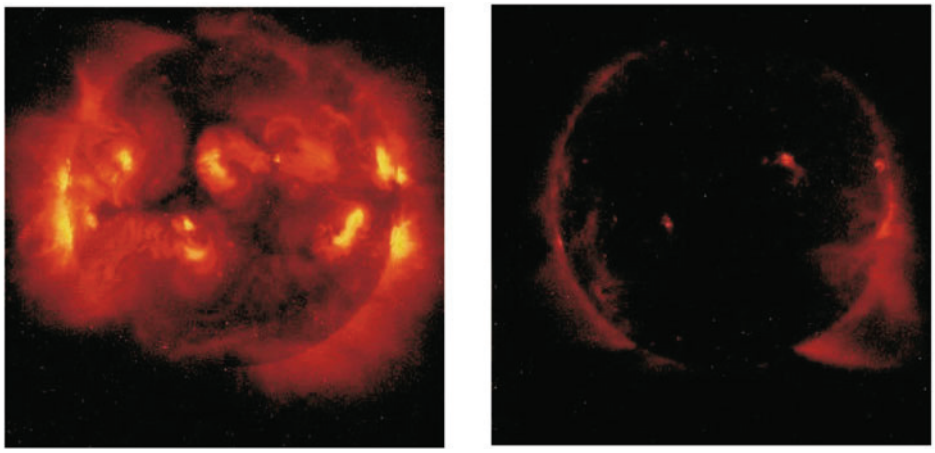

Fig. 7.24 The Sun in the X-ray region – left March 1993 (Sun very active), right near minimum March 1995 (photo: YOHKOH)

According to this, X-rays can be divided into: (a) hard X-rays 10–100 keV, (b) soft X-rays 1–10 keV.

Consider the time evolution of *flares:* Hard X-ray radiation is mostly released during the impulsive initial phase, soft X-ray radiation reaches the maximum with a time delay (some minutes). For the first time, hard X-ray radiation was observed by the *Solar Maximum*

Mission (SMM) around 1980. It was found that there are two sources of this X-ray radiation localized at the foot points. The suggests non-thermal electrons moving down to the foot points from the corona into the denser chromosphere. The microwave emission is also related to this. The slow increase in the soft X-ray region corresponds to the time integral of the hard X-ray emission radiation→*Neupert effect.*

The high temperatures in the course of flares lead to different radiation mechanisms:

- *Thermal bremsstrahlung:* protons attract free electrons; electrons change their velocity, bremsstrahlung occurs, observed as soft X-rays. In thermal bremsstrahlung the particles of the emitting plasma have a defined velocity v, and the distribution function corresponds to of a *Maxwell distribution:*

$$f(v) = 4\pi \left(\frac{m}{2\pi kT}\right)^{3/2} v^2 \exp\left[\frac{-mv^2}{2kT}\right] \tag{7.18}$$

  The emission from this plasma is then called thermal bremsstrahlung, and the radiation power (in [W m^{-3}]) is

$$P_{\mathrm{BR}} = \frac{Z_i^2 n_i n_e}{(7.69 \times 10^{18})^2} T_e[\mathrm{eV}]^{1/2} \tag{7.19}$$

  where n_i, n_e ion or electron density, Z_i the charge number of the deflecting charge and T is the temperature below which the energy is insufficient to emit a photon (frequency ν) in the X-ray range ($kT = \hbar\nu$).
- Synchrotron radiation: electrons with very high velocities are accelerated along magnetic field lines. High energy electromagnetic waves are emitted tangential to the direction of motion.
- Non-thermal bremsstrahlung: electrons with very high energy, no Maxwell distribution.

Coronal Holes Almost always to be observed at the poles of the sun ; they appear dark in X-ray light, the gas density (4×10^{14} electrons m^{-3}) as well as the temperature ($\approx 1 \times 10^6$ K) are lower than in the surrounding area. The expansion is about 700 to 900 $\times$ 10^6 m. The magnetic fields in the coronal holes are open and thus charged particles can escape at high speed; this is the high speed solar wind. Before the minimum of the activity cycle they cover the poles, near the maximum the polar holes shrink, and near the solar equator smaller holes appear.

Other phenomena of the corona are arcs of active regions ("active region loops"), which have an extent of about 10^7 m, temperatures of $2 - 4 \times 10^6$ K and an electron density of $1 - 7 \times 10^{15}$ m^{-3} as well as X-ray bright points whose extent is $5 - 20 \times 10^6$ m, and T = 2.5×10^6 K and $\rho_e = 1.4 \times 10^{16}\,\mathrm{m}^{-3}$.

At the time of the sunspot maximum, there are many bright coronal arcs *(loops),* at the time of the minimum the Sun appears very faint in X-ray light.

In the chromosphere and the corona the plasma follows the magnetic field lines because of the low density.

7.4 The Space-Weather-Solar-Terrestrial Relations

We have discussed numerous phenomena on the Sun or in its atmosphere, where energetic short-wave radiation or particles are released.

Under the term space weather we summarize their effects on the physics of the Earth and near-Earth space, or in general their influence on the planets.

In the solar system these processes can be studied in detail and they are also of great importance in clarifying the question of habitability of Exoplanets.

7.4.1 The Solar Activity Cycle

Sunspot counts are among the oldest scientific records ever. After the first telescopic observations in 1610 by Galileo and others, interest in sunspots waned. The cause, as we now know, was the fact that there were almost no sunspots, especially between 1645 and 1715 → Maunder Minimum.

The German amateur astronomer *Samuel Heinrich Schwabe* (1789–1875) wanted to find planets within Mercury's orbit, so he observed sunspots very carefully. He did not discover an intramercurial planet, but he did discover the eleven-year sunspot cycle. The Swiss astronomer *Rudolf Wolf* (1816−1893) then introduced the *Sunspot relative number R* ("Zurich number"). Today the relative number R is defined as the mean of observations from different observatories,[5] and one forms monthly averages. The Greenwich Heliophysical Observatory made records from 1874 to 1976, then the Debrecen Heliophysical Observatory.

With the *Sunspot cycle* other solar activity phenomena also change, such as the frequency of flares and CMEs.

[5] SIDC Sunspot number, Solar Influences Data Center, Brussels.

- Variation of CMEs: 1/day at minimum–6/day at maximum
- Solar wind

  (a) Minimum: fast component (800 km/s) emitted almost all over the Sun, slow component (400 km/s) in low latitude regions.
  (b) Maximum: slow component becomes dominant; greater symmetry.

- Flares: the number of M and X flares, N_M resp. N_X, is correlated with the *sunspot relative number* R, and one finds the following approximate formula:

$$N_M = 2.86R \qquad N_X = 0.23R \tag{7.20}$$

  Besides the variation with the activity cycle, there appear to be other cycles of flare activity with periods of multiples of 24 days.

Other longe periods of solar activity are the *Gleissberg cycle* (about 90 years) as well as the 22-year magnetic Cycle *(Hale cycle).*

7.4.2 Time Series, Period Analysis

Such periods can be analyzed by means of a *power spectrum* of relative numbers. The power spectrum of a time series is essentially the square of its Fourier transform (Chap. 17). Let us take a sine-function. This has a period, and the associated power spectrum therefore has one *peak*. For a function with two periods, two peaks are found, and so on. From the individual peaks in the power spectrum one can therefore conclude on periods of a signal.

There are numerous programs for data analysis in the field of astronomy, which can be downloaded from the internet. Especially widespread in the field of professional astrophysics are IRAF, MIDAS, ANA and of course the programming language Python, in which there are numerous ready-made astronomy packages. These are freely downloadable without license fees. IDL has a fee, but is very often used in the field of solar physics; a demo version, which runs for about eight minutes without restrictions, can also be obtained from the Internet. All mentioned programs work with a PC under Windows, Linux or MacOS. As a good exercise try to download such a program and perform experiments with power spectra.

To clarify the question whether the parts of the power spectrum at high frequencies are periodic or not, one examines the underlying attractor. An attractor in the *phase space* is a subspace of the phase space when, if $t \to \infty$, is taken. One uses the correlation integral to determine the *fractal dimension* of this attractor. A high fractal dimension means *Turbulence,* Chaos. Periodic or multiply periodic systems have an integer dimension, the value of which depends on the number of modes. If one has a low fractal dimension, then

the system can be described with a few ordinary differential equations. Suppose the data are given as time series:

$$x(t_1), \ldots, x(t_n)$$
$$x(t_1 + \Delta t), \ldots, x(t_N + \Delta t)$$
$$x(t_1 + (d-1)\Delta t), \ldots., x(t_N + (d-1)\Delta t)$$

Let $x_1 = [x(t_i), x(t_i + \Delta t), \ldots, x(t_i + (d-1)\Delta t)]$ a be a d-dimensional vector describing a point in the d-dimensional space. So we can reconstruct an attractor from a scalar time series in this way, from a single variable. The real attractor, which has generated this data sequence, is of course embedding this d-dimensional attractor, if $d \to \infty$. Therefore one determines $|x_i - x_j|$ for $d = 1$ and calculate the correlation integral of q-th order $C^{(q)}_{d=1}(r)$. Then one increases the dimension of the artificial phase space and calculates $C^{(q)}_{d=2}(r)$. This is repeated until of increase of the correlation integral does not change any more. The Embedding theorem from *Takens* says that $d \geq 2n + 1$ is sufficient, where n is the actual but unknown dimension of the attractor.

This shows that one can arrive at a complete description of a physical system using a time series.

7.4.3 The Solar Irradiance

Is the brightness of the Sun changing, and if so, what effect might this have on the Earth's climate?

Since 1979 the *solar irradiance* has been measured by satellites (ACRIM, ERBE, SOHO, . . .). In principle, there are several components of its change, probably on different time scales:

$$\frac{\Delta S_\odot}{S_\odot} = \frac{\Delta S_S}{S_\odot} + \frac{\Delta S_F}{S_\odot} + \frac{\Delta S_N}{S_\odot} + \frac{\Delta S_{\mathrm{DO}}}{S_\odot} + \frac{\Delta S_{\mathrm{NM}}}{S_\odot} \tag{7.21}$$

Thus, the solar irradiance changes go back to:

- ΔS_S Spots;
- ΔS_F flares;
- ΔS_N network, this is seen well in Ca light; it coincides with the *Supergranulation cells* (about 30,000 km diameter of each cell);
- ΔS_{DO} caused by deep magnetic fields; these cause disturbances in the heat transport at the base of the *Convection zone* and could show up as brightenings or darkenings at the surface;
- ΔS_{NM} non-magnetic origin.

The Maunder Minimum

The American astronomer *Douglass* studied tree rings on felled trees around 1900 and found that they had a specific pattern that was repeated at eleven-year intervals. Between 1645 and 1715 this periodicity disappeared. The English astronomer *Maunder* sent in 1922 Douglass a letter stating that virtually no sunspots were seen at that very period. Climate records from this period revealed what is known as the Little Ice Age in Europe. That gives you the context:

> High solar activity → global temperature increase on Earth.

Since sunspots are more than 1000 K cooler than the surrounding photosphere, this at first seems like a contradiction. Less energy is emitted in sunspots, but this radiation deficit is overcompensated by enhanced radiation in the bright and hot flare regions.

A few years later *Eddy* found the connection between solar activity and the ^{14}C-Concentrations in tree rings. The sun emits electrically charged particles. But energetic particles also reach us from sources outside the solar system (supernova explosions, the nucleus of the galaxy, etc.). If the earth had no magnetic field, these particles would hit the earth's surface unhindered.

We are doubly protected from cosmic ray particles:

- *Earth's magnetosphere* mainly protects us from cosmic ray particles, rays coming from the sun itself.
- The *magnetic field of the Sun* extends into interplanetary space, as do solar wind particles in this space, which is called the *heliosphere*. The *Heliopause* is located at about 100 AU. In the area of the *Termination Shock* the solar wind particles are decelerated from supersonic velocity of the particles to a velocity below the local sound velocity of the plasma, i.e. from about 350 km/s to 150 km/s. The medium is compressed, heating occurs. The medium compresses, heating occurs. Behind the termination shock is the *heliosheath,* which has an extension of several 10 AU. At the heliopause the influence of the solar wind ends. On 30 August 2007 Voyager 2 reached[6] the Termination Shock, which was located at a distance of 84 AU. The distance of the shock is determined by the solar activity.

The *Solar Activity* is linked to the Sun's magnetic field: When activity is high, the density of the interplanetary magnetic field is higher than when solar activity is low. Therefore, when solar activity is low, more energetic fractions of cosmic rays can reach the Earth's atmosphere, where they then produce secondary particles and neutrons. When a neutron

[6] Launched on 20 August 1977.

collides with a nitrogen nucleus ^{14}N the radioactive ^{14}C isotope is produced. The plants then take this up, and you can therefore measure from the ^{14}C how much solar activity there has been. However, the whole thing only occurs with a time delay (about 20 years). Since year 1, the following minima or maxima have been found:

- Maunder minimum: 1645–1715,
- Spörer minimum: 1460–1550,
- Medieval maximum: 1100–1250 (unusually warm period, Greenland means green land),
- Medieval minimum: 640–710,
- Roman Maximum: 20–80.

In addition to the eleven-year cycle, there is probably the approximately 90-year Gleissberg cycle.

So we can use the following indicators *(proxies)* back into the past. :

- Relative numbers, spots;
- Cosmogenic isotopes: ^{14}C; Be-isotopes .
- Polar Ice Drilling : The particles cannot move crosswise to the magnetic field lines and preferentially arrive at the poles; thus the effects are greatest here.

So does the sun change our climate? Generally speaking *Climate changes* occur due to the following causes:

- *Circulation* in the Earth's atmosphere or in the oceans (cf. Gulf Stream); this is related to the movement of continental plates over the course of Earth's history (plate tectonics).
- *Mountain formation:* Mountains and plateaus have great influence on climate; on the side where winds rise you have precipitation, on the other side you have drought. Ex: Andes: On the eastern slopes you have dense forests, on the western slopes deserts.
- Changes of the *Earth's orbit:* Due to the interference of the other planets, the eccentricity of the Earth's orbit changes by 6% in a cycle of 100,000 years. The tilt of the Earth's axis changes by about 3° with a period of 41,000 Years.
- *Greenhouse Effect:* Since the beginning of industrialization around 1750, the CO_2-content in the earth's atmosphere increased from 280 ppm to 360 ppm. But not only the CO_2 is responsible for the greenhouse effect, but also the methane content, which has more than doubled. This greenhouse effect could raise the global temperature between 1 °C and 3.5 °C (associated with a rise in sea level of 50 cm, which would currently affect 100 million people).

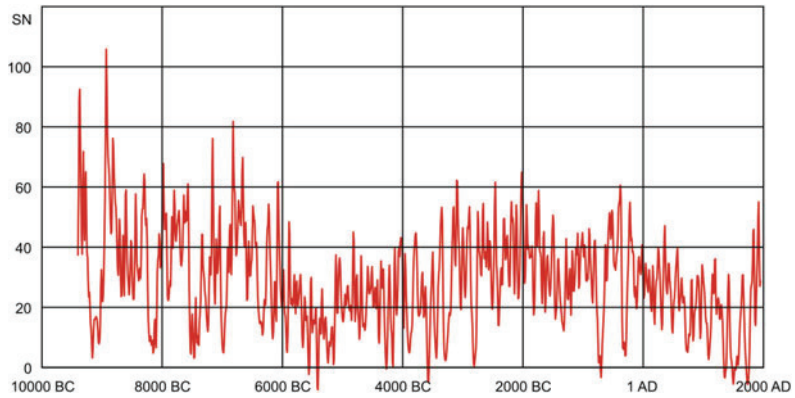

Fig. 7.25 Reconstruction of the sunspot relative numbers. It can be seen that solar activity has been increasing again since 1900 and that there are long periods of varying solar activity (according to Solanki)

- Solar activity: at the time of maximum, the Sun is about 0.1% brighter, corresponding to 1.3 W/m^2. Studies have shown that a 0.1% change in solar radiation leads to a global temperature change of 0.2 °C.

Since solar activity has been increasing overall since 1900, some of the temperature increase could be caused by the sun. Note here the increase since 1900 in Fig. 7.25. However, the observed increase in solar activity since 1900 is only sufficient to explain the Earth's temperature increase up to about 1970, i.e., the presently observed rapid temperature increase since 1970 is certainly due to the *anthropogenic greenhouse effect* (CO_2-increase).

So in the long run, the sun certainly determines our climate.

Space Weather

The Earth's magnetic field and the effects of the solar wind have already been discussed in Sect. 6.3.3 also the effects of incoming particles (Van Allen belt, auroras).

Changes in solar activity can influence currents in the Earth's atmospherere *(GIC, geomagnetically induced currents).* These can cause surges in overhead power lines and thus destroy transformers, paralyzing the power supply to large areas (this occurred in Quebec in 1989). Geomagnetic activity is described by the *K*-, *Ap* and *Kp index*.

X-rays are produced during the eruption of a solar flare. This increases the ionization in the Earth's atmosphere, the ion density as well as the electron density increase. A sudden ionospheric perturbation occurs, *sudden ionospheric disturbance, SID*). Radio signals are already absorbed in the D layer of the atmosphere and radio communication is interrupted. On the other hand, at the maximum of solar activity, higher frequencies are reflected in the Earth's atmosphere, increasing the range for RF transmissions. High-energy particles from the solar wind cause the effect of bit reversal in computers, resulting in incorrect

commands; satellites can get out of control. The Earth's upper atmosphere is heated by increased shortwave radiation during a flare, it expands, and near-Earth satellites can thus be severely slowed and crash to the surface. Solar flares also pose a significant radiation threat to astronauts.

That's why people all over the world are now trying to predict what is known as Space Weather. When and with which intensity is the outbreak of a solar flare or CME to be expected? What precautionary measures can be taken?

7.5 Helioseismology

In the year 1962 it was discovered that the upper photosphere oscillates up and down with a period of 5 min *(5 minute oscillation.)* In reality there is a superposition of many oscillations. Waves wander into sun-inside, where temperature is much higher, and there waves are reflected upward again (Fig. 7.26). The reflection at the solar surface occurs due to the extreme decrease in density and temperature.

The sun therefore oscillates like a *(resonant cavity).* By studying different frequencies, one can therefore detect different layers.

The propagation speed of sound waves is

$$v = \sqrt{\kappa \Re T/M} \tag{7.22}$$

$\kappa = c_p/c_v$, $\Re = 8.31\,\mathrm{J/(molK)}$.

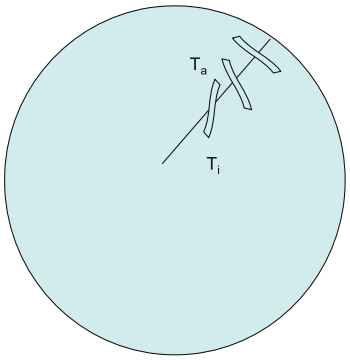

Fig. 7.26 Propagation of a wave front into the solar interior. Because of $T_i > T_a$ the speed of sound is also greater there, and the wave front is bent upwards

Table 7.2 Absorption lines and oscillations observed in the centres of the lines

Line [nm]	Element [nm]	Period [s]	v [km/s]
39.37	Ca II	150	2.00
656.28	H_α	180	1.34
516.87	Ni I	300	0.31

The most pronounced is the 5-minute oscillation. The higher the spectral lines originate in the solar atmosphere (photosphere), the greater the amplitude of the oscillation. In addition, the period (frequency) changes with altitude (cf. Table 7.2).

7.5.1 Mathematical Description

As will be shown in more detail in the chapter on stellar structure, one can start from the equations of an equilibrium state of a star: In such a state of equilibrium one has $\rho = \rho_0(r)$, $P = P_0(r)$, $\Phi = \Phi_0(r)$, $\mathbf{v} = 0$ i.e. density, pressure and gravitational potential depend only on the distance from the center r . If Φ the gravitational potential, $\mathbf{v}$ the velocity of a fluid, Γ the ratio of the specific heats, then holds:

$$\rho \frac{d\mathbf{v}}{dt} = -\operatorname{grad} P + \rho \operatorname{grad} \Phi \tag{7.23}$$

$$\frac{d\rho}{dt} + \rho \operatorname{div} \mathbf{v} = 0 \tag{7.24}$$

$$\frac{1}{P}\frac{dP}{dt} = \frac{\Gamma}{\rho}\frac{d\rho}{dt} \tag{7.25}$$

$$\nabla^2 \Phi = -4\pi G\rho \tag{7.26}$$

The first equation is the equation of motion, the second the equation of continuity, the third the adiabatic equation, and the fourth the Poisson's Equation. Now suppose one can take any variable f in the form: $f = f_0 + f_1$ with

$$f_1 = \operatorname{Re}\left[\exp(i\omega_{\mathrm{nl}}t)\bar{f}_1(r)Y_l^m(\Theta, \phi)\right] \tag{7.27}$$

where Re is the real part and $Y_l^{\mathrm{m}}(\Theta, \phi)$ the spherical function.

$$Y_l^m(\Theta, \phi) = P_l^m(\Theta)\exp(im\phi), \tag{7.28}$$

where $P_l^{\mathrm{m}}(\Theta)$ is the associated Legendre function. If a star is spherical, then its oscillation frequency does not depend on m. Only when the deviations from the spherical shape are small do the above formulas hold. In the case of the sun one has different m-modes with different frequencies. The oscillation frequency depends on l and n. The numbers n, l,

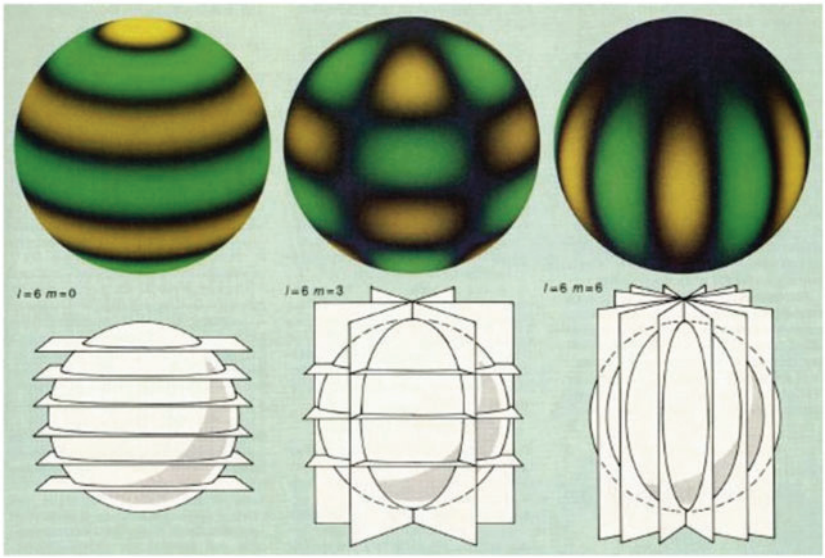

Fig. 7.27 Oscillation modes of the sun

m indicate how often the function f_1 in the radial as well as in the θ- and ϕ-direction vanishes. Furthermore $|m| \leq l$ (Fig. 7.27).

In solving the system of equations one has the problem of boundary conditions. At the center of a star, everything is clear. But stars do not have a defined surface. One could simply assume that all waves are reflected back at the surface of the Sun (since there, by definition P, ρ disappear). In reality, however, some energy is transferred outward into the solar atmosphere.

If the changes in gravitational potential due to the oscillations are negligible, we have a 2nd order DE (differential equation). This is sufficient for most perturbations: certain parts of the star move outward, other parts move inward. In the case of radial oscillations only, a perturbation vector ξ may be introduced as:

$$\mathbf{v} = \frac{d\xi}{dt} \tag{7.29}$$

and further:

$$\Psi = c_s^2 \rho_0^{1/2} \mathrm{div}\, \xi \tag{7.30}$$

Thereby c_s is the speed of sound in the undisturbed star:

$$c_s = (\Gamma P_0/\rho_0)^{1/2} \tag{7.31}$$

The equation for the radial part is then simply:

$$\frac{d^2\Psi}{dr^2} = -\frac{1}{c_s^2}\left[\omega^2 - \omega_c^2 - S_l^2\left[1 - \frac{N^2}{\omega^2}\right]\right]\Psi \tag{7.32}$$

We therefore have, in addition to ω the three frequencies:

- ω_c *acoustic cutoff frequency*

$$\omega_c^2 = \left(c_s^2/4H_p^2\right)(1 - 2dH_p/dr) \tag{7.33}$$

- S_l *Lamb frequency*

$$S_l = c_s[l(l+1)]^{1/2}/r \tag{7.34}$$

- *N Brunt-Väissälä frequency:*

$$N^2 = g\left[\frac{1}{\Gamma P}\frac{dP}{dr} - \frac{1}{\rho}\frac{d\rho}{dr}\right] \tag{7.35}$$

where the pressure scale height is given by:

$$H_p = |\rho/(d\rho/dr)| \tag{7.36}$$

and

$$g = GM/r^2 \tag{7.37}$$

It can be seen that: S_l is always real, ω_c, N can become imaginary. If N^2 becomes imaginary, one has convection (chapter about star-construction!).

Equation 7.32 can be written as:

$$\frac{d^2\Psi}{dr^2} + K_r^2\Psi = 0 \tag{7.38}$$

- $K_r^2 > 0$: behavior of solution depends on radius.
- $K_r^2 < 0$: exponential behaviour, the modes fall exponentially (*evanescent modes*).

There are two domains where K_r^2 is positive:

- High frequencies $\omega > S_l, \omega_c$: Then the pressure fluctuations become important, one speaks of p-modes.
- Low frequencies $\omega < N$: One speaks of *Gravity mdoes* (engl. *gravity modes*), *g-modes.*

S_l, ω_c, N depend on location in the sun. S_l decreases monotonously from center to surface, N becomes imaginary in the *Convection zone*. The p-modes can propagate into the solar interior up to the Lamb frequency, and at the surface they terminate at the acoustic cut off frequency. The g-modes are absorbed or reflected in the convection Zone. Therefore the p-modes can be observed more easily than the g-modes, because g-modes are exponentially attenuated in the convection zone. The p-modes of smallest order (l) penetrate deepest into the Sun. Together with the g-modes, they thus provide clues to the deep interior of the Sun.

The Sun is not strictly spherical: one must consider rotation and magnetic field. For a rotating star, the oscillation frequency depends on m, each frequency ω_{nl} thus splits into the $2\,l + 1$ frequencies ω_{nml}. From this rotational splitting, one can study how the Sun's rotational velocity changes in the interior.

7.5.2 Observational Results

The SOHO-MDI- the VIRGO instruments have been used to measure vertical velocities propagating through the Sun. With VIRGO oscillations of the solar brightness were measured. Figure 7.28 shows deviations from the mean rotation of the Sun (left) and temperature deviations in the interior of the Sun (right). A temperature increase has been detected at the transition zone between the convection zone and the radiation zone. At this zone, called *tachoclyne,* also occurs a jump in the rotation speed of the sun:

- The interior rotates slower and like a rigid body,
- the outer layers rotate faster and differential.
- Therefore, shearings occur; these shearings cause the solar dynamo.

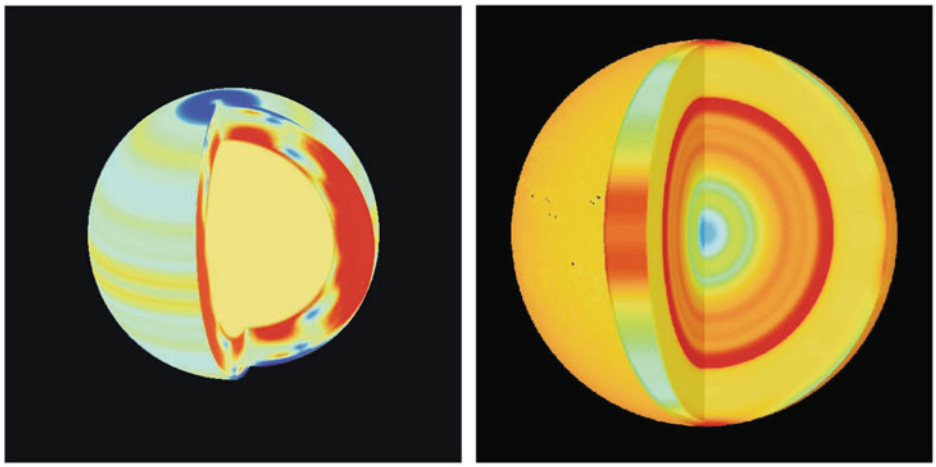

Fig. 7.28 Temperature deviations in the Sun (right), deviations from the mean solar rotation (left) (NASA/ESA SOHO)

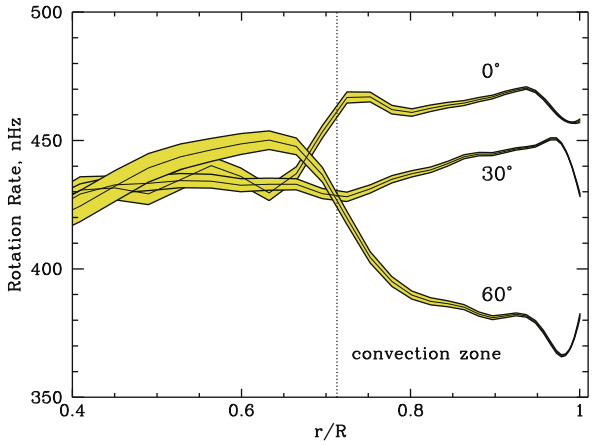

Fig. 7.29 Course of solar rotation at the surface (differential, at $r/R = 1$); from the so-called tachoclyne the Sun rotates like a rigid body (SOHO-MDI, ESA/NASA)

The zone in the centre of the sun, where the nuclear reactions take place, indicates that this is 0.1% cooler than the assumed 15 million K. So possibly the sun is producing less energy today.

With the *Michelson Doppler Imager* (MDI) on board SOHO, the rotation of the Sun has also been measured. In Fig. 7.28, left, dark means faster rotation than average, light means smaller. A band-like structure is found that rotates slightly faster than the surrounding area, and this structure extends about 20 000 km into the depths. Sunspots form at the edges of these bands.

In Fig. 7.29 results of SOHO-MDI observations are reproduced, showing the pattern of rotation as a function of distance from the center of the Sun. At the solar surface ($r/R = 1$) one can clearly see the differential rotation, i.e. higher frequency at the equator than e.g. at 60° heliographic latitude. At the transition layer between the convection zone and the radiation zone (tachoclyne) the solar rotation changes into a rigid rotation. This results in strong shear in the tachoclyne region.

SOHO/VIRGO was used to measure the brightnesses of the Sun at various wavelengths. The data can then be transformed into Fourier space and the *power spectrum* calculate. This shows over which frequencies a signal is distributed. In the data one can see the p-modes as well as the granulation and supergranulation.

Since February 2010 the NASA mission SDO (Solar Dynamics Observatory) has been sending data. The EVE (Extreme UV Variability Experiment) can be used to obtain images of the Sun every 10 s in the range 0.1 to 105 nm. With HMI (Helioseismic and Magnetic Imager) one can determine the variation of the magnetic field, and with AIA (Atmospheric Imaging Assembly) one gets an image every 10 s in nine different UV-ranges and at visible range.

Objective of SDO: Evolution and formation of activity regions on the Sun.

7.6 Magnetohydrodynamics of the Sun

The *magnetohydrodynamics (MHD)* studies the connection between magnetic fields and plasma motions.

We give a brief overview with applications to solar physics.

7.6.1 Maxwell's Equations

We want to give here briefly the basic equations. Starting point are the Maxwell's equations:

$$\nabla \times \mathbf{B} = \mu \mathbf{j} + \frac{1}{c^2} \frac{\partial \mathbf{E}}{\partial t} \tag{7.39}$$

$$\nabla . \mathbf{B} = 0 \tag{7.40}$$

$$\nabla \times \mathbf{E} = - \frac{\partial \mathbf{B}}{\partial t} \tag{7.41}$$

$$\nabla . \mathbf{E} = \frac{\rho_e}{\epsilon} \tag{7.42}$$

B—magnetic induction, **E**—electric field strength, **j**—electric current density, ρ_e—electric charge density, ϵ—dielectric constant, μ—magnetic permeability.

In astrophysics we assume $\epsilon,\ \mu$ as constant and $\epsilon \approx \epsilon_0 = 8.854 \times 10^{-12}\,\mathrm{F\,m^{-1}},\ \mu \approx \mu_0 = 4\pi \times 10^{-7}\,\mathrm{H\,m^{-1}}$. Further it is to be noted that the properties of the plasma are isotropic except for one exception: The *thermal heat conduction* κ is preferentially along the magnetic field lines!

The simplified *Ohm's law* is:

$$\mathbf{j} = \sigma (\mathbf{E} + \mathbf{v} \times \mathbf{B}) \tag{7.43}$$

In the case one has a plasma consisting of electrons and only one type of ions, then:

$$\mathbf{j} = n_i Z_i e \mathbf{v_i} - n_e e \mathbf{v}_e \tag{7.44}$$

$$\rho_E = n_i Z_i e - n_e e \tag{7.45}$$

n_i—Number of ions, n_e—number of electrons, $\mathbf{v}_e$—velocity of the electrons. $Z_i e$—charge of the ion, -e—charge of the electron.

In general, in almost all astrophysical cases one assumes that magnetic fields are permanent and electric fields can be neglected.

There are no magnetic monopoles ($\nabla \mathbf{B} = 0$). Electric fields are produced by changing magnetic fields. Magnetic fields, which are generated by the displacement

current $1/c^2 \partial \mathbf{E}/\partial t$ are negligible. If one has a high current density $\mathbf{j}$ then magnetic fields are generated (cf. 1st Maxwell equation). For a stationary medium holds:

$$\nabla \times B = \mu \mathbf{j} \tag{7.46}$$

$$\nabla \times \mathbf{E} = -\partial \mathbf{B}/\partial t \tag{7.47}$$

$$\mathbf{j} = \sigma \mathbf{E} \tag{7.48}$$

This gives the following equation insert (7.48 into 7.46 and then form the vector product):

$$\frac{\partial \mathbf{B}}{\partial t} + \frac{1}{\mu_0 \sigma} \nabla \times \nabla \times \mathbf{B} = 0 \tag{7.49}$$

and because of $\nabla \times \nabla \times \mathbf{B} = \text{grad}\,\text{div}\mathbf{B} - \nabla^2 \mathbf{B}$ and $\text{div}\mathbf{B} = 0$:

$$\frac{\partial \mathbf{B}}{\partial t} = \frac{1}{\mu_0 \sigma} \nabla^2 \mathbf{B} \tag{7.50}$$

In Cartesian coordinates, one then obtains, e.g.:

$$\frac{\partial \mathbf{B_x}}{\partial t} = \frac{1}{\mu_0 \sigma} \left[\frac{\partial^2 \mathbf{B_x}}{\partial x^2} + \frac{\partial^2 \mathbf{B_x}}{\partial y^2} + \frac{\partial^2 \mathbf{B_x}}{\partial z^2} \right] \tag{7.51}$$

The solution of this equation indicates how magnetic fields decay, along with the currents they produce. One can estimate the approximate decay time:

$$\tau_D = \mu_0 \sigma L^2 \tag{7.52}$$

$L \ldots$ within this distance the currents should change. From the DG 7.51 it also follows that if at time $t = 0$ a field of the form $B_x = B_0 \exp(iky)$ is given, the equation is:

$$B_x = B_0 \exp(iky) \exp(-k^2 t/\mu_0 \sigma) \tag{7.53}$$

$\lambda = 2\pi k$ Is the wavelength of the spatial change of the field.

In the laboratory, the currents decay very quickly because the material has a low expansion. In stars, one has a high conductivity as well as a large L. That is why there is a fossil field here, which comes from the time of star formation.

7.6.2 Induction Equation

With the *induction equation* we describe how a magnetic field develops with plasma movements.

From 7.43 one eliminates $\mathbf{E} = \mathbf{j}/\sigma - (\mathbf{v} \times \mathbf{B})/\sigma$. Thus, Eq. 7.41 to:

$$\nabla \times \frac{1}{\sigma}[\mathbf{j} - \mathbf{v} \times \mathbf{B}] = -\frac{\partial \mathbf{B}}{\partial t}$$

Since the velocities under consideration are small compared to c, one can use in 7.39 the term $1/c^2(\partial \mathbf{E}/\partial t)$ omit and $\nabla \times \mathbf{B} = \mu_0 \mathbf{j}$ (*induction equation*):

$$\frac{\partial \mathbf{B}}{\partial t} = \nabla \times (\mathbf{v} \times \mathbf{B}) + \eta_0 \nabla^2 \mathbf{B} \tag{7.54}$$

where $\eta_0 = (\mu_0 \sigma)^{-1}$ is the magnetic diffusivity, σ the electrical conductivity.

- The ratio $\nabla \times (\mathbf{v} \times \mathbf{B})/(\eta_0 \nabla^2 \mathbf{B})$ is known as *magnetic Reynolds number* $R_m = l_0 v_0/\eta_0$.
- Diffusion $\sim \eta_0 \nabla^2 \mathbf{B}$.
- $R_m \gg 1$ then one can neglect the diffusion $\rightarrow$ magnetic field is frozen in the plasma and one can also write $\mathbf{E} = -\mathbf{v} \times \mathbf{B}$.

7.6.3 Plasma Equations

Now we can write down how plasma moves. Here the total derivative with respect to time is composed of

- Space point fixed, time derivative, thus $\partial/\partial t$
- Time point fixed, difference of velocity at different space points: $\mathbf{v}\nabla$.

  Therefore is the *substantial derivative:*

$$\frac{D}{Dt} = \frac{\partial}{\partial t} + \mathbf{v}\nabla \tag{7.55}$$

One has the *Mass continuity:*

$$\frac{D\rho}{Dt} + \rho \nabla \mathbf{v} = 0 \tag{7.56}$$

The *Lorentz force* is given by :

$$F_L \approx \mathbf{j} \times \mathbf{B} \tag{7.57}$$

The *Equation of motion* of plasma becomes:

$$\rho \frac{D\mathbf{v}}{Dt} = -\nabla p + \mathbf{j} \times \mathbf{B} + \rho \mathbf{g} + \rho \nu \nabla^2 \mathbf{v} \tag{7.58}$$

and thereby is: ∇p a pressure gradient, $\mathbf{j} \times \mathbf{B}$ the Lorentz force, $\rho\mathbf{g}$ the force of gravity (gravitational acceleration $g_\odot$ =264 m s^{-2}), $\rho\nu\nabla^2\mathbf{v}$ viscosity.

Furthermore, one still needs an energy equation. Into this goes the thermal conductivity. For the corona, note:

$$\frac{\kappa_\perp}{\kappa_\parallel} \approx 10^{-12} \tag{7.59}$$

I.e. heat conduction occurs mainly along the field lines.

The magnetic force on a moving charge ($\mathbf{v}$) is

$$\mathbf{F} = q\mathbf{v} \times \mathbf{B} \tag{7.60}$$

If one has a magnetic field in a conducting fluid, then the force exerted by it is:

$$\mathbf{F_{mag}} = \mathbf{j} \times \mathbf{B} = \frac{1}{\mu_0}\nabla \times (\mathbf{B} \times \mathbf{B}) \tag{7.61}$$

(here we have Eq. 7.46 used). This can be written as:

$$\mathbf{F_{mag}} = -\text{grad}\,(B^2/2\mu_0) + \mathbf{B}\nabla\mathbf{B}/\mu_0 \tag{7.62}$$

The two right-hand terms mean:

1. Gradient of an isotropic pressure,
2. Stress along the field lines.

Therefore, if one has a *magnetic flux tube* with the pressure P_i and if the pressure in the surrounding medium is P_o, then the equilibrium is:

$$P_o = P_i + \frac{B^2}{2\mu_0} \tag{7.63}$$

$P = \Re\rho T/\mu$... gas pressure. If holds $T_i = T_o$ then it follows:

$$\rho_i < \rho_a \tag{7.64}$$

So our flux tube is lighter than the surroundings and rises upwards, *magnetic buoyancy.*

There is a connection between the plasma and the fields:

- The plasma determines the motion of the magnetic fields (photosphere of the Sun); we speak of frozen field lines.

- The magnetic field determines the motion of the plasma (when the density of the plasma is low, e.g. corona).

The speed of sound in a gas is:

$$c_s = \sqrt{\gamma P/\rho} \tag{7.65}$$

Hydromagnetic waves propagate with the *Alfvén velocity*:

$$c_H = \sqrt{B^2/\mu_0 \rho} \tag{7.66}$$

7.6.4 Motion of a Particle in a Magnetic Field

Now let's consider the motion of a single charged particle in an electromagnetic field; q...particle charge; the equation of motion (Lorentz force) reads:

$$m\frac{d\mathbf{v}}{dt} = q(\mathbf{E} + \mathbf{v} \times \mathbf{B}) \tag{7.67}$$

If $\mathbf{b}$ is a unit vector, then we decompose the fields into two components:

$$\mathbf{B_0} = B_0\mathbf{b} \tag{7.68}$$

$$\mathbf{E} = E_\parallel \mathbf{b} + \mathbf{E}_\perp \tag{7.69}$$

$$\mathbf{v} = v_\parallel \mathbf{b} + \mathbf{v}_\perp \tag{7.70}$$

Since $\mathbf{v} \times \mathbf{B_0} = B_0(\mathbf{v}_\perp \times \mathbf{b})$ perpendicular to $\mathbf{b}$, we get from the equation of motion above:

$$m\frac{dv_\parallel}{dt} = qE_\parallel \tag{7.71}$$

$$m\frac{dv_\perp}{dt} = q[\mathbf{E}_\perp + B_0(\mathbf{v}_\perp \times \mathbf{b})] \tag{7.72}$$

From the first equation, we immediately have:

$$v_\parallel = (qE_\parallel/m)t + v_{\parallel 0} \tag{7.73}$$

So: the motion of the particles is parallel to the field lines. Particles of different charges q move in opposite directions! The solution of the second equation results in a circular motion around $\mathbf{b}$ with the Frequency $|q|B_0/m$ and the *Gyration radius* $r_g = mv_{\perp 0}/|q|B$.

Example
An electron has the Gyration frequency $1.8 \times 10^{11}(B/\mathrm{T})\,\mathrm{Hz}$ and a gyration radius of $6 \times 10^{-9}(v_{\perp 0}/\mathrm{km\,s^{-1}})/(B/T)\,\mathrm{m}$.
If there is an additional non-magnetic force **F** normal to **B** then the result is a Drift velocity of:

$$\mathbf{v}_{\mathrm{DF}} = \mathbf{F} \times \mathbf{B}/qB^2 \tag{7.74}$$

If $\mathbf{F} = m\mathbf{g}$, i.e. gravitation, then one sees that the *Drift velocity* is proportional to the ratio m/q, i.e. the *Ion drift* is much larger than *electron drift.* This drift of particles in different directions produces currents.
Now to understand understand Flares, one needs the concept of *magnetic reconnection.* of Suppose two oppositely directed magnetic field lines are brought closer together by plasma motion. When the field lines approach each other, the gradient becomes large, and between them there is a neutral point where the field disappears. Dissipation now causes reconnection of the field lines, and the plasma then moves in the opposite direction to the original motion. This causes a release of magnetic energy in the vicinity of the neutral point.

Solar Dynamo
The activity cycle of the sun can be explained with the *dynamo theory*. The starting point is a poloidal field extending from pole to pole along the z-axis. Due to the differential rotation of the sun (rotation is faster at the equator than at the poles, ω-Effect), the magnetic field lines are wound up in the toroidal direction, and a toroidal field is formed (Fig. 7.30). From the toroidal field, Coriolis force and convection again produce a poloidal component (α-effect).

For the mathematical description the principle of *mean field electrodynamics* is used: The magnetic induction and the velocity are divided into a mean and a fluctuating part written:

$$\mathbf{B} = \mathbf{B_0} + \mathbf{b}, \qquad \mathbf{v} = \mathbf{v_0} + \mathbf{u} \tag{7.75}$$

The average magnitudes $\mathbf{B_0}$, $\mathbf{v_0}$ change only slowly with time. **u** let be given, **b** shall be found: Put above approach and get for the mean and fluctuating part:

$$\frac{\partial \mathbf{B_0}}{\partial t} = \nabla \times (\mathbf{v_0} \times \mathbf{B_0}) + \nabla \times < \mathbf{u} \times \mathbf{b} > + \eta \nabla^2 \mathbf{B_0} \tag{7.76}$$

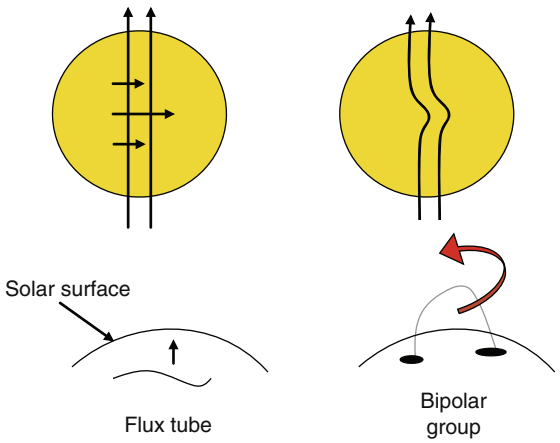

Fig. 7.30 Principle of the solar dynamo. The ω-effect is the winding up of the field lines at the equator due to differential rotation. A poloidal field is transformed into a toroidal one. Flux tubes rise from the interior of the sun to the surface due to magnetic buoyancy and pierce the photosphere forming a bipolar group. Due to the α effect (twisting of the field lines by convection and Coriolis force) the toroidal field again becomes an inverted poloidal field

and:

$$\frac{\partial \mathbf{b}}{\partial t} = \nabla \times (\mathbf{b_0} \times \mathbf{b}) + \nabla \times (\mathbf{u} \times \mathbf{B_0}) + \nabla \times (\mathbf{u} \times \mathbf{b} - < \mathbf{u} \times \mathbf{b} >) + \eta \nabla^2 \mathbf{B} \tag{7.77}$$

$\eta = 1/\mu_0 \sigma$—magnetic resistance, <>—mean value.

Corona Heating

The following energy densities can be given for the corona:

- Kinetic energy

$$E_{\text{kin}} = \frac{1}{2} m_p n v^2 \tag{7.78}$$

  with $n = 10^{15}\,\text{m}^{-3}$ as particle density and $v = 1000\,\text{km/s}$ one obtains for the energy density $8 \times 10^{-4}\,\text{J m}^{-3}$.
- Thermal energy

$$E_{\text{therm}} = nkT \tag{7.79}$$

  with $T = 10^6\,\text{K}$ one obtains for the energy density $1 \times 10^{-2}\,\text{J m}^{-3}$

- Potential energy

$$E_{\text{pot}} = nm_p gh \tag{7.80}$$

m_p mass of the proton, $h = 10^5$ km The energy density is $5 \times 10^{-2}\,\text{J}\,\text{m}^{-3}$

- Magnetic energy:

$$E_{\text{magn}} = \frac{B^2}{2\mu_0} \tag{7.81}$$

with 10^{-2} T the energy density is $40\,\text{J}\,m^{-3}$. The magnetic energy dominates the corona.

Finally, we address the problem of *Heating* of the corona.

- Earlier idea: the solar surface (lower photosphere) is convective, sound waves are generated there; these have an energy density of:

$$\frac{1}{2}\rho v^2 \tag{7.82}$$

Thereby ρ the density of matter and v is the velocity of the particles carrying the waves. This energy is conserved as the waves propagate upward. As the wave moves into a region of lower density (the density naturally decreases from the photosphere into the corona), the wave will increase in amplitude. Eventually it will become a shock wave, releasing its energy into the surrounding medium.

- MHD waves: Energy dissipation as soon as the *Alfvén velocity* c_H is greater than the local speed of sound c_s is. Another possibility would be magnetic reconnection. Magnetic field lines often enter the corona in large arcs, their foot points migrating by convection. From the corona holes, which correspond to open magnetic field configurations, the solar wind flows away. In the ecliptic plane, the typical velocity is 400 to 500 km/s. Ulysses was a space mission in which a probe was to study primarily the poles of the Sun. To do this, the probe was first sent to Jupiter, where it received the necessary *gravity assist* Got to get out of the ecliptic plane. To the great surprise of solar physicists, it was found in 1995 (minimum solar activity) that there are also coronal holes at the poles from which the solar wind flows off at up to 700 km/s.
- Spicules:

(a) Type I; amounts to $T < 100{,}000$ K, then cool plasma sinks back down,
(b) type II; amounts to $T > 1{,}000{,}000$ K, then hot plasma rises upward into the higher corona. This has been established with HINODE satellite observations. In most spicules, plasma heating occurs only up to about 100,000 K, but there are some where the temperature rises to much higher values.

Heating causes the corona to expand → Solar wind.

7.7 Further Literature

We give a small selection of recommended further reading.
An Introduction to Waves and Oscillations in the Sun, S. Narayanan, Springer, 2012
Magnetohydrodynamics of the Sun, E. Priest, Cambridge Univ. Press, 2017
The Sun from Space, K. Lang, Springer, 2008
The Sun, M. Stix, Springer, 2004
The Sun and Space Weather, A. Hanslmeier, 2006

Tasks

7.1 Compare the solar radiation on Venus with that on Earth!

Solution
$\frac{F_{\text{Venus}}}{F_{\text{Earth}}} = \frac{E_{\text{Sun}}}{4\pi d^2_{\text{Sun-Venus}}} / \frac{E_{\text{Sun}}}{4\pi d^2_{\text{Sun-Earth}}} = \frac{1^2}{0.72^2} = 1.9$

7.2 The sun loses about $3 \times 10^{-14}\,\mathrm{M}_\odot/yr$. How much of this does the earth absorb?

Solution
The earth takes the fraction
$\frac{A_{\text{Earth}}}{A_{1\,AU}} = \frac{\pi R^2_{\text{Earth}}}{4\pi R^2_{1\,AU}} = \frac{(6\times10^6)^2}{4(1.5\times10^{11})^2} = 4 \times 10^{-9}$
and thus $M = 8.8 \times 10^9$ kg/day. So the captured solar wind makes the Earth heavier by almost nine billion kg per day. What simplifications have been made here?

7.3 Jupiter is about 5 times as far from the Sun as the Earth. How large does the sun appear in Jupiter's sky?

Solution
1/5 of the diameter in Earth's sky.

7.4 Determine the kinetic energy of a proton in the solar wind and compare it with the energy of a X-ray photon.

Solution
$E_{\text{kin}} = 1/2mv^2 = \frac{1}{2}(1.7 \times 10^{-27}) \times 450,000^2\,\mathrm{J} = 1.7 \times 10^{-16}\,\mathrm{J}$ (Solar wind: $v = 450$ km/s). An X-ray photon at a frequency of 10^{18} Hz has an energy of $E = h\nu = 6.626 \times 10^{-34} \times 10^{18}\,\mathrm{J} = 6.626 \times 10^{-16}\,\mathrm{J}$ Thus protons have an energy of the same order of magnitude as X-ray photons and can destroy cells, for example.

7.5 Calculate how long it takes the solar wind to reach the system Alpha Centauri ($d = 1.33$ pc) to reach.

Solution
$1.33\,\text{pc} = 3.9 \times 10^{13}\,\text{km}$ and $t = d/v = (3.9 \times 10^{13})\,\text{s}/450 = 8.7 \times 10^{10}\,\text{s} = 2700\,\text{years}$

7.6 Estimate the magnetic Reynolds number in an active region of the solar surface! Typical values are: $l_0 \approx 700\,\text{km}$, $\eta_0 = 1\,\text{m}^{-2}\,\text{s}^{-1}$, $v_0 \approx 10^4\,\text{m/s}$.

Solution
$R_m = 7 \times 10^9 \gg 1$, therefore magnetic field is frozen in the plasma.

State Variables of Stars

8

In this section we deal with the determination of the most important properties or state variables of a star: radius, temperature, mass, density, gravitational acceleration, chemical composition, magnetic field and rotation. First, we briefly review the trigonometric distance determination. Although the distance of a star is not a state variable characterizing the star itself, its knowledge is necessary for the determination of other physical parameters of stars.

8.1 Distance, Magnitudes

The apparent brightness of a star depends on its true luminosity and its distance. Thus, although the distance of a star is not a quantity characterizing the star itself, it is important for deriving other essential physical state quantities.

8.1.1 Apparent Brightness

How bright is a star? The brightness depends on:

- the true luminosity of the star,
- the distance of the star.

In antiquity the concept of *magnitude classes,* lat. *magnitudo,* was introduced. The brightest stars called 1st magnitude stars, the faintest stars just visible to the naked eye are then 6th magnitude stars.[1]

[1] Because of light pollution in big cities you can only see stars up to about 3rd magnitude.

A. Hanslmeier, *Introduction to Astronomy and Astrophysics*,
https://doi.org/10.1007/978-3-662-64637-3_8

Table 8.1 Apparent brightnesses Stars

Sun	$-26.^{m}8$
Full Moon	-12^{m}
Venus	$-4.^{m}5$
Sirius	$-1.^{m}6$
Polaris	$+2.^{m}12$
Faintest stars visible to the naked eye	$+6.^{m}0$

Note Magnitude classes in astrophysics refer to stellar brightnesses and have nothing to do with the size (diameter) of a star!
Sensory perceptions (eye, ear) are always proportional to the logarithm of the stimulus; this is known as the *Weber-Fechner law*. To accommodate both the brightness scale of ancient astronomers and Weber-Fechner law it was defined: Given are two stars with the apparent magnitudes m_1, m_2. Let the intensity of their radiation be I_1 respectively. I_2. Then:

$$m_1 - m_2 = -2{,}5 \log(I_1/I_2) \tag{8.1}$$

$$I_1/I_2 = 10^{-0{,}4(m_1 - m_2)} \tag{8.2}$$

m comes from the Latin term magnitudo. Furthermore, it was determined that for a difference of $\Delta m = 1$ the intensity ratio is 2.512. If $\Delta m = 2$ then the intensity ratio is 2.512×2.512 etc. To a $\Delta m = 5$ corresponds to an intensity ratio of 100 (2.512^5). This scale can also be used to indicate very bright objects as the sun and the moon (Table 8.1).

One can also convert the astronomical magnitudes into the usual physical values: The magnitudes depend on the spectral range—take, for example, the visual range, V, which is defined around a central wavelength of 550 nm, then the following holds: The flux at $V = 0$ is 3640 Jy, the $d\lambda/\lambda = 0.16$, where

$1\,\text{Jy} = 1.51 \times 10^7$ Photons s^{-1} m^{-2} $(d\lambda/\lambda)$.

Let's calculate how many photons arrive outside the Earth's atmosphere (a) for a star $V = 0$ and (b) $V = 20.0$.

Solution

(a) $1.51 \times 10^7 \times 0.16 \times 3640 = 8794 \times 10^6$ photons $\text{m}^{-2} \approx 10^6$ photons cm^{-2}.

(b) At a brightness of $V = 20$ holds $10^{-0.4V} = 10^{-8}$ and thus $10^{-8} \times 1.51 \times 10^7 \times 0.16 \times 3640 = 8794 \times 10^{-2}$ photons $\text{m}^{-2} \approx 10^{-2}$ photons cm^{-2}.

How do you set the zero point of the scale? This is done using the international *pole sequence,* a series of Stars around the celestial north pole.

Star magnitudes are given in magnitude classes. The larger this value, the fainter the star.

8.1.2 Distance

The annual movement of the earth around the sun leads to the *stellar parallaxes.*

A nearby star is seen at different angles against more distant background stars, so the position of a nearby star in the sky shifts slightly with a period of one year.

The main objection to the *heliocentric system* was always that such parallaxes could not be detected. Only in 1838 *Bessel* determined the parallax of the star 61 Cygni and *Struve* those from Wega. The problem lay in the accuracy of the measurement, since all stellar parallaxes are below $1''$. If a is the distance sun-earth and r the distance earth-star, then for the parallax of a star is valid

$$\pi[\text{rad}] = a/r \tag{8.3}$$

A star is located at a distance of 1 pc (1 pc = 206,265 AU), if its parallax is $1''$ is 1.

$$r[\text{pc}] = 1/\pi[''] \tag{8.4}$$

8.1.3 Absolute Brightness, Distance Modulus

As already mentioned, the *apparent magnitude m* of a star depends on the luminosity and the distance:

$$m = m(L, r) \tag{8.5}$$

The apparent brightness says nothing about the true brightness (luminosity).

Therefore one still has the term *absolute brightness, M.* The absolute brightness is understood to be the apparent magnitude that a star would possess at a unit distance of 10 pc = 32.6 light-years.

Relationship between apparent and absolute brightness:

$$m - M = 5 \log r - 5 \tag{8.6}$$

The expression

$$m - M \tag{8.7}$$

is called *Distance modulus.*

Table 8.2 Absolute magnitudes of various objects

Object	Absolute brightness
Brightest galaxies	−23
Supernova 1987 A	−15.5
Globular cluster	−10...−6
Brightest stars	−9
Sun	+4.79
Weakest stars	∼ 20

Table 8.3 HIPPARCHOS parallax measurements of some bright stars

Star	HIP no.	Brightness in V	Parallax in $''$
Sirius	32349	−1.44	0.37931
Canopus	30438	−0.62	0.01043
Rigil Kent	71683	0.01	0.74212
Arcturus	69673	−0.05	0.08885
Vega	91262	0.03	0.12893

The absolute brightness of the sun is about $4.^m8$. At a distance of 10 pc it would therefore be an inconspicuous star, just visible to the naked eye.

In Table 8.2 the absolute luminosities of some objects are given. Thus, a supernova at a distance of 10 pc would shine much brighter than the full Moon.

Using the HIPPARCHOS satellite one could measure the parallaxes of 18,000 stars with an accuracy of 10^{-3}. The mission (carried out by the European Space Agency ESA) took place between 1989 and 1993. A total of 120,000 astrometric and photometric data were recorded (Table 8.3).

ESA's *GAIA* (Global Astrometric Interferometer for Astrophysics, launch Dec. 2013) mission measures parallaxes of more than 10^9 Stars in our Milky Way. Similar to the solar satellite SOHO, GAIA was positioned at one of the Lagrange points in the Sun-Earth system (in this case L_2). The satellite measured each star about 70 times during the five-year mission. The measurement accuracy for stars up to the 15th magnitude class is 20 μas where $1\,\mu as = 10^{-6}$ arcseconds. In April 2018, the DR2 catalog was released, covering more than 1.7 billion stars.

The main objectives of the GAIA mission (see Fig. 8.1) were:

- Astrometry: accurate position determination, parallax determination, determination of proper motion of objects.
- Radial velocity measurements of more than 100 million stars (brighter than 17^m).
- Determination of important physical parameters such as mass, temperature.
- Accurate tests of general relativity (by measuring curvature of space).
- Discovery of exoplanets.

Other methods of determining the distance of stars are discussed in the following chapters.

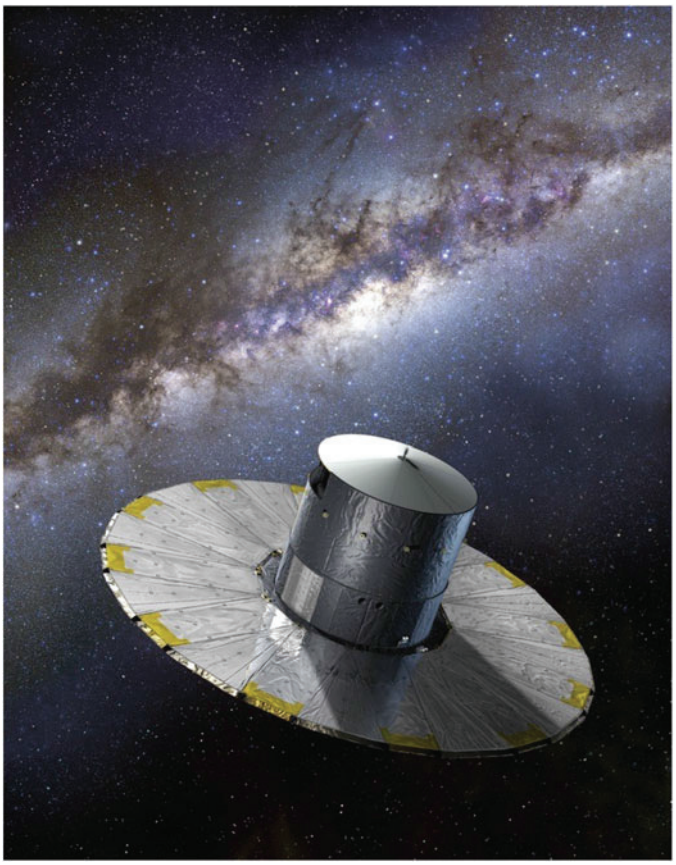

Fig. 8.1 The GAIA satellite. ESA

8.1.4 Bolometric Brightness

Stars do not only radiate in the visible range, but also e.g. in the UV, IR, X-ray range. The measured luminosities in the visible spectral range are therefore too low. In order to get a measure for the total radiation of a star, one introduced the term *bolometric brightness*.

The *bolometric correction B.C.* is used to correct for these missing amounts of energy. The bolometric brightness refers to the entire spectrum.

Example The absolute brightness bolometric brightness of the Sun is $4.^{\mathrm{M}}87$. The absolute bolometric magnitude $4.^{\mathrm{M}}74$.

The brightest stars reach -9^M, the faintest $+17^M$.

All magnitudes must still,be corrected for the amount of interstellar extinction.

The bolometric magnitude measures the total radiation of a star.

8.2 Stellar Radii

In this section we address the problem of determining the true stellar diameters. Since the stars are far away, it is very difficult to determine the angular diameters.

8.2.1 Basic Principle

An object with the true diameter D appears at a distance r at an angle Θ:

$$\Theta\,[''] = 206,265\frac{D}{r} \tag{8.8}$$

This formula is valid only for small angles.

For the *sun* one determines the radius trigonometrically. The apparent solar diameter is $32'$ and with the solar distance of $r = 149 \times 10^6$ km one obtains the Solar radius to

$$R_\odot = 6.96 \times 10^5\,\text{km} \tag{8.9}$$

For stars, the problem is to measure the extremely small apparent diameter as a consequence of their large distance.

8.2.2 Stellar Interferometer

The starlight is directed into a normal telescope by two mirrors placed at a distance D (several meters) apart (Fig. 8.2). Since stars are extended objects, albeit of extremely small angular extent. For simplicity, let us imagine a stellar disk consisting of two halves separated by a distance of $\alpha/2$ from each other. The light passes through both mirrors. As a result of the angular extent of the star, the wavefronts are inclined with respect to each other by the angle Φ. Therefore, the following superpositions occur:

- First wave: comes, for example, from the left edge of the star. After reflection from the two mirrors, the rays are combined, interference occurs, and amplification occurs when the path difference is a multiple of the wavelength: $\Phi = n\frac{\lambda}{D}$.
- Second wave: comes from the right edge of the star. It forms with the first one an angle of $\alpha/2$. Thus again a *Interference occurs.*

Both systems amplify when

$$\frac{\alpha}{2} = n\frac{\lambda}{D}. \tag{8.10}$$

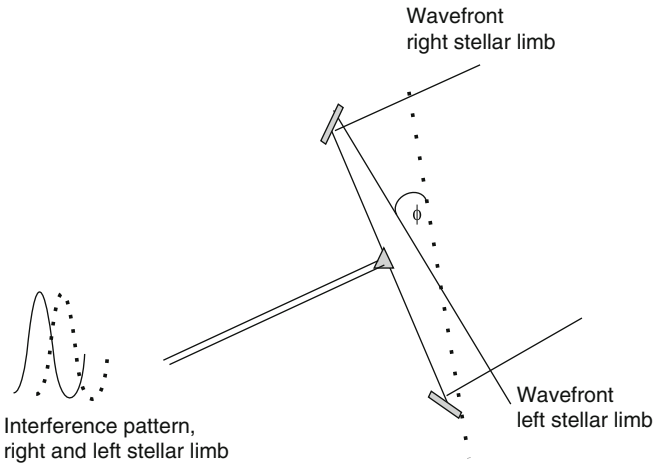

Fig. 8.2 Schematic of the Michelson interferometer Michelson interferometer

As long as $\alpha \ll \Phi$ the star is also point-like for the interferometer. But as soon as

$$\Phi = \alpha = \frac{\lambda}{D} \tag{8.11}$$

the interference system disappears. D, the distance between the two mirrors, can therefore be varied until the interference system disappears. But from this then follows the angular diameter α of the star. If one still knows the distance, then one has the linear diameter.

This type of interferometer is also called *Michelson interferometer* (*Michelson,* around 1920). There are also intensity interferometers.

8.2.3 Stellar Occultations by the Moon

The Moon runs in the course of time on an orbit slightly inclined to the ecliptic over the sky. If the moon occults a star, a diffraction figure is formed by the diffraction of the light at the moon's edge, and due to the small but finite diameter of the star, it does not disappear immediately behind the moon's limb. Thus one can determine the diameter of a star, but this is only possible for stars which can be occulted by the moon, i.e. which are located along a narrow band around the ecliptic (Fig. 8.3).

Theoretically one could argue that such star occultations can also be produced artificially at the telescope and so the diameter can be determined. The problem here, however, is that as a result of the air turbulence in the Earth's atmosphere, there are constant changes in the position of the stars's position, making measurements impossible. In the moon-star system, on the other hand, the atmospheric conditions are the same for both the lunar limb profile and the star at the moment of occultation.

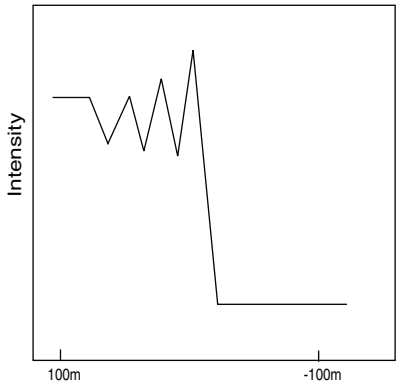

Fig. 8.3 Shortly before the moon occults a star, there are diffraction phenomena because of the lunar limb and the unevenness at the lunar limb

8.2.4 Eclipsing Variable Stars

At least half of all eclipsing variable stars are double or multiple systems. If we lie in the line of sight of a double star system, then it comes to *occultations.* A star 1 has a diameter D and is eclipsed by a star 2 with diameter d orbiting with the velocity v. The whole system has a relative velocity of V. If star 2 approaches the observer as a result of its orbit, then one measures the following *Doppler shift:*

$$\frac{\Delta\lambda_1}{\lambda_0} = \frac{V + v}{c} \tag{8.12}$$

If star 2 moves away because of its orbit, then:

$$\frac{\Delta\lambda_2}{\lambda_0} = \frac{V - v}{c} \tag{8.13}$$

and thus:

$$\frac{\Delta\lambda_1 - \Delta\lambda_2}{\lambda_0} = 2\frac{v}{c} \tag{8.14}$$

Consider, a binary star system as in Fig. 8.4, consisting of a large star 1 and a smaller companion star 2.

If star 2 disappears behind 1, an occultation occurs (Fig. 8.4, 1'–4'), the brightness of the whole system decreases. Similarly, if star 2 passes in front of star 1 as seen from us (transit), the brightness of the system decreases. The time t_1 is the time when star 2 starts to cover star 1, at t_2 it is completely in front of star 1 and so on. We therefore obtain for

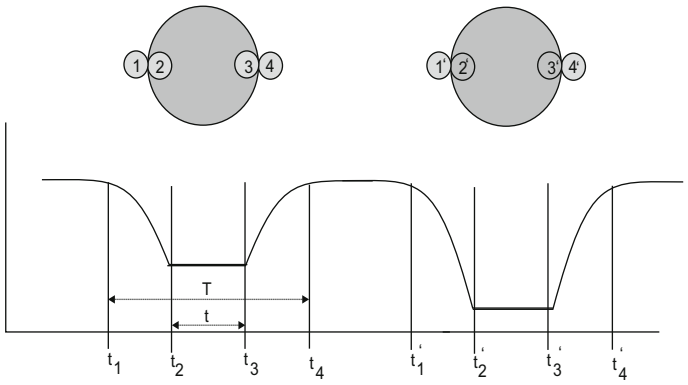

Fig. 8.4 Diameter determination in eclipsing variable stars. For 1 to 4, a transit occurs; for 1'–4', the smaller star is eclipsed by the larger one

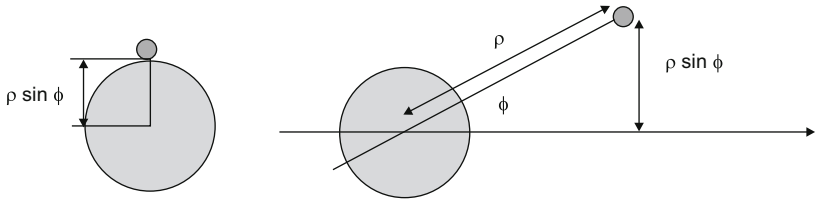

Fig. 8.5 Geometry of eclipsing stars

the diameters of the two components:

$$D + d = v(t_4 - t_1) \tag{8.15}$$

$$D - d = v(t_3 - t_2) \tag{8.16}$$

However, there are several uncertainties in this method:

- instead of circular, orbit is elliptical;
- star is not exactly spherical;
- surface brightness of stars is not uniform (cf. center to limb variation of the Sun);
- in reality both stars move around the common center of gravity.

In Fig. 8.5 it is shown that the inclination of the orbit must be very small in relation to the line of sight of the observer, in order to observe occultation.

Interesting is the star Betelgeuse (α Ori), which is about 200 pc away and is a triple system. The closest component orbits the main star in only 2.1 years, passing through the widely extended Chromosphere of Betelgeuse (Fig. 8.6). On December 12, 2023,

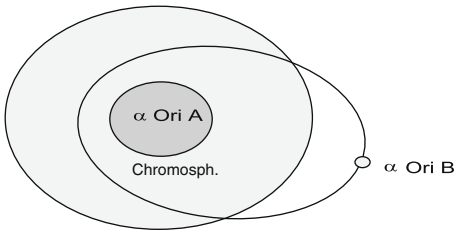

Fig. 8.6 α Ori with its inner component

the asteroid Leona will occult Betelgeuse. The extent of Betelgeuse varies between 290 million and 480 million km, so Earth's orbit would fit comfortably within the star.

8.2.5 Speckle Interferometry

The Speckle interferometry technique uses short exposures of stars to eliminate the *Seeing*. The turbulence of the Earth's atmosphere has longer periods, so exposures are made around 1 ms and therefore images are obtained that are close to the resolution limit of a telescope. If one has an unresolved point light source, then its image brightness depends on the exposure time. In *speckle interferometry* the optimal integration time is $\approx \lambda^{1.2}$. If one has longer exposure times, the image becomes blurred to a seeing disc *(blurring)* and is about $1''$ large. If the exposure times are smaller than the coherence time $t_c \approx 10$ ms (in the optical range, in the IR 100 ms), then we obtain a group of bright *Speckles* whose size is approximately that of the Airy disk (r_0).[2] Thus, the influence of the atmosphere is frozen. The speckles are distributed over an area of diameter λ/r_0, the number of speckles is of the order of the sub-apertures D^2/r_0^2. The observed image I' is a convolution between the true image and the so-called *point spread function* (PSF) of the telescope. This indicates how an ideal point source of light behaves after passing through the telescope. In classical spectral analysis one tries to restore the original amplitude, and in bispectral analysis one also tries to restore the phases. One has thus (F stands for the Fourier transform):

$$F(I') = F(I)F(b) \tag{8.17}$$

I—Original intensity distribution of the object, b—PSF of the telescope. High spatial frequencies are not affected by the Earth's atmosphere, but low ones are, and therefore low spatial frequencies are disturbed by seeing.

[2] Corresponds to the resolving power of a telescope.

8.2.6 Microlensing

With the methods described above, radii can only be determined for relatively large evolved stars (cf. HRD, Sect. 8.5). For small main sequence stars, the determination of radii is difficult because their angular diameter is too small. Under the term *Microlensing* one understands the deflection of light by an object according to the general theory of relativity, which, however, does not lead to separate images as in the case of galaxies (multiple images of a galaxy or quasar—due to lens effect of a n unseen galaxy lying between the observer and the galaxy), but only to an increase in brightness. The lens moves through the connecting line earth-star, and the latter changes its brightness analogously. The change in brightness is symmetrical, and the event lasts a few weeks or months. By evaluating the photometric light curve one can determine the diameters of the objects. Such events are more frequent in double stars.

8.3 Stellar Masses

The Mass of stars is the most difficult to determine; however, it is a fundamental state variable on which many other parameters depend: Stellar evolution, age of stars, nuclear fusion, etc.

8.3.1 Kepler's Third Law

Directly derivable is the mass only, if a star with a mass M_1 has a companion with a mass M_2 so it is a double star or multiple system. One can also use exoplanets to determine the mass of a star. The third Kepler's Law reads:

$$\frac{(M_1 + M_2)}{a^3} U^2 = \text{const} = 1 \tag{8.18}$$

The units here are: mass M in solar masses, a the distance between star and companion in AU and the orbital period U in years. We therefore get the mass sum:

$$M_1 + M_2 = \frac{a^3}{U^2} \tag{8.19}$$

How can one now determine the necessary quantities $a,\ U$?

- Visual binary stars: both components observable, $\rightarrow a$ in AU once their distance is known. Then follows the mass sum. The mass ratio follows from the analysis of the

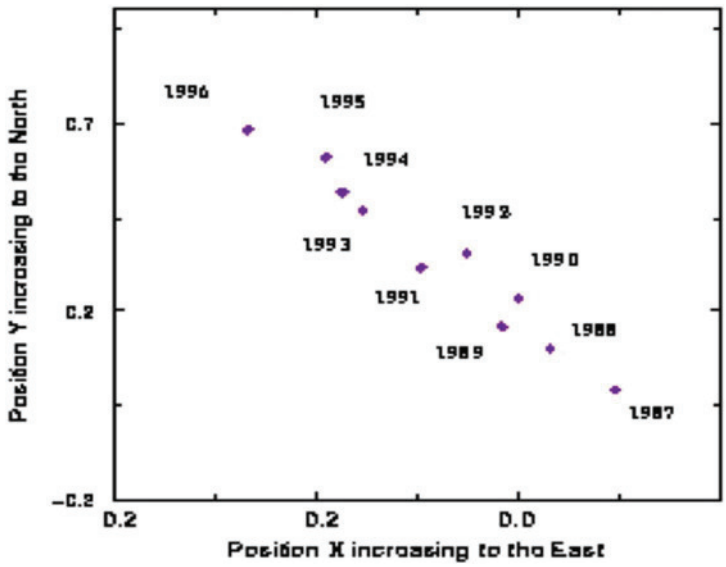

Fig. 8.7 Double star in which only one component is visible, but which clearly shows regular variations (HIPPARCHOS)

absolute orbit, i.e., one must know the motion of the two components about their common center of mass.

$$M_1/M_2 = a_2''/a_1'' \tag{8.20}$$

- Only bright component visible: in most cases, however, the fainter component is not directly observable and only the absolute orbit of the brighter component is known (Fig. 8.7).

$$a_1/a = M_2/(M_1 + M_2) \tag{8.21}$$

This is estimated according to a resolved and inserted:

$$(M_1 + M_2)\left(\frac{M_2}{M_1 + M_2}\right) = \frac{a^3}{U^2} \tag{8.22}$$

- Exoplanets: This can be simplified for extra solar planets where: $M_2 \ll M_1$ and therefore $M_2 + M_1 \approx M_1$.
- Spectroscopic binary stars: One does not see the double stars separatedly, but due to the motion of the two components there is a periodic shift of the spectral lines due to the

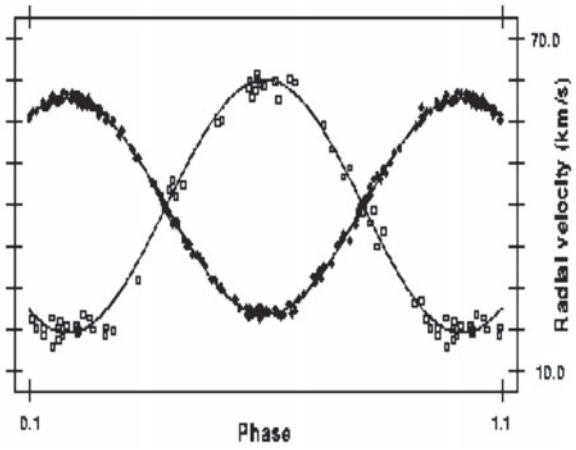

Fig. 8.8 Spectroscopic double star (α Aur). The masses of the two components are about 2.5 solar masses [HIPPARCHOS]

Doppler effect. Problem: Orbital inclination i is unknown. Let v is the orbital velocity in the direction of the observer, then we get:

- $a_1 \sin i$, when only one spectrum is known;
- $(a_1 + a_2) \sin i = a \sin i$ when both spectra are visible and only relative line shifts can be measured;
- $a_1 \sin i$ and $a_2 \sin i$ when both spectra are visible and absolute shifts have been measured (Fig. 8.8).
  The problem is the orbital inclination i. From mathematics one has for the averaging over the orbital inclinations i:

$$\overline{\sin^3 i} = 0.59 \tag{8.23}$$

- Spectroscopic eclipsing variability: Here is $i = 90°$.

Overall, there are good mass determinations for only a few 100 stars.

8.3.2 Gravitational Red Shift

For stars with large gravitational acceleration, the *relativistic red shift* apply: Light consists of photons of energy $E = h\nu$. One can attribute the photons a mass m (rest mass = 0):

$$E = mc^2 = h\nu \rightarrow m = h\nu/c^2 \tag{8.24}$$

The photons did work against gravity, lose energy, which $\propto \lambda^{-1}$ and the light appears reddened according to the classical derivation:
Gravitational red shift:

$$\frac{\Delta\lambda}{\lambda} = \frac{GM}{Rc^2} \tag{8.25}$$

Where R is the radius of the star. From this formula, we see that the relativistic red shift is large for stars of large mass that are very compact (small R).

As an example, consider white dwarfs. These final stages of the evolution of stars below 1.4 solar masses are very compact; $M \approx 1\,M_\odot$, $R \approx 0.01\,R_\odot$; white dwarfs have a relativistic red shift of is 10^{-4}.

8.3.3 Microlensing

Microlensing can also be used for mass determination. There are several projects. One of them is to find neutron stars and black holes using the Hubble Space Telescope. So far, the masses of neutron stars and black holes are only known if they are companions in a binary system. Masses of isolated neutron stars and black holes can be determined by microlensing. For this purpose one regularly records star fields and

- examines them for symmetrical variations in brightness (in the case there occurs an alignment of earth-neutron star or black hole—another star in thee field)
- make precise position measurements of the stars, astrometry.

To increase the probability of a microlensing event, one chooses dense stellar fields in the Galactic plane, since the stellar density is high there.

Important: The mass of a star determines its lifetime and evolution.

8.3.4 Derived Quantities

Density is directly obtained from the mass and radius

$$\rho = \frac{M}{\frac{4\pi}{3}R^3} \tag{8.26}$$

Also one immediately gets the *Gravitational acceleration* of a star:

$$g = GM/R^2 \tag{8.27}$$

A first evaluation for many stars results in the following value ranges for:

- Mass: 0.2–60 $M_\odot$,
- Radius: 0.1–500 $R_\odot$.

Although there are several methods for determining stellar masses, their determination is difficult but extremely important because it determines the further evolution of a star.

8.4 Stellar Temperatures

There are many different temperature terms. The values derived from the different methods do not match exactly because stellar radiation does not behave exactly like that of a black body.

8.4.1 Stars as Black Bodies

Here there are different definitions. Basically one assumes that the stars radiate like a *Black body*, and then defines:

- *Effective temperature:* The temperature of a star that corresponds to the radiation from a blackbody emitting the same energy per unit area as the star.
- *Radiative Temperature:* The temperature which corresponds to the radiation of a black body in a narrow wavelength range.
- *Color temperature:* The Temperature corresponding to the radiation of a black body in a spectral range (= color).
- *Gradation temperature:* The temperature whose intensity-wavelength curve at a given wavelength has the same slope as that of the intensity curve of a black body.
- *Wien's temperature:* Follows from the maximum of the intensity distribution.

For an A0-V star, one has (e.g. $T_F(500)$ is the temperature at a wavelength of 500 nm):
$T_{\text{eff}} = 9500\,\text{K}$ $T_F(425\,\text{nm}) = 16{,}700\,\text{K}$ $T_F(500\,\text{nm}) = 15{,}300\,\text{K}$.

The differences between these temperature terms indicate that the radiation of stars is only to a first (but mostly good) approximation that of a black body.

8.4.2 Other Temperature Terms

Temperature can also be defined in terms of kinetic temperature, or in terms of atomic states of excitation and ionization.

- *Kinetic temperature:* From of the kinetic theory of gases we know that particles move with the most probable velocity

$$v_{\text{th}} = \sqrt{\frac{2\Re T}{\mu}} \tag{8.28}$$

  ($\Re$ is the gas constant). This thermal velocity is also partly responsible for the *width* of the spectral lines.

The thermal velocity of particles depends on the temperature and the particle mass.

- *Electron temperature* T_e: Defined through the kinetic temperature of the electrons (note: $m_e = (1/1800)m_p$, electrons have only 1/1800 of the proton mass).
- *Ionization temperature* T_{ion}: Results from the ratio of the number of atoms in different ionization states (Saha formula, is a function of temperature and pressure).
- *Excitation temperature* T_{exc}: The Boltzmann formula is used to obtain the relative atomic numbers in different excited states (which depends on temperature).
- *Band temperature:* molecules generate dark bands in the spectrum due to their rotational or vibrational transitions.

8.5 Classification of Stars, HRD

We now come to one of the most important diagrams in astrophysics. If we plot the temperatures of the stars against their luminosities, we obtain the Hertzsprung-Russell diagram, HRD.

Stars can be classified according to their line spectrum.

8.5.1 Spectral Classification

A single star spectrum is obtained when starlight is focused through a telescope and falls on a spectrograph where it is split. The spectrum itself is recorded either photographically or by CCD.

Angelo Secchi has introduced *Spectral types* around 1863. The classification still in use today was introduced in 1910 by *Annie Cannon*. This is also known as the *Harvard Classification.* Cannon herself classified 400,000 stars *(Henry Draper catalogue).*

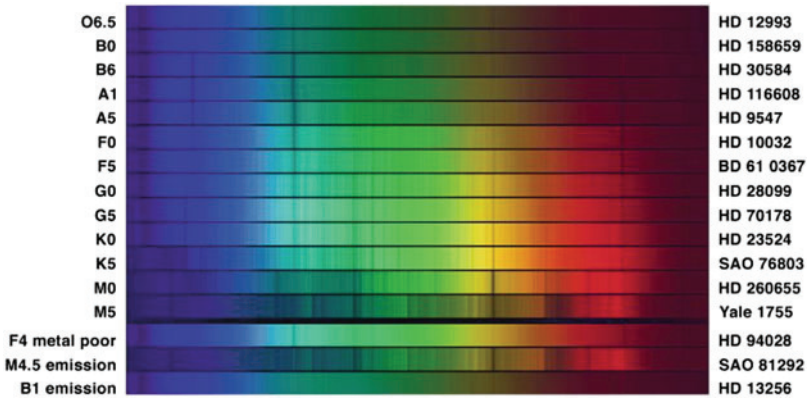

Fig. 8.9 Spectra of the stars. Hydrogen lines are most prominent in A stars, the later the spectral type, the more lines are visible in the spectrum (Copyright: KPNO 0.9-m Telescope, AURA, NOAO, NSF, Princeton)

Originally stars were classified according to the strength of their hydrogen lines. The stars with the strongest hydrogen lines were given the designation A and so on. Today one uses a sequence of descending temperature and therefore the strange order:
O – B – A – F – G – K – M
These are simply remembered: **o***h* **b***e* **a** **f***ine* **g***irl (***g***uy)* **k***iss* **m***e*. Further, one still subdivides decimally. We briefly discuss the individual types (Fig. 8.9):

- O: The hottest stars, bluish, He-II lines; He-I lines increase from type O5; there are also lines of Si IV, O III, N III, and C III. *Balmer lines* of hydrogen are present, but relatively weak compared to the other lines.
- B: White-blue stars; He I dominates, no He II; the hydrogen lines become stronger; Mg II and Si II. Very often they are surrounded by envelopes, which are noticeable by characteristic shapes of the spectral lines (Fig. 8.10).
- A: White stars; H lines dominate; at A0 the strength of H lines is greatest; lines of ionized metals (Fe II, Si II, Mg II). Ca II lines become stronger (Fig. 8.11).
- F: White to slightly yellowish stars, strength of hydrogen lines decreases, neutral *metal lines* appear. Ca II H and K lines become stronger; neutral metals (Fe I, Cr I).
- G: Yellowish stars; Ca II dominates; at G2 the H and K lines of ionized calcium (Ca II) are strongest; neutral metals become stronger, no more ionized metals (Fig. 8.12).
- K: Reddish stars; first appearance of *molecular bands;* neutral metals. Bands of TiO.
- M: Coolest, red stars; neutral metal lines strong, molecular bands dominant.

Since the radiation of stars conforms to a Planck curve to a first approximation, one has problems at both ends of the spectral sequence:
For very hot stars the maximum of the intensity distribution is in the UV region, for very cool stars it is in the IR region.

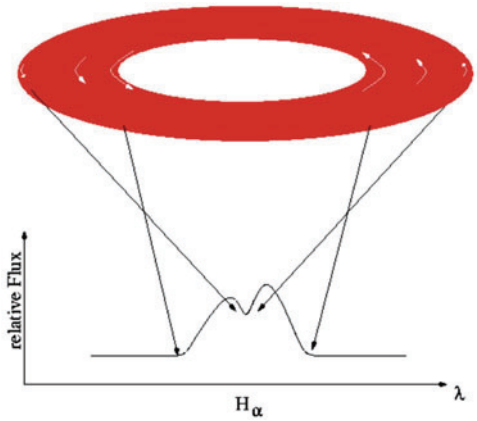

Fig. 8.10 Stars with an envelope: formation of the characteristic line profile of the hydrogen line H_α. The emission comes from the envelope, the displacement from its rotation

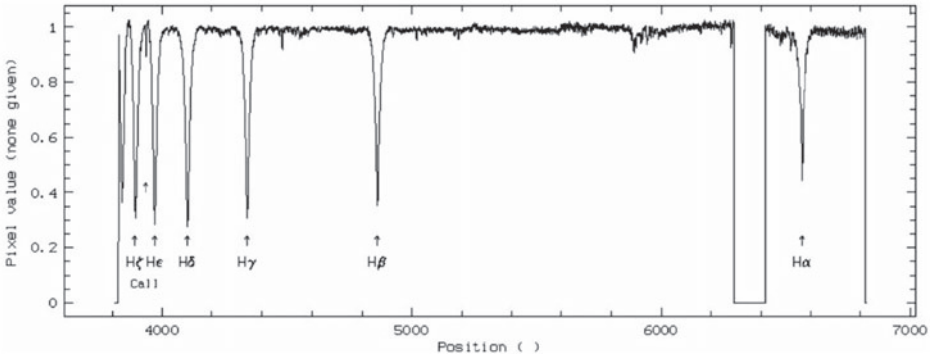

Fig. 8.11 Spectrum of the star Vega (A0)

Fig. 8.12 The line-rich spectrum of a G star

8.5.2 The Hertzsprung-Russell Diagram

In 1911 *Hertzsprung* established the most important diagram for stellar astrophysics. The absolute brightness of the stars (corresponding to the true luminosity of the stars) is plotted against their spectral type (Fig. 8.13). However, one must consider selection effects:

- If one creates a *Hertzsprung-Russell diagram* for stars in the solar neighborhood, mostly faint stars are found there.

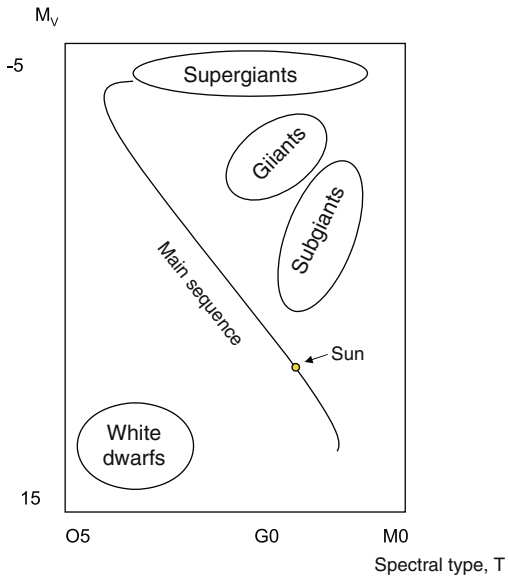

Fig. 8.13 The Hertzsprung-Russell diagram

- If one generates such a diagram for bright stars, then obviously stars of large luminosity are preferred.

→ Most important result: the stars are not randomly arranged in an HRD:

- Diagonally runs in the HRD the main sequence from top left to bottom right.
- On the upper left there are hot luminous stars,
- and on the lower right, cool stars of low luminosity.
- More than 90% of all stars fit into this *main* sequence. *main sequence*).
- Furthermore, the HRD shows that there are stars which are clearly above the main sequence at a given temperature, but whose luminosity is higher.

So in the HRD, we plot: spectral type and luminosity of the stars. Since stars radiate like black bodies in a good approximation, one can use the temperature instead of the spectral type or even more simply the color or the color index of the stars. Color index *(color index, CI)* is the difference of brightnesses:

$$\text{color index} = m_{\text{short wave}} - m_{\text{long wave}} \tag{8.29}$$

The Hertzsprung-Russell diagram is fundamental in astrophysics. One plots the temperature (spectral type, color) against the luminosity (absolute brightness) of the stars.

Standardized *color systems* have been introduced. Very often the *UBV system* is used:

- U stands for brightness in the near UV,
- B for brightness in the blue range,
- V for brightness in the visual range.

So one measures brightnesses with these filters and then simply speaks of a brightness in U, B, V and often writes instead of m_U, $m_B, \ldots$ simply $U, B, \ldots$ For the spectral type A0 is defined : $U - B = B - V = 0$.

The *color index* C.I. is given by the difference of brightnesses in different wavelengths:

$$\text{C.I.} = \text{m}_{\text{short wave}} - \text{m}_{\text{long wave}} \tag{8.30}$$

From the color index, one can immediately determine *temperature*; e.g., for $B - V$:

$$B - V = 7090\frac{1}{T_{\text{eff}}} - 0.71 \tag{8.31}$$

In Fig. 8.14 a *Color-brightness diagram,* CBD, is shown.

In Table 8.4 shows some photometric systems.

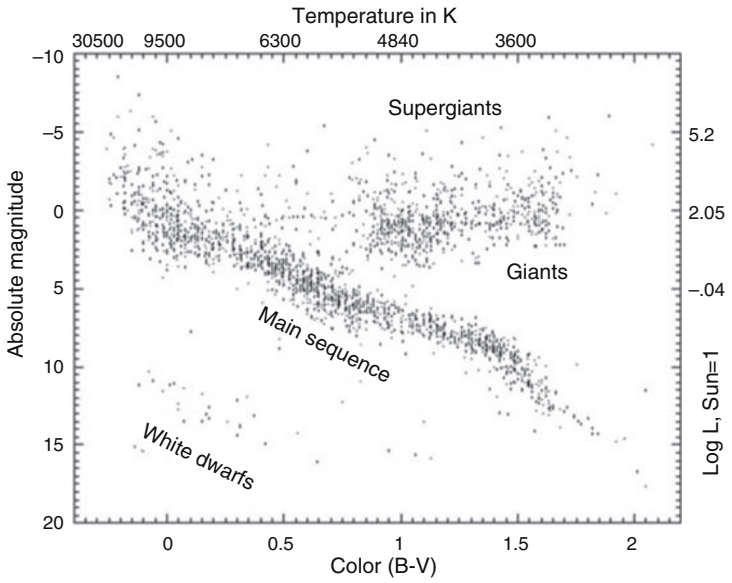

Fig. 8.14 Hertzsprung-Russell diagram with color index B-V as the x-axis. This is called a color-brightness diagram (CBD)

Table 8.4 Photometric systems

Designation	Central wavelength [nm]	Filter width [nm]
U	365	70
B	440	100
V	550	90
R	720	138
I	806	149
Z	900	–
Y	1020	120
J	1220	213
H	1630	307
K	2190	390
L	3450	472
M	4750	460
N	10,500	2500
Q	21,000	5800

What is the sign of $U - B$ for our sun? Our Sun is a cool star with maximum intensity at 550 nm. Therefore its brightness in U is lower than in B, lower brightness means higher value for the magnitude class, therefore $m_U > m_B \rightarrow m_U - m_B > 0 \rightarrow U - B > 0$

An important parameter is the metallicity (*abundance of metal*), defined as

$$\mathrm{Fe/H} = \log \frac{(\mathrm{Fe/H})_{\mathrm{Star}}}{(\mathrm{Fe/H})_{\mathrm{Sun}}} \tag{8.32}$$

Metal Poor Stars have a negative metallicity. A metallicity of -1 means that the object shows only about 1/10 of the metal abundance in the spectrum as our Sun.

8.5.3 Luminosity Classes

The *luminosity* of a star is given by its surface $4\pi r^2$ and the *Stefan-Boltzmann law* $\sigma T_{\mathrm{eff}}^4$:

$$L = 4\pi r^2 \sigma T_{\mathrm{eff}}^4 \tag{8.33}$$

If a star has a much higher luminosity at a given temperature, then its surface area must be larger, therefore it is called a *giant star.*

Temperature alone is not sufficient to define the location of a star in the HRD. Therefore, a star of given temperature may be a normal main sequence star or may be above it; then

it is a giant star. For this reason in 1937 the *Morgan-Keenan luminosity classes* have been introduced:

- I: supergiants (Ia, Ib, Ic);
- II: bright giants (IIa, IIb, IIc),
- III: giants (IIIa, IIIb, IIIc),
- IV: subgiants, (IVa, IVb, IVc),
- V: dwarf stars (Va, Vb, Vc), main sequence stars.
- VI: subdwarfs.

In the HRD, therefore, above the main sequence on the right are the supergiants, below them the bright giants, and so on. A G2 supergiant is 12.5 magnitudes brighter than our Sun.

The absolute brightness of the Sun is $4\overset{\text{m}}{.}6$; a supergiant of similar spectral type (G2) at this distance would have a brightness of $-7\overset{\text{m}}{.}9$; for comparison, Venus reaches about $-4\overset{\text{m}}{.}5$!

The next star is α Cen and has the same spectral type as our Sun (G2V). Its brightness is $V = -0.33$ the distance is 1.3 pc, and the absolute magnitude is $4\overset{\text{m}}{.}5$. The star Capella (α Aur) is of the type a G8 III, has $V = 0.09$ and a distance of 14 pc. Its absolute brightness is therefore -0.59. Here,V means the brightness measured in the visual band.

In Table 8.5 the characteristic state variables of the main sequence stars are listed.

The position of stars in the HRTD: main sequence stars (about 80% of all stars) in the diagonal; hot, massive stars are on the left; cool, low-mass stars are on the lower right.

Table 8.5 Characteristic state variables from main sequence stars

Spectral type	Mass[$M_\odot$]	Luminosity[$L_\odot$]	Temperature[K]	Radius Sun = 1
O5	40	7×10^5	40.000	18
B0	16	27×10^4	28.000	7
A0	3.3	55	10.000	2.5
F0	1.7	5	7500	1.4
G0	1.1	1.4	6000	1.1
K0	0.8	0.5	5000	0.8
M0	0.4	0.05	3500	0.6

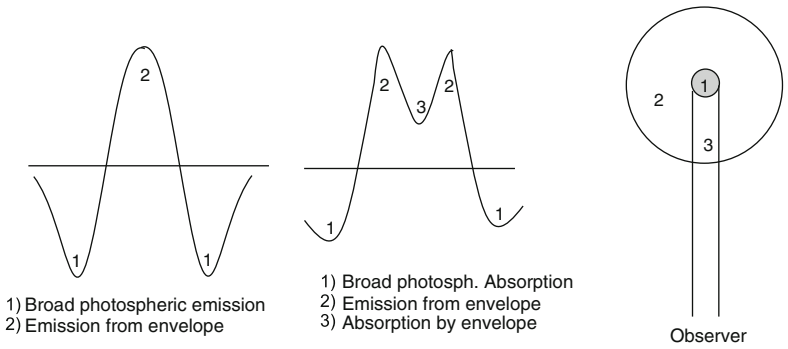

Fig. 8.15 The origin of the typical line profile a stellar envelope

Special features in the spectrum are indicated by:

- n: diffuse blurred lines; nn very diffuse; indicates rapid rotation of the star;
- s (sharp) sharp lines;
- e: emission lines (suggesting an extended envelope around the star from which these lines originate) (Fig. 8.15);
- v (variable); spectrum variable;
- k (K line); strong interstellar Ca-II line;
- p (peculiar); any peculiarities in the spectrum. Here Metallic stars there are the Ap stars or the Am stars *(metallic line stars).*

8.5.4 Balmer Discontinuity

In the so-called *Paris classification* one determines:

- *D*: Size of the Balmer*discontinuity* at $\lambda = 370\,\text{nm}$. This results from the extended continua in the short-wavelength and in the long-wavelength region of 370 nm.
- λ_1: Location of the Balmer discontinuity = intersection of the registered continuum with the parallel to the long-wavelength continuum through the bisector of the Balmer discontinuity.

The Balmer discontinuity *D* does not occur at the theoretical series limit, but occurs earlier because the higher order transitions converge. This happens earlier the higher the electron pressure. Therefore *D* is determined by the temperature and thus defines the spectral type; λ_D Is defined by pressure and is therefore characteristic of luminosity. Giant stars have a very extended atmosphere and therefore low pressure, and their spectral lines appear sharp.

Another possibility of spectral classification is the *narrow band classification,* where one measures the intensity within a narrow bandwidth (3–15 nm) at defined points in the spectrum.

Objective prism spectra have only a low *dispersion* ($\approx$ 50 nm/mm), and therefore one uses as a criterion:

- Size and sharpness of the Balmer discontinuity,
- intensity of the Balmer lines,
- Ca-II line intensity.

8.5.5 Star Population and FHD

In astrophysics, all elements heavier than He are called *Metals* .

According to the metal content one distinguishes between two *stellar populations:*

- Population I: young Stars, 2−4 % heavy elements,
- Population II: old stars, low content of heavy elements (less than 1%).

We will talk about this later in the stellar evolution.

From the observational side, a *color-brightness diagram, CBD,* is still easier to obtain. One plots color (a measure of temperature and therefore spectral type) against luminosity (absolute brightness). To determine the color, one simply measures the brightness with two different color filters (e.g., in the B and V filters, Fig. 8.16). In a *two-color diagram* for example, one plots B-V against U-B. The result is a wave in the diagram. At A0 the Balmer depression decreases, U becomes brighter, opposite to the temperature response; at F5 the Balmer depression decrease predominates again. The influence of a reddening

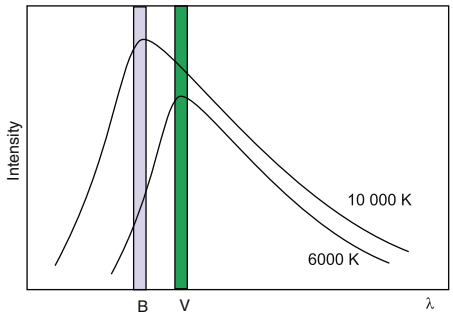

Fig. 8.16 Determination of the B-V brightness. Let a star **a** have a temperature of 10,000 K, and the maximum of its radiation, given by a Planck curve, lies in the B region. A second star **b** has the maximum of its radiation in the V-range

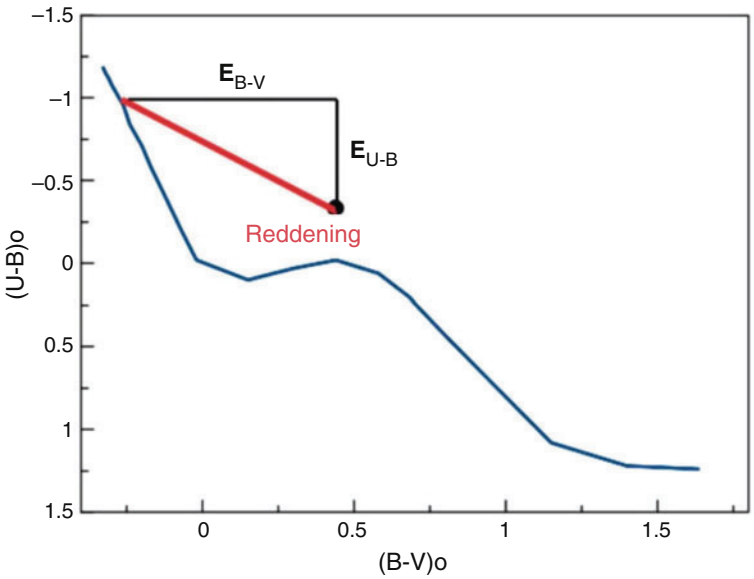

Fig. 8.17 In the two-color diagram, the color index U-V is plotted against B-V. A possible reddeing of the colors of the stars of a star cluster, caused by interstellar matter, is indicated

by interstellar matter has the effect of a shift in the diagram. Let us assume that we are looking at a two-color diagram of the stars of a star cluster, which are practically all at the same distance from us. Then the reddening due to interstellar matter affects all stars equally and is shown in Fig. 8.17.

8.5.6 The Mass-Luminosity Relation

For main sequence stars there is a *mass-luminosity relationship*:

$$L \approx M^{3.5} \tag{8.34}$$

Thus, if we know the luminosity of a main sequence star, it follows its a mass. The masses decrease along the main sequence from the top left to the bottom. Right downwards.

From the position of a star in the HRD follows its temperature, luminosity and mass.

8.6 Rotation and Magnetic Fields

Both effects are important for the activity of a star. In the spectrum, rotation is noticeable by an elliptical line profile, magnetic fields also lead to a broadening *(Zeeman effect)*.

8.6.1 Rotation

Solar rotation can be determined directly:

- by so-called tracers, e.g. migration of sunspots due to solar rotation, the equatorial solar rotation velocity is $v_{\mathrm{rot}\odot} = 2\,\mathrm{km/s}$,
- spectroscopically.

For some eclipsing binaries, one also proceeds by the spectroscopic method. If the right or the left edge of the star becomes visible for a short time, there is a bump in the radial velocity curve (Fig. 8.18).

Indirectly, the rotation of a star can only be determined from the width of its spectral lines. This *line broadening* occurs because, in effect, one half of the star is moving toward the observer (hence blue shift) and the other away from it (hence red shift). Rotating stars provide an elliptical line profile. Again, of course, the inclination of the rotation axis is

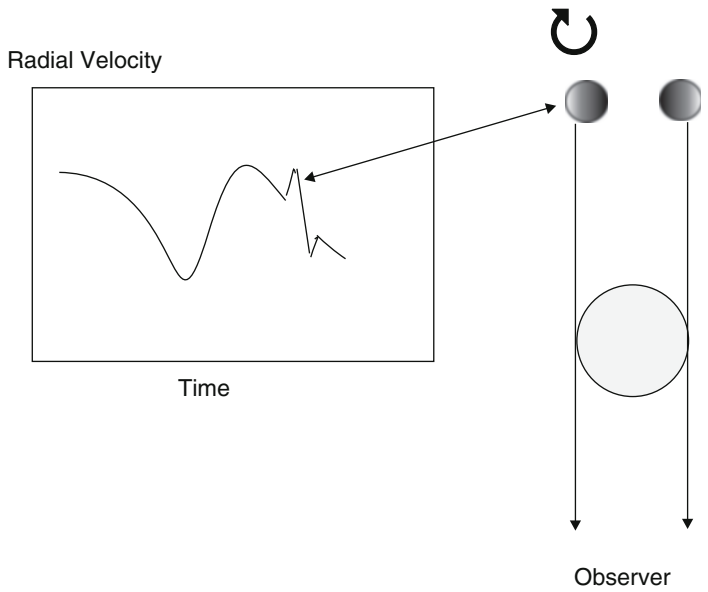

Fig. 8.18 So-called bump in the radial velocity curve of a star, when a component is close to before or after total occultation

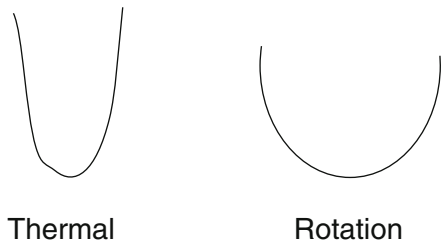

Fig. 8.19 Line broadening; thermal (left) and due to rotation of a star (right)

unknown, and we obtain (v_{eq}—rotational velocity at the equator):

$$v_{eq} \sin i. \tag{8.35}$$

If $i = 0$ then one looks at the pole of the star, and one observes no rotation broadening.
The limit for rotation follows from the condition:
Gravitational acceleration = Centrifugal acceleration.

$$\frac{GM}{R^2} = \frac{v_{rot}^2}{R} \qquad v_{rot} = 440\sqrt{M/R}\ \text{km/s} \tag{8.36}$$

Rotation changes as stars evolve.

Protoplanetary disks slow down the rotation. The Spitzer-telescope;[3] is equipped by a 0.85-m mirror, and one observes in the IR between 3 and 180 μm. It has been found that young stars in the Orion Nebula region (a so-called *star forming region*) rotate more slowly when there are protoplanetary disks around them that show up in IR radiation. Stars without detectable protoplanetary disks on the other hand rotate more rapidly.

Stellar rotation (Fig. 8.19) influences stellar evolution and star formation.

There are already some 10^5 Stars whose $v \sin i$ is know:

- Early types, i.e. spectral type O, B, A, and early F: 50−400 km/s, i.e. high rotation rate.
- Late types, i.e. spectral type G, K, M: rotate slower, $v_{rot} \sin i < 50$ km/s
- Trend in HRD: rotation rate decreases with stellar mass; the lower the mass, the slower stars rotate.

Rotation mixes elements or can explain anomalies; rotation affects stellar activity (starspots, winds, ...). High rotation rates cause an outflow of stellar matter at the equator, which accumulates in a shell *(shell stars)*.

[3] Launched 2003.

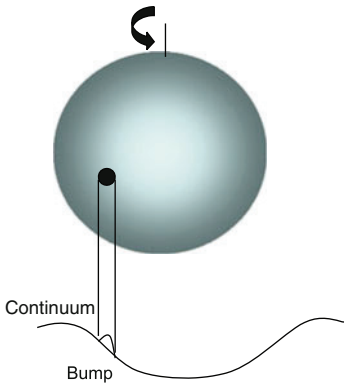

Fig. 8.20 Principle of Doppler imaging for the detection of starspots. The starspot makes the line profile appear less deep (sketched below); rotation of the star changes the position of this bump

8.6.2 Magnetic Fields

The direction of the angular momentum axis of the atoms is quantized; in the presence of a magnetic field, the terms split → Line splitting, Zeeman effect.

By means of "Doppler Imaging" (*Vogt, Penrod,* 1983) we can detect *stellar spots* as magnetically active regions. Let us take a stellar photospheric line which is Doppler broadened by the rotation of the star. If a large starspot now moves across the stellar disk as a result of the rotation, then this can be seen in the spectrum. Due to he spot

1. Continuum shifted down to entire line profile;
2. Component of the spot Doppler-shifted due to rotation.
3. Measured line: subtract 1−2; less light is subtracted at the point of Doppler shift.
4. → Bright "bump" due to spot in line profile (Fig. 8.20).

Another way to detect starspots is by using a technique called *Zeeman Doppler imaging* or by observing eclipses of stellar spots in active binary stars. Many magnetically active stars are close binary systems *(close binaries),* and one or both components rotate extremely rapidly due to tidal interaction.

One can also see fine structures in the *Balmer lines of* hydrogen, which can be traced back to matter motions in the stellar chromospheres or coronae → stellar prominences.

Here again the hydrogen line Hα is a useful proxy. This line originates in stellar atmospheres usually in the chromosphere. The calcium lines (H and K lines) are also used to determine the magnetic activity of stars: One measures their *equivalent width.*

Starspots, prominences etc. can only be detected by special spectroscopic techniques.

8.7 Peculiar Stars

We discuss here some special stars. First the particularly bright stars (bright therefore, because they are either very close to or actually shine very brightly); then some special types of stars, such as eclipsing variable stars, where there a *Mass Exchange* between the components occurs.

8.7.1 Bright Stars

We give in Table 8.6 the brightest stars visible in the northern sky.

Compare in Table 8.6 the actual luminosities of the stars Deneb and Sirius! As a measure of Luminosity we use the absolute Brightness.

$m - M = 5 \log r - 5$, where r in [pc]. Deneb: $m = 1.25$ and $r = 3227.7/326 = 990\,\text{pc} \rightarrow M = -8.73$. Sirius: $M = 1.43$. Deneb is therefore 10.15 magnitudes brighter than Sirius.

Table 8.6 Brightest Stars at north sky

Name	Designation	Brightness (V)	Distance [Ly]	Spectral type
Sirius	α CMa	−1.46	8.6	A1Vm
Arcturus	α Boo	−0.04	312.6	K1 III
Vega	α Lyr	0.03	25.3	A0V
Capella	α Aur	0.08	42.2	G5IIIe
Rigel	β Ori	0.12	772.5	B8a
Procyon	α CMi	0.38	11.4	F5IV-V
Betelgeuse	β Ori	0.50	427.3	M1Ia
Altair	α Aql	0.77	16.8	A7V
Aldebaran	α Tau	0.85	65.1	K5III
Antares	α Sco	0.96	603.7	M1I
Spica	α Vir	0.98	262.1	B1III
Pollux	β Gem	1.14	33.7	K0III
Fomalhaut	α PsA	1.16	25.1	A3V
Deneb	α Cyg	1.25	3227.7	A2Ia
Regulus	α Leo	1.35	77.5	B7V
Bellatrix	γ Ori	1.64	242.9	B2III

Table 8.7 Some known eclipsing binaries

Name, designation	Distance [Lj]	Period	Variation
Algol, β Per	93	2d 20h 48m	$2^{m}.3$–$3^{m}.5$
Sheliak, β Lyr	1000	12.9 d	$3^{m}.4$–$4^{m}.6$

8.7.2 Algol and Eclipsing Binaries

Eclipsing variables like Algol Stars *(eclipsing binaries)* have already been mentioned in the discussion of the methods for the mass- and diameter determination of stars. *Algol*[4] is the second brightest star in the constellation Perseus (β Pers). Its name (Devil's Star) comes from the fact that it is variable (Table 8.7). It is a triple system; two components, closely adjacent and occulting each other as seen from us, are orbited by a third far away. In the *Algol stars*, the occulting components are still round, i.e., not deformed by gravitational interaction; for the *Beta Lyrae stars* (named after the prototype β Lyr), the two components are elliptically deformed. The data of β Lyr can also be found in Table 8.7.

In the spectrum of β Lyr one sees the continuum with emission lines of the B8 giant, an absorption spectrum of the B5 star and an emission spectrum. In the B8 spectrum one sees periodic Doppler shifts of ± 180 km/s while the lines of the B5 spectrum show no shifts and originate from the gas envelope.

The Roche sphere *(Roche lobe)* is the region around a star within which matter is gravitationally bound to the star. In a binary star, one of the components may expand over the Roche sphere → Matter outside the Roche sphere falls on the other star. The point at which the Roche spheres of the two stars M_1, M_2 touch, corresponds to thereby the Lagrange point L1 (Fig. 8.21).

For the β-Lyr stars, the B8 component fills the Roche sphere; the second component is smaller and less luminous, but has the larger mass. Just before the occultation of the B8 component, so-called satellite lines are produced, which are red shifted. These are produced by the rotation of the gas disk (accretion).

For Algol stars, one component fills the Roche limit.

Narrow binary systems are classified as follows (Fig. 8.22):

- D, *detached,* separated systems; the two masses M_1, M_2 are much smaller than the Roche interface.
- SD, *semi detached,* semi separated systems. One component extends to the interface.
- C, *contact*, contact systems, both components reach the interface.

The *W-Ursae-Majoris stars* are short-period contact systems.

One can estimate how large the mass transfer is by measuring the change in period.

[4] al-gu-l, the demon.

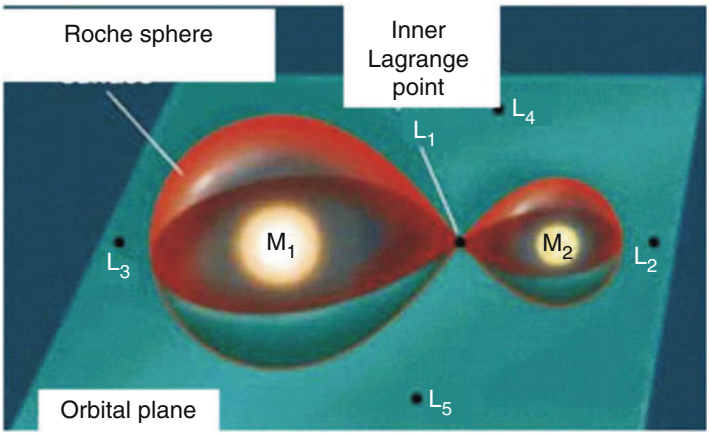

Fig. 8.21 The Roche boundaries around two stars M_1, M_2 where $m_1 > m_2$. As soon as one star fills its Roche sphere (up to the point L1), mass transfer occurs to the other star

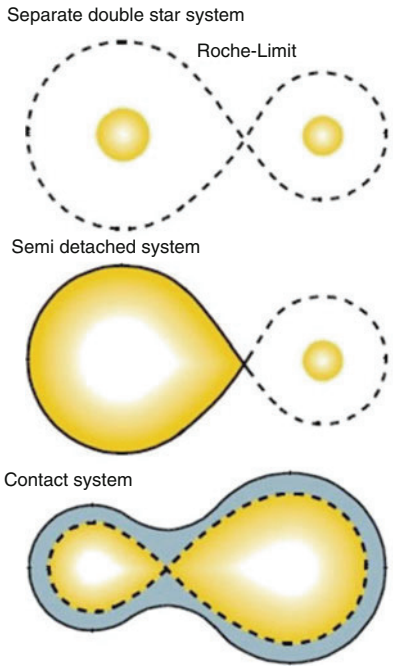

Fig. 8.22 Kopal classification of close binary star systems. From Stars and Space

8.8 Further Literature

We give a small selection of recommended further reading.
Astrophysics for Physicists, A.R. Chourdhuri, Cambridge Univ. Press 2010
An Introduction to Modern Astrophysics, B.W. Caroll, D.A. Ostlie, Cambridge Univ. Press, 2017
Astrophysics—a very short introduction, J. Binney, Oxford Univ. Press, 2016
An Introduction to Stellar Astrophysics, F. LeBlanc, Wiley, 2010

Tasks

8.1 Calculate the absolute brightness of the sun: $m = -26.7$, distance of the Sun in pc = 1/206,265.

Solution
$M = -5 \log r + 5 + m = -5 \log(1/206.265) + 5 - 26.7 = 4.87$

8.2 Take a cool supergiant with $T = 3000$ K with a luminosity of $10^4 L_\odot$. What is its magnitude?

Solution
$R_* = 400\, R_\odot$.

8.3 A galaxy has an absolute luminosity of -20^{M}. How bright does it appear to us at a distance of (a) 1 Mpc, (b) 1000 Mpc?

Solution
(a) 5^{m}, (b) 20^{m}.

8.4 Discuss which sign(s) the bolometric correction has.

Solution
Always negative.

8.5 Aldebaran (α Tau) has $\alpha = 0.023''$. The Distance d is 20.8 pc. Calculate the true diameter.

Solution
$D = (1.1 \times 10^{-7})(20.8\,\text{pc}) = 2.3 \times 10^{-6}\,\text{pc} = 7.2 \times 10^{7}\,\text{km}$. Thus Aldebaran has 50 times the diameter of the sun.

8.6 Calculate the relativistic red shift for our sun.

Solution
$\Delta\lambda/\lambda = 10^{-6}$.

Stellar Atmospheres

9

The term stellar atmosphere is very broad: In principle, it is understood to mean those layers of a star in which the spectral lines are formed. In our *sun* this essentially occurs in the *photosphere,* (only 400 km thick) but also in Chromosphere and even in the Corona.

The physics of stellar atmospheres deals with the formation and interpretation of spectra → qualitative and quantitative spectral analysis. First we want to sketch a quantum mechanical description of the emission-absorption processes.

Important input parameters for the physics of stellar atmospheres are temperature and gravitational acceleration.

The homogeneity of stellar atmospheres is no longer given as soon as one considers e.g. center to limb variation or large spots. Magnetic fields or stellar winds also cause anisotropy of the plasma. Let us consider two extreme cases:

Sun: Atmosphere (photosphere) very thin, plane-parallel approximation possible.
Super giants: Atmosphere extremely extended, so spherical models better.

9.1 Quantum Mechanical Description

In this section, we will give a brief overview of the quantum mechanical description of a particle to understand the origin of the spectral lines, as well as the quantum mechanical parameters to describe the electron configuration.

9.1.1 Description of a Particle

$\psi(x, y, z, t)$ let be a complex function with which the state of a particle can be completely described quantum mechanically.

A. Hanslmeier, *Introduction to Astronomy and Astrophysics*,
https://doi.org/10.1007/978-3-662-64637-3_9

The probability $dw(x, y, z, t)$ of finding a particle at time t at the location $\mathbf{r} = (x, y, z)$ is given in quantum mechanics by the absolute square of the *Wave function*:

$$dw(x, y, z, t) = |\psi(x, y, z, t)|^2 dV \tag{9.1}$$

The normalization simply states that the probability of finding the particle anywhere must equal 1:

$$\int |\psi^2| dV = 1 \tag{9.2}$$

9.1.2 Schrödinger Equation

The classical *energy* is given by the sum of kinetic and potential energy:

$$E = \frac{\mathbf{p}^2}{2m} + V(\mathbf{r}, t) \tag{9.3}$$

In quantum mechanical description, one replaces energy and momentum by the *operators:*

$$E \rightarrow i\hbar \frac{\partial}{\partial t} \tag{9.4}$$

$$p \rightarrow -i\hbar \nabla \tag{9.5}$$

The operator on the right-hand side of the Schrödinger equation is also known as the *Hamilton operator* and denoted by H. With this the *Schrödinger equation* becomes

$$i\hbar \frac{\partial}{\partial t} \psi(\mathbf{r}, t) = H\psi(\mathbf{r}, t) \tag{9.6}$$

respectively:

$$\mathrm{i}\hbar \frac{\partial}{\partial t} \psi(\mathbf{r}, t) = \frac{\hbar^2}{2m} \nabla^2 \psi(\mathbf{r}, t) + V(\mathbf{r}, t)\psi(\mathbf{r}, t) \tag{9.7}$$

The Schrödinger equation is a non-relativistic equation. If one wants to understand spin, for example, one needs the relativistic Dirac equation (it predicts, among other things, the

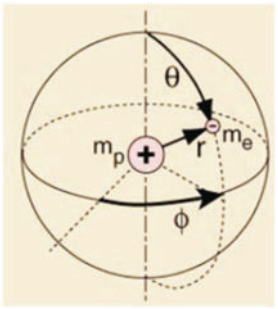

Fig. 9.1 Hydrogen atom, in the center is the proton, p^+, mass m_p, surrounded by an electron e^- mass m_e

spin of the electron, and the existence of antiparticles[1]).

$$i\hbar\frac{\partial\psi}{\partial t} = \left(c\alpha\mathbf{p} + \beta mc^2\right)\psi \tag{9.8}$$

And $\alpha = (\alpha_x, \alpha_y, \alpha_z)$ consists of 4×4-matrices and $\mathbf{p} = \frac{\hbar}{i}\nabla$.

$$\beta = \begin{pmatrix} 1&0&0&0\\ 0&1&0&0\\ 0&0&-1&0\\ 0&0&0&-1 \end{pmatrix} \qquad \alpha_x = \begin{pmatrix} 0&0&0&1\\ 0&0&1&0\\ 0&1&0&0\\ 1&0&0&0 \end{pmatrix} \tag{9.9}$$

$$\alpha_y = \begin{pmatrix} 0&0&0&-i\\ 0&0&i&0\\ 0&-i&0&0\\ i&0&0&0 \end{pmatrix} \qquad \alpha_z = \begin{pmatrix} 0&0&1&0\\ 0&0&0&-1\\ 1&0&0&0\\ 0&-1&0&0 \end{pmatrix} \tag{9.10}$$

9.1.3 Wave Functions for Hydrogen

Only for the hydrogen atom, the Schrödinger equation can be solved analytically. Let us use *Polar coordinations* r, Θ, Φ (Fig. 9.1). One separates the wave function in

$$\psi(r, \Theta, \Phi) = R_{\mathrm{nl}}(r)Y_{\mathrm{lm}}(\Theta, \Phi) \tag{9.11}$$

- radial solutions: $R_{\mathrm{nl}} \rightarrow$*Laguerre polynomials.* The square again gives the probabilities at what distance one can find the particle.
- Y_{lm} *Spherical harmonics.*

[1] Discovery of the positron in 1932.

The Laguerre polynomials are solutions of the Laguerre differential equation

$$x\,y''(x) + (1-x)\,y'(x) + ny(x) = 0 \qquad n = 0, 1, \ldots \tag{9.12}$$

And one finds :

$$\begin{aligned} L_0(x) &= 1 \\ L_1(x) &= -x + 1 \\ L_2(x) &= \frac{1}{2}\,(x^2 - 4\,x + 2) \\ L_3(x) &= \frac{1}{6}\,(-x^3 + 9\,x^2 - 18\,x + 6) \end{aligned}$$

resp. the formula of *Rodriguez:*

$$L_n(x) := \frac{e^x}{n!}\frac{d^n}{dx^n}(x^n e^{-x}) \tag{9.13}$$

For the associated Laguerre polynomials the DE is:

$$z\,y''(x) + (k+1-x)\,y'(x) + (p-k)\,y(x) = 0 \tag{9.14}$$

where $n = 0, 1, \ldots k \leq n$, and one finds:

$$\begin{aligned} L_0^k(x) &= 1 \\ L_1^k(x) &= -x + k + 1 \\ L_2^k(x) &= \frac{1}{2}\left[x^2 - 2\,(k+2)\,x + (k+1)(k+2)\right] \end{aligned}$$

The formula of *Rodriguez* reads:

$$L_n^k(x) = \frac{e^x\,x^{-k}}{n!}\,\frac{d^k}{dx^k}\,(e^{-x}\,x^{n+k}). \tag{9.15}$$

In the radial part of the wave function one has then:

$$R_{\mathrm{nl}}(r) = D_{\mathrm{nl}}\,e^{-\kappa\,r}\,(2\,\kappa\,r)^l\,L_{\mathrm{n+l}}^{2\,l+1}(2\,\kappa\,r) \tag{9.16}$$

Where D_{nl} is a normalization constant, κ a characteristic length and n is the principal quantum number, l the orbital angular momentum quantum number.

The spherical harmonic functions are defined as follows:

$$Y_{\mathrm{lm}}(\theta,\phi) = \frac{1}{\sqrt{2\pi}} N_{lm} P_{lm}(\cos\theta) e^{im\phi} \tag{9.17}$$

where $P_{\mathrm{lm}}(x)$ are the assigned Legendre polynomials

$$P_{\mathrm{lm}}(x) := \frac{(-1)^m}{2^l l!}(1-x^2)^{\frac{m}{2}} \left(\frac{\partial}{\partial x}\right)^{l+m} (x^2-1)^l \tag{9.18}$$

and N_{lm} are the normalization factors:

$$N_{\mathrm{lm}} = \sqrt{\frac{2\,l+1}{2} \cdot \frac{(l-m)!}{(l+m)!}} \tag{9.19}$$

For bound states, the solution to the Schrödinger equation is:

$$E_n = -\frac{\mu Z^2 e^4}{8\,h^2 \epsilon_0^2} \frac{1}{n^2} = -R\frac{Z^2}{n^2} \tag{9.20}$$

For the transitions of an electron between two states n_1, n_2 (see Table 9.1), we find the following wavelength of emission or absorption of a photon:

$$\frac{1}{\lambda} = \frac{1}{hc}\left(E_{n_1} - E_{n_2}\right) = R_H \left(\frac{1}{n_1^2} - \frac{1}{n_2^2}\right) \tag{9.21}$$

Table 9.1 Hydrogen atom: important transitions

Series		n_i	n_j	λ
Lyman	Lα	1	2	121.6 nm
	Lβ	1	3	102.6
	Lγ	1	4	97.3
	Lδ	1	5	94.9
Balmer	Hα	2	3	656.3
	Hβ	2	4	486.1
	Hγ	2	5	434.0
	Hδ	2	6	410.2
Paschen	Pα	3	4	1875.1
	Pβ	3	5	1281.8
	Pγ	3	6	1093.8
	Pδ	3	7	1005.0

R_H the *Rydberg constant.* It holds

$$R_H = \frac{\mu}{m_e} R_\infty = \left(\frac{M_\mathrm{H}}{M_{\mathrm{H}+m_e}} \right) R_\infty \tag{9.22}$$

and $R_\infty = 109{,}737.31\,\mathrm{cm}^{-1}$.

In addition to hydrogen, the universe also contains Deuterium, but only at about 2×10^{-4} of the hydrogen abundance. The Rydberg constant for deuterium is:

$$R_D = \frac{\mu_D}{\mathrm{H}} R_H \tag{9.23}$$

and the reduced masses are:

$$\mu_\mathrm{H} = \frac{M_\mathrm{H} + m_e}{m_\mathrm{H} m_e} \qquad \mu_\mathrm{D} = \frac{M_D + m_e}{M_D + m_e} \tag{9.24}$$

and $\mu_\mathrm{H}/\mu_\mathrm{D} = 1.00027$. From this follows for the wave numbers of the Hα-line:

H: $15238.7\,\mathrm{cm}^{-1}$ D: $15233\,\mathrm{cm}^{-1}$.

9.1.4 Quantum Numbers

One has four quantum numbers:

- three quantum numbers give space geometry,
- the 4th quantum number the spin.

Thus:

- *R(r) principal quantum number,* $n = 1, 2, 3, \ldots$
- $\Theta(\theta)$: orbital number, $l = 0, 1, 2, \ldots n - 1$; identifies the *Orbital angular momentum* of the electron, gives the shape of the orbital.
- $\Phi(\phi)$: *magnetic quantum number,* $-l, -l + 1, \ldots, l - 1, l$; $2l + 1$ Values
- $m_s = \pm\frac{1}{2}$ *Spin quantum number.*

In the field of IR spectroscopy the *rotational quantum number J* and the *vibrational quantum number v* are important, and *k* describes the *precession motion* of a molecule around its rotation axis. Furthermore, there is also the *nuclear spin quantum number.*

In IR spectroscopy, the excitation of the molecules plays an important role: they can oscillate or rotate, but these states are quantized.

Table 9.2 Quantum numbers and orbitals

Quantum number	Character	Range	Designation
Main quantum number	n	1,2,3,...	K,L, M,...
Secondary quantum number	l	0,..., n−1	s,p,d, f,...
Magnetic quantum number	m	−l,..., l	
Spin quantum number	s	−1/2,+1/2	

9.1.5 Electron Configurations

Pauli Principle In a *Quantum Cell* electrons must differ in at least one quantum number. Therefore, all electrons in an atom distribute themselves to different states.

A summary is given in Table 9.2.

The principal quantum numbers define the *shells;* the minor quantum numbers define the subshells.

Each shell can be occupied at most by $2n^2$ electrons, and one denotes the shells by K (for $n = 1$), L (for $n = 2$), M (for $n = 3$), etc. The outermost shell determines the chemical behavior *(valence shell)*. The occupation is in this order:

1. 1 s
2. 2 s 2p
3. 3 s 3p
4. 4 s 3d 4p (Hund's rule)...

Electron configuration is important for labeling radiative transitions. Suppose there are five electrons in the 2nd sub shell of the 2nd shell, then they are given as follows:

$2p^5$

Where p stands for the 2nd subshell.

9.1.6 Hydrogen Fine Structure

The *electron spin* is a consequence of the relativistic treatment of quantum mechanics → Coupling between Orbital angular momentum l and spin s⇒ total angular momentum j of the electron.

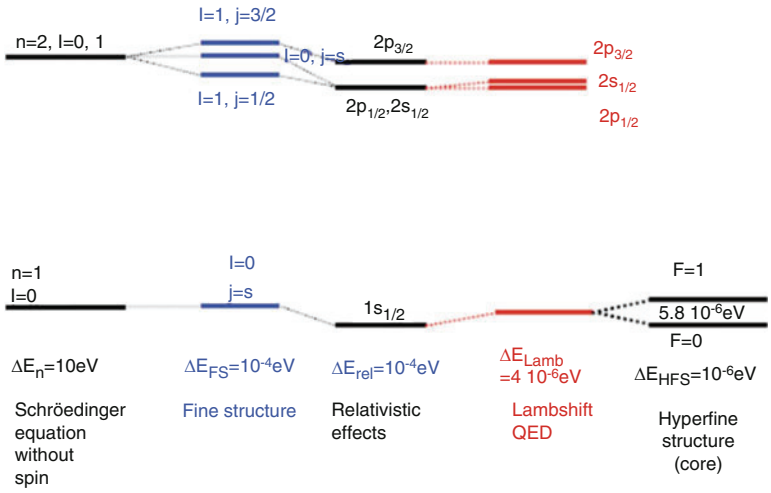

Fig. 9.2 Fine structure or hyperfine structure in the hydrogen atom.

Hydrogen: $s = 1/2$, therefore for $l \neq 0 : j = l \pm 1/2$.

Besides there is the *hyperfine structure*. Here the *nuclear spin, i*, must be taken into account. Thus one has

$$f = j \pm \frac{1}{2} \tag{9.25}$$

Because of the nuclear spin, the ground state can be divided into two levels $f = 0$ resp. $f = 1$ can be split. The energy difference is only 6×10^{-6} eV and the transition corresponds to a frequency of 1420.4 MHz or a wavelength of 21 cm (chapter on galaxies) (Fig. 9.2).

9.1.7 Complex Atoms

For an atom with N electrons and charge number Z is the Schrödinger equation:

$$\left[\sum_{i=1}^{N}\left(-\frac{\hbar^2}{2m_e}\nabla_i^2 - \frac{Ze^2}{4\pi\epsilon_0 r_i}\right) + \sum_{i=1}^{N-1}\sum_{j=i+1}^{N}\frac{e^2}{4\pi\epsilon_0|\mathbf{r}_i - \mathbf{r}_j|} - E\right]\psi(\mathbf{r}_1, \ldots \mathbf{r}_N) = 0 \tag{9.26}$$

In the first sum stands the kinetic energy as well as the Coulomb attraction between electron and atomic nucleus. In the second sum stands the expression for the repulsion between electron-electron. This makes the equation no longer analytically solvable.

Atomic ions containing the same number of electrons belong to the so-called isoelectronic series.

A splitting of the spectral lines occurs trough[2] interaction of the orbital angular momentum of an electron with the spin. Because of the electron spin, the electron has a magnetic moment. This is coupled to the magnetic moment of the nucleus → for one spin direction the energy increases, for the other it decreases. → Increase of the number of the Energy levels, hence more lines.

One distinguishes:

- light atoms (e.g. C): spin-orbit coupling, LS coupling (Russel-Saunders coupling). Here the electrostatic interaction of all electrons is large compared to the spin-orbit interaction of single electrons. Thus the spin-orbit coupling of an electron is broken, and the total momentum is:

$$\mathbf{J} = \sum_i \mathbf{l}_i + \sum_i \mathbf{s}_i \tag{9.27}$$

- jj-coupling applies to heavy atoms. The electrostatic interaction of all electrons is small compared to the sum of all spin-orbit interactions of individual electrons:

$$\mathbf{J} = \sum_i \mathbf{j}_i \tag{9.28}$$

9.2 Excitation and Ionization

In this section we discuss the distribution of electrons/atoms among the different

- Excitation states: this leads to the Boltzmann formula,
- ionization states: this leads to the Saha formula.

This can then be used to explain why hydrogen lines are only faintly visible in very hot stellar atmospheres.

[2] Very well known: Splitting of the D line of Na.

9.2.1 Thermodynamic Equilibrium

In thermodynamic equilibrium, TE, the internal energy is distributed uniformly by collisions among all particles.

Example of a non-equilibrium: an extremely thinly distributed gas (e.g. interstellar matter); collisions hardly occur there because of the low density; likewise in thin atmospheres (corona of the sun, etc.).

Within TE one can calculate particle-speeds by the *Maxwell distribution*:[3]

$$F(v) = \sqrt{\frac{2}{\pi}} \left(\frac{m_M}{kT}\right)^{3/2} v^2 \exp\left(-\frac{m_M v^2}{2kT}\right) \tag{9.29}$$

Where $F(v)$ is the distribution function of the velocities, m_M is the particle mass, $k = 1.38 \times 10^{-23}\,\mathrm{JK}^{-1}$ Boltzmann constant. The probability that a particle has a velocity in the interval v_1, v_2 is calculated from

$$w = \int_{v_1}^{v_2} F(v)dv \tag{9.30}$$

and the fraction of particles in a small velocity interval Δv is approximately

$$f = F(v)\Delta v \tag{9.31}$$

The most probable velocity is obtained from the maximum of the distribution function, i.e., one sets the derivative of Eq. 9.29 to zero.

$$v_{\max} = \sqrt{\frac{2kT}{m_M}} \tag{9.32}$$

The root mean square velocity is found from the kinetic theory of gases:

$$pV = \frac{1}{3} n M \bar{v}^2 \qquad pV = n\Re T \tag{9.33}$$

[3] 1860 Maxwell, Boltzmann.

Hence

$$\sqrt{\overline{v^2}} = \sqrt{\frac{3kT}{m}} = \sqrt{\frac{3\Re T}{M}} \tag{9.34}$$

A doubling of the temperature increases the root mean square velocity by a factor of $\sqrt{2}$.

For the mean kinetic energy per particle we find:

$$E_{\text{kin}} = \frac{3}{2}kT \tag{9.35}$$

Maxwell distribution is valid for thermodynamic equilibrium.

9.2.2 Boltzmann Formula

We assume thermal equilibrium. The average state of the atoms is not supposed to change. Any excitation in which an electron jumps from a level A to a level B is compensated by a transition from B to A, one therefore has equilibrium:

$$A \rightarrow B = B \rightarrow A \tag{9.36}$$

N_A, N_B let be the number of atoms in state A and B respectively, where state B is said to have a higher energy than A , $B > A$.

The Boltzmann formula gives the distribution over the different excited states.[4]

$$\frac{N_B}{N_A} = \frac{g_B}{g_A} \exp[(E_A - E_B)/kT] \tag{9.37}$$

g is the multiplicity of the level *(statistical weight)* and E is the energy. Please note:

1. N_B/N_A increases with increasing temperature
2. If the temperature is given, then the ratio N_B/N_A increases when $E_B - E_A$ decreases between two energy levels.
3. In plasma physics, one often computes with:

$$\frac{1\text{eV}}{k} = \frac{1.60 \times 10^{-19}\,\text{J}}{1.38 \times 10^{-23}\,\text{J/K}} = 1604\,\text{K} \tag{9.38}$$

[4] *Ludwig Boltzmann,* 1844−1906.

4. Consider a volume of gas containing H and He atoms. Both atoms produce spectral lines, but which lines are stronger? Let the number of H atoms in state 2 compared to state 1 be $N_2/N_1 = 1/10$. The ratio N_2/N_1 for He, however, will be much lower, since other (higher) excitation energies are required.

The strength of a line therefore depends on the element and the temperature T.

Let us examine the effect of temperature on the distribution of hydrogen atoms in a stellar atmosphere in the ground state and in the first excited state.

1. Number of hydrogen atoms in the ground state N_0, statistical weight $g_0 = 2$.
2. Number of hydrogen atoms in the first excited state N_1, statistical weight $g_1 = 8$.

Further $E_1 - E_0 = 10.2\,\text{eV}$, and from the Boltzmann formula

$$\frac{N_1}{N_0} = \frac{g_1}{g_0}\exp(-(E_1 - E_0)/(kT)) \tag{9.39}$$

we get $T = 3000\,\text{K}$:

$$\begin{aligned}\frac{N_1}{N_0} =& \frac{8}{2}\exp\left(-\frac{10.2 \times 1.6 \times 10^{-19}}{1.38 \times 10^{-23} \times 3000}\right)\\ =& 3 \times 10^{-17}\\ T =& 6000\,\text{K} : 10^{-8}\\ T =& 12{,}000\,\text{K} : 10^{-4}\end{aligned}$$

Up to a temperature of about 10,000 K the intensity of the spectral line increases according to this formula, which agrees with observations. However, at higher temperatures, it must be taken into account that the ionization also increases!

9.2.3 Saha Equation

At higher temperatures, the atoms become ionized. Therefore, a hot gas consists of neutral atoms, ions, and free electrons. The higher the electron density N_e the higher the probability that an ion captures an electron and becomes neutral. Therefore, two processes are relevant to the distribution among the different ionization states:

- Ionization
- Recombination

If the rate of ionization equals the rate of recombination, then again we have equilibrium:

$$X \rightleftharpoons X^+ + e^- \tag{9.40}$$

The Indian physicist *Saha* has established the equation named after him: N_{i+1} is the number of ions in the $(i+1)$-th ionization state, N_i the number of ions in the i-th ionization state, χ_i is the ionization potential.

$$\frac{N_{i+1}}{N_i} = \frac{A(kT)^{3/2}}{N_e} \exp\left(-\chi_i / kT\right) \tag{9.41}$$

In A stand atomic constants as well as the partition function (degeneracy) resulting from the statistical weights.

We consider N_+/N_0 for hydrogen as a function of temperature. It is found that below 7000 K most H is neutral. The ratio N_2/N_1 increases with T, but at high temperature T there are no more neutral H atoms. The curve N_2/N reaches a maximum at 10,000 K. The transitions from $n > 2$ to $n = 2$ is called *Balmer series.* The strength of the Balmer lines is greatest at $T = 10{,}000$ K.

The general form of the Saha equation is (u_i partition function or degeneracy, P_e electron pressure):

$$\frac{N_{i+1}}{N_i} P_e = 2\frac{u_{i+1}}{u_i} \frac{(2\pi m_e)^{3/2}(kT)^{5/2}}{h^3} \exp\left(-\frac{\chi_i}{kT}\right) \tag{9.42}$$

Written logarithmically:

$$\log\left(\frac{N_{i+1}}{N_i} P_e\right) = -\chi_i \Theta + \frac{5}{2}\log T - 0.48 + \log\frac{2u_{i+1}}{u_i} \tag{9.43}$$

Where P_e in dyn (1 dyn = 1 cm g s^{-2} = 10^{-5} N), χ in eV and $\Theta = 5040/T$.

One can make a very simple estimate of the temperature of a stellar atmosphere. Suppose a particular ion is very abundant, i.e., its associated spectral line is very strong. Then its ionization potential becomes $\approx kT$.

9.3 Radiation Transport

The transport of radiation is described by a transfer equation. This involves (i) emission, (ii) absorption; both processes are described by macroscopic coefficients.

9.3.1 Transfer Equation

Inside of a stellar atmosphere there is a flow of energy outwards. Energy transport is possible in principle by:

- Heating, conduction,
- Radiation,
- Convection.

In radiative transfer, which is most important to the physics of stellar atmospheres, photons are continuously absorbed and then re-emitted in all directions. As a result, less intensity reaches the observer, and dark spectral lines are seen. What is important here is the temperature gradient, the amount by which the temperature decreases with altitude. You have lower and hotter layers radiating energy to the higher lying, cooler layers.

We now examine the main laws of this radiative transfer. The radiation field can be described by the intensity I_ν. In general, this also depends on the direction of the radiation. The frequency dependence is described by the index ν. The radiation energy dE_ν that is emitted in the frequency interval $[\nu, \nu + d\nu]$ during the time dt through a perpendicular surface dF into the solid angle $d\omega$ is:

$$dE_\nu = I_\nu dt dF d\omega d\nu \tag{9.44}$$

Note: In exact thermal equilibrium, the radiation is independent of the direction of radiation, hence isotropic. The intensity distribution is then given by the Planck function:

$$I_\nu = B(\nu, T) \tag{9.45}$$

Now we make a balance: what happens when the radiation passes through a thin layer of matter of thickness ds (Fig. 9.3)?

→ **Absorption:** the change in intensity when passing through ds is:

$$dI_\nu = -I_\nu \kappa_\nu ds \tag{9.46}$$

For this an *Absorption coefficient* κ_ν is introduced. This has the dimension $1/L$, L—length, and is a function of chemical composition of the matter and of the degree of ionization and excitation, i.e. of T and P (cf. Saha equation).

→ **Emission:** this causes an increase in intensity, and we introduce the *Emission coefficient* ϵ_ν:

$$dI_\nu = \epsilon_\nu ds \tag{9.47}$$

Again, this coefficient depends on temperature and pressure.

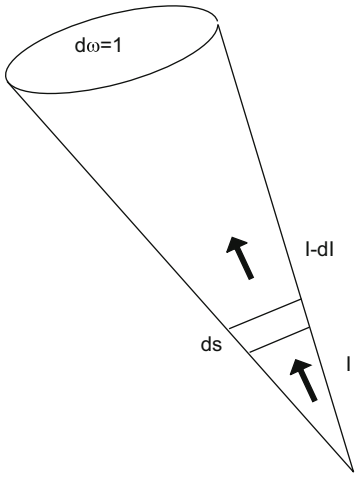

Fig. 9.3 Change in the instensity I coming from the stellar interior as it passes through a layer ds. Absorption changes the intensity to $I - dI$

If thermal equilibrium holds, then:

$$\frac{\epsilon_\nu}{\kappa_\nu} = B(\nu, T) \tag{9.48}$$

which is known as *Kirchhoff's theorem*. Note:

> In general, a stellar atmosphere is not in thermal equilibrium, because this would mean the same temperature for every depth T and isotropic radiation.

In reality, we observe a net outward radiation flux, and the temperature drops. If we use the approximation for thermal equilibrium locally, then we speak of a *LTE (local thermodynamic* equilibrium).

Now we complete the balance: The change of intensity dI_ν when passing through a layer ds is equal to emission minus absorption:

$$dI_\nu = -I_\nu \kappa_\nu ds + \epsilon_\nu ds \tag{9.49}$$

We divide this by ds: $\frac{dI_\nu}{ds} = -I_\nu \kappa_\nu + \epsilon_\nu$.

One introduces the *optical depth* τ_ν:

$$\tau_\nu = \int \kappa_\nu ds \tag{9.50}$$

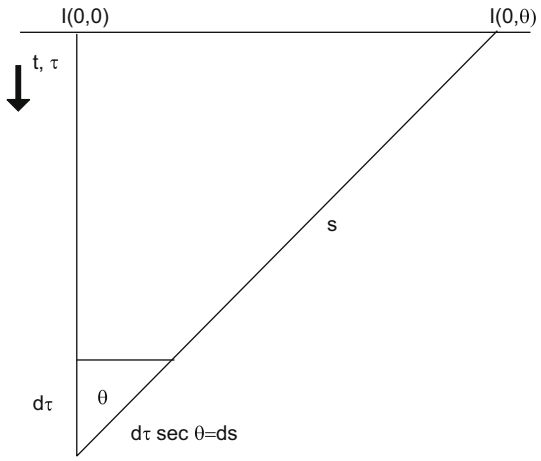

Fig. 9.4 Relationship between optical depth τ, geometric depth t resp. geometricdepth s, seen from an angle Θ

If one has only one absorption, it follows from 9.49

$$dI_\nu = -I_\nu \kappa_\nu ds$$
$$-\int dI_\nu / I_\nu = \int \kappa_\nu ds = \tau_\nu$$
$$I_\nu = I_{\nu,0} e^{-\tau_\nu}$$

Extreme cases:

- $\tau_\nu \ll 1$ *optically thin,*
- $\tau_\nu \gg 1$ *optically thick.*

Let's estimate the thickness of the solar photosphere. The mean value for the absorption coefficient is:[5] $\bar{\kappa} = 3 \times 10^{-8}\,\mathrm{cm}^{-1}$. For an optical depth of 1, according to the above formula, the intensity falls to the (1/(*e*)-th part. Therefore, we find the thickness of the photosphere Δs from the relation

$$\bar{\kappa} \Delta s = \tau \sim 1$$

and thus $\Delta s = 300\,\mathrm{km}$.

Let us go back again to our considerations about the radiation intensity. Let us assume that our surface element dF forms an angle with the normal θ. The depth t and the path distance s are related via (Fig. 9.4):

$$\cos\theta = -d\tau / ds \tag{9.51}$$

[5] Averaging over all frequencies ν.

Applying Kirchhoff's theorem, we find:

$$\cos\theta \frac{dI_\nu(t,\theta)}{d\tau_\nu} = I_\nu(t,\theta) - B_\nu(T(t)) \tag{9.52}$$

At radiative equilibrium, the radiative flux is independent of the depth t:

$$F = \int_{\theta=0}^{\pi}\int_{\nu=0}^{\infty} I_\nu(t,\theta) 2\pi \cos\theta \sin\theta d\theta d\nu = \sigma T_{\text{eff}}^4 \tag{9.53}$$

At the stellar surface the incident radiation vanishes, i.e. $I_\nu(0,\Theta)$ for $0 < \theta < \pi/2$. The solution becomes simple if one assumes that the absorption coefficient is independent of the frequency: this is called as *grey stellar atmosphere* . One can also assume an averaged absorption coefficient for example the *Rosseland's opacity coefficient:*

$$\bar{\tau} = \int_{-\infty}^{t} \bar{\kappa} dt \tag{9.54}$$

9.3.2 Solutions of the Transfer Equation

The *source function* is:

$$S_\nu = \epsilon_\nu/\kappa_\nu, \tag{9.55}$$

With this the transport equation becomes:

$$\cos\theta \frac{dI_\nu}{d\tau_\nu} = I_\nu(\tau,\theta) - S_\nu(\tau) \tag{9.56}$$

In American literature one often finds : $\mu = \cos\theta$. To solve, substitute:

$$\sec\theta = 1/\cos\theta \qquad \tau/\cos\theta = \tau\sec\theta = \xi$$

and substitute this into the transgfer equation:

$$\frac{dI}{d\xi} - I = -S$$

Now we multiply this by the integrating factor $e^{-\xi}$:

$$\frac{d(Ie^{-\xi})}{d\xi} = -Se^{-\xi} \qquad \frac{dIe^{-\xi}}{d\xi} = \frac{dI}{d\xi}e^{-\xi} - e^{-\xi}I$$

and we get

$$Ie^{-\xi} = -\int Se^{-\xi'}d\xi'$$

and therefore:

$$Ie^{-\tau\sec\theta} = -\int Se^{-\tau'\sec\theta}d\tau'\sec\theta$$

and finally

$$I = -\int_{\infty}^{\tau} S(\tau')e^{-(\tau'-\tau)sec\theta}d\tau' sec\theta$$

Let us now consider the most important case for us: radiation at the surface: Then $\tau = 0$, and we get (the $'$ omitted):

$$I_\nu(0,\theta) = \int_0^{\infty} S_\nu(\tau)e^{-\tau_\nu sec\theta}d\tau_\nu sec\theta \tag{9.57}$$

So this is the intensity reaching the observer. If one looks vertically into a stellar atmosphere ($\theta = 0$), and the same temperature prevails (S_ν independent of τ_ν):

$$I_\nu = S_\nu \int e^{-\tau\nu}d\tau_\nu = S_\nu(1 - e^{-\tau_\nu})$$

Now we can apply to this the two cases optically thick and optically thin:

- optically thick: $\tau \gg 1$, then $e^{-\tau} = 1/e^{\tau} \to 0$ and you have $I_\nu = S_\nu$;
- optically thin: $\tau \ll 1$, from $e^{-\tau} = 1 - \tau$ follows: $I_\nu = S_\tau\tau_\nu$.

The general solution of 9.57 can be integrated numerically. However, we study one approach.

Eddington-Barbier Approximation
One expands the soruce function:

$$S(\tau) = S(\tau') + (\tau - \tau')\frac{dS}{d\tau}\bigg|_{\tau'} + \frac{(\tau - \tau')^2}{2}\frac{d^2S}{d\tau^2}\bigg|_{\tau'} + \ldots$$

This is put into the formula 9.57, and obtains for the first two terms:

$$I_\nu(0,\theta) = \int_0^\infty \left(S(\tau') + (\tau - \tau')\frac{dS}{d\tau} \right) \exp^{-\tau \sec\theta} d\tau \sec\theta$$
$$= - S(\tau')\exp^{-\tau \sec\theta}\Big|_0^\infty + (\cos\theta - \tau')\frac{dS}{d\tau}\Big|_{\tau'}$$

and integrating term by term.

If $\tau' = \cos\theta$ is, then the second term disappears, and it follows:

$$I(0,\theta) = S_{\tau=\cos\theta} \tag{9.58}$$

One can easily show that then the next term of the series expansion becomes a minimum. We have therefore, to a good approximation:

The outgoing intensity is equal to the source function at the optical depth $\tau = 2/3$.

This also provides a simple relation for the *Center to limb variation* .

Gray Atmosphere, Milne Solution
One replaces the frequency-dependent absorption coefficient with an appropriate mean value, $\kappa_\nu \to \kappa$, and then obtains:

$$\cos\theta \frac{dI(\tau,\theta)}{d\tau} = I(\tau,\theta) - S(\tau)$$
$$I = \int_0^\infty I_\nu d\nu \qquad S = \int_0^\infty S_\nu d\nu$$

The source function is then equal to $S(\tau) = J(\tau) = \int\int I(\tau,\theta)d\omega/4\pi$, i.e. the intensity integrated over the sphere. With the conditions $F^+ = F$, $F^- = 0$ one obtains

$$S(\tau) = \frac{3}{4\pi} F[\tau + q(\tau)] \tag{9.59}$$

Where $1/2 \le q(\tau) \le 1$; $q(0) = 1/\sqrt{3} = 0.5774$. In practice one calculates with:

$$q(\tau) = 0.7104 - 0.1331\exp^{-3.4488\tau} \tag{9.60}$$